Validation of Hydrogenography for the search of promising hydrogen storage materials

This work was funded as a part of the EU project 'NESSHY' (Novel Efficient Solid Storage for Hydrogen, contract # 518271).

The work was carried out at

Vrije Universiteit Amsterdam
Condensed matter physics
Faculteit Exacte Wetenschappen
De Boelelaan 1081,
1081 HV Amsterdam

And

Technische Universiteit Delft
Faculty of Applied Sciences
Department of Chemical Engineering
Materials for Energy Conversion and Storage (MECS)
Julianalaan 136,
2628 BL Delft

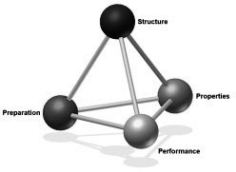

Validation of Hydrogenography for the search of promising hydrogen storage materials

Proefschrift

ter verkrijging van de graad van doctor
aan de Technische Universiteit Delft,
op gezag van de Rector Magnificus prof. ir. K.C.A.M. Luyben,
voorzitter van het College voor Promoties,
in het openbaar te verdedigen op dinsdag 24 januari 2012 om 15.00 uur

door

YEVHENIY PIVAK

Master of Science in Semiconductor Microelectronics,
Lviv Polythechnic National University
geboren te Lviv, Ukriane

Dit proefschrift is goedgekeurd door de promotoren:

Prof. dr. B. Dam

Prof dr. R. Griessen

Samenstelling promotiecommissie:

Rector Magnificus,	voorzitter
Prof. dr. B. Dam,	Technische Universiteit Delft, promotor
Prof. dr. R. Griessen,	Vrije Universiteit Amsterdam, promotor
Prof. dr. A. Pundt,	University of Göttingen (Germany)
Prof. dr. ir. B.J. Kooi,	Rijksuniversiteit Groningen
Prof. dr. A. Schmidt-Ott,	Technische Universiteit Delft
Prof. dr. F.M. Mulder,	Technische Universiteit Delft
Prof. dr. H.W. Zandbergen,	Technische Universiteit Delft

Cover: Blue Lagoon geothermal spa and geothermal power plant Svartsengi in Iceland

Printed by: Gildeprint drukkerijen

ISBN 978-94-6108-260-2

Посвящается Диане

Contents

Chapter 1

1.1 Introduction

Hydrogen storage in metal hydrides is one of the ways to store this clean energy carrier. It is a very promising method as it relatively safe and may provide higher gravimetric and volumetric densities over hydrogen storage in gas or liquefied form.

This makes metal hydrides a very attractive and effective option for storing hydrogen for automobile applications. The practical use of metal hydrides is, however, still limited due to their relatively high stability. The stability of a metal hydride depends on thermodynamic parameters such as the enthalpy and entropy of formation, which define the operating pressure and temperature window. The thermodynamic parameters of the most studied metal hydride systems fall outside the desired range (273-373 K at 1 bar H_2 pressure), resulting in too high temperatures (423-573 K) of hydrogen release or uptake, Therefore, a lot of work is undertaken at the moment to identify new promising candidates and/or modify the existing ones.

This thesis addresses the question of the applicability of a new combinatorial thin film technique called *Hydrogenography* to: (1) the study of the thermodynamic behavior of metal hydride thin films in relation to the corresponding bulk materials and (2) the identification of new promising hydrogen storage materials.

The applicability of *Hydrogenography* to the investigation of the thermodynamics of metal hydrides thin films depends on several critical issues. First of all, we need to validate the method. In other words, we should answer the question whether our optical thin film approach gives the same thermodynamic properties as compared to common bulk techniques. Secondly, the applicability of Hydrogenography depends on the question whether the presence of the substrate can alter the thermodynamic and hysteresis behavior of thin films as compared to bulk.

In thin films, the volumetric expansion on hydrogenation is constrained by the presence of the substrate. As a result, in general, more plastic deformation is to be expected to occur. In the course of our research we developed a simple (stress-strain) model, which allows to quantify the difference between films and bulk behavior and provides a possibility to recalculate bulk properties from the *Hydrogenography* results. The proposed model is of particular interest not only from the practical, but also from the fundamental point of view, as it shides light on the hysteresis, a widely observed phenomenon in many metal-hydride systems. While the theory was developed for interstitial hydrides such as Pd, we have explored its applicability to a wide range of (complex) metal hydrides with and without a structural transformation.

In this thesis I will show that thin films can advantageously be used to explore the thermodynamics of metal hydrides, if the effect of substrate clamping is properly taken into account.

1.2 Why hydrogen storage

The depletion of the fossil fuel reserves and the climate change due to CO_2 emission force mankind to shift from the energy system based on oil and gas towards cleaner and more renewable energy sources. One of the possible future scenarios is based on hydrogen.

Hydrogen is a clean energy carrier. It can be obtained in a sustainable way by means of electrolysis of water with electricity, produced from sources like sunlight, wind or nuclear power. Hydrogen can be stored and then used in a stationary or mobile application. In the latter case it can be utilized in combination with an internal combustion engine or a fuel cell. As it is a carbon-free fuel, hydrogen combustion just results in the production of water, which completes the hydrogen cycle (Fig. 1.1).

In the context of automotive applications, hydrogen storage remains the main problem, as at normal conditions H_2 is a gas. At ambient temperature it can be stored under very high pressures (up to 700 bars) in gas cylinders. This is now the method of choice of the car industry although energy losses due to compression, and large volumes (a small volumetric capacity) are unavoidable drawbacks of this option. A better volumetric density can be achieved in liquid hydrogen at temperatures of 21 K at ambient pressure. However, the liquefaction process is extremely inefficient and requires about 40% of the higher heating value of the hydrogen combustion [1]. In addition, imperfect thermal isolation will inevitably lead to a boiling off of hydrogen, which makes this storage possibility unpractical for long-term mobile applications. The third way to store hydrogen is by chemical storage in materials. This is a relatively safe method, which provides a higher volumetric capacity and has a potential to work near ambient temperatures and pressures.

The last point is very important if one wants to combine a hydrogen storage medium with a PEM fuel cell, which has a limited operating range of temperatures and pressures.

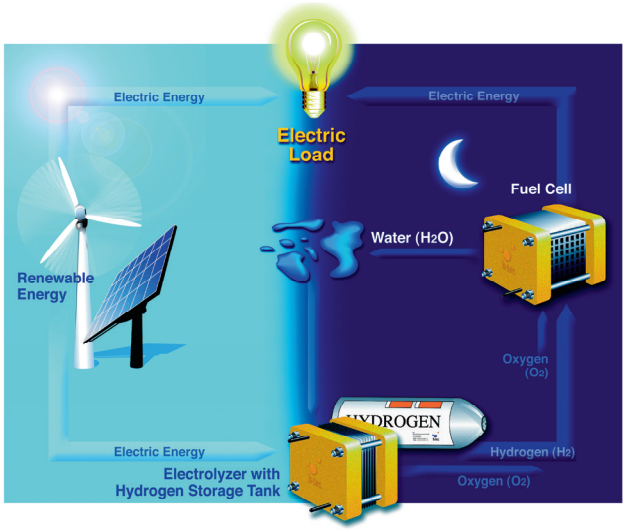

Fig. 1.1. The solar hydrogen cycle [1].

There are different types of materials, which can store hydrogen. The nature of the hydrogen interaction with a material, whether in a molecular or atomic form, distinguishes physisorption and chemisorption storage systems, respectively. Porous materials such as carbon, zeolites and metal –organic frameworks belong to the first class. The second class includes two large groups of materials, namely metal hydrides and complex metal hydrides. Metal hydrides, which are of particular interest for this thesis, absorb hydrogen interstitially in the tetrahedral or octahedral sites of the metal lattice, whereas in complex hydrides hydrogen forms metal-hydride complexes. Many lightweight metals can bind hydrogen and do it reversibly, making metal hydrides promising hydrogen storage systems in this field.

1.3 Thermodynamics of hydrogen storage in metals

The absorption of hydrogen by a metal depends on temperature and pressure and can be described by the Pressure-Concentration-Isotherm (PCI). In the PCI's, shown in Fig. 1.2, the logarithm of the hydrogen pressure (y axis) is plotted against the hydrogen concentration (x axis) stored in a material.

At low pressures, hydrogen atoms are typically present in a diluted solid solution (H/M<0.1), the so-called α-phase (Fig. 1.2). As the pressure increases, hydrogen continues to be absorbed until H-H interactions become important and a nucleation of the β-phase takes place. At this point α- and β-phases coexist in the equilibrium with each other and with the hydrogen gas. The subsequent growth of the β-phase occurs at the expense of the α-phase at a constant pressure and can be observed as a plateau in the PCI diagram. The hydrogen concentration increases up to a certain value, which represents the point where all of the α-phase is transformed into the β-phase. When the pressure again rises, the overall hydrogen concentration continues to increase as hydrogen is dissolved as a solid solution in the β hydride phase.

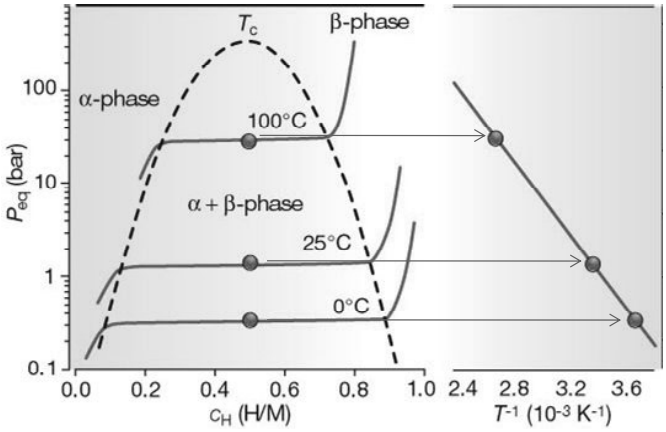

Fig. 1.2. Typical pressure-concentration-isotherms and the corresponding Van 't Hoff plot of an interstitial hydrogen storage material [1].

The hydrogen pressure at which the α-β phase transformation takes place, is called the equilibrium pressure plateau, P_{eq}. The plateau disappears completely at the critical point, T_c (Fig. 1.2a), above which there is a smooth transition from the α-phase to the β-phase.

As a function of temperature, the plateau pressure is given by the Van 't Hoff equation:

$$\ln \frac{p_{eq}}{p_o} = \frac{\Delta H}{RT} - \frac{\Delta S_o}{R} \tag{1.1}$$

where $p_o = 1.013 \times 10^5$ Pa is the standard pressure, R is the gas constant, T is the absolute temperature and ΔH and ΔS_o is the enthalpy (kJ molH_2^{-1}) and entropy (J K^{-1}molH_2^{-1}) of hydride formation, respectively.

The entropy change, ΔS_o, is the difference between the partial molar entropy ($\overline{S}_H = \frac{S_\beta - S_\alpha}{c_\beta - c_\alpha}$) of the hydride phase and the standard entropy of hydrogen gas (ΔS_{H_2}). However, for most metal-hydride systems, ΔS_o is mainly determined by the loss of entropy when H_2 gas molecule is dissociated and adsorbed by the metal, i.e. $\Delta S_o \cong \Delta S_{H_2} = -130.7$ J K^{-1}molH_2^{-1}. Taking this into account and assuming that metal hydride storage system should release hydrogen in a temperature range of 273–373 K at a pressure of 1 bar or more, the ideal hydrogen storage material should be characterized by a heat of hydride between approximately -36 and (-48) kJ molH_2^{-1}. Thus information on the enthalpy of formation is essential for practical applications since it has a direct impact on whether a hydrogen storage material can be used for on-board hydrogen recharging. Van 't Hoff plots are commonly used to determine the thermodynamic properties of hydrogen storage materials (Fig. 1.2b). In general, using a standard bulk technique such as volumetry (Sievert's method), a number of PCI's are measured at different temperatures to generate the Van 't Hoff plot. The enthalpy and entropy of the hydride formation can then be calculated by means of a regression analysis from the slope of the line and from the intercept with the y-axis, respectively (Fig. 1.2b).

1.4 Thermodynamics measurements using Hydrogenography

Hydrogenography is an alternative to the conventional volumetric method used to study the thermodynamic properties of hydrogen storage materials. Unlike bulk techniques, *Hydrogenography* is applied to thin films of metal hydrides. It is an optical technique, based on the fact that metallic films change their optical properties upon hydrogen loading and unloading (Fig. 1.3).

The *Hydrogenography* approach is similar to the conventional Sievert's technique with the difference that the hydrogen concentration cannot be measured directly during the experiment. Instead, we monitor the change in the optical transmission of metal thin films while increasing and decreasing the hydrogen pressure during loading and unloading, respectively (Fig. 1.4).

Fig. 1.3. $Mg_{0.7}Ti_{0.3}$ thin film in the metallic (left) and in the hydrided (right) state during hydrogenation [2].

An abrupt change in optical transmission occurs when two phases coexist. Using the same experimental data in different coordinates, namely $P(H_2)$ vs. $\ln(T/T_M)$ we plot the so-called Pressure-Transmission-Isotherms (PTI's). According to the Lambert-Beer law, the logarithm of the normalized optical transmission is proportional to the hydrogen concentration in the two-phase region. Note, that the method is not confined to materials showing a metal insulator transition on hydrogenation: even materials such as Pd- that show quite small optical changes in transmission on hydriding- can be studied by *Hydrogenography* as long as the layer thickness is below 90nm. This makes the PTI's equivalent to the Pressure-Concentration-Isotherms (PCI's) obtained with standard volumetric or gravimetric methods, with the advantage that, due to the thin film geometry, the diffusion issues encountered during the recording of PCI's are minimized.

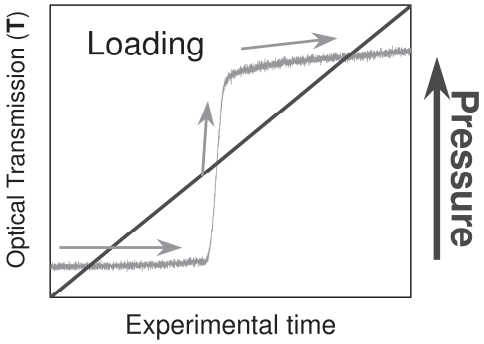

Fig. 1.4. Optical transmission changes in a metallic thin film during hydrogenation.

The optical transmission is used only as an indicator of the (de)/hydrogenation plateau pressure. The determination of the absolute hydrogen concentration falls outside the scope of *Hydrogenography*. In the two-phase region, the hydrogen concentration can be derived from the optical transmission, when the limiting hydrogen concentration of the alpha and beta phase are known and when there is an abrupt change in optical properties on forming a hydride (i.e. relatively flat plateau). To accurately estimate the amount of hydrogen dissolved we use electrochemistry or nuclear resonance reaction methods (N-15).

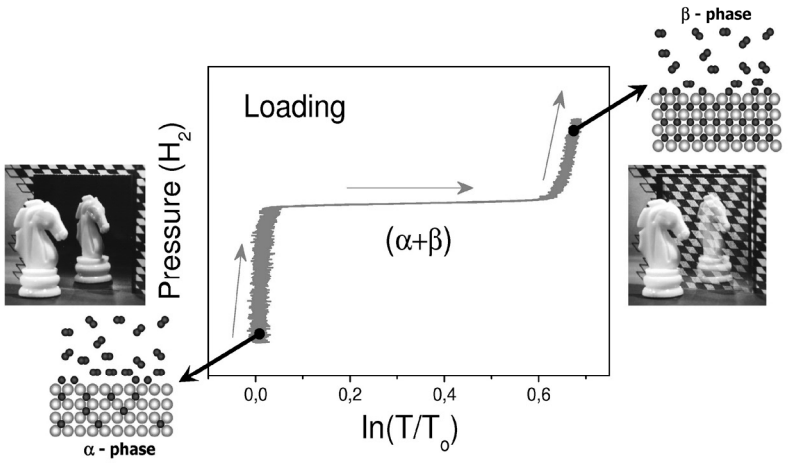

Fig. 1.5. Typical Pressure-Transmission-Isotherm of a metal hydride with two coexisting phases.

Through the recording of pressure–transmission isotherms at several temperatures the Van 't Hoff plot can be constructed and the corresponding thermodynamic parameters (ΔH, ΔS_o) of hydride formation and decomposition are derived.

A big advantage of *Hydrogenography* over the conventional methods is the possibility to measure a large number of chemical compositions simultaneously. This combinatorial high-throughput technique is capable of exploring the thermodynamic behavior of about 10^3 samples by using large area gradient films with controlled chemical composition (Fig. 1.6). These can be created by co-deposition of two, three or more metal constituents simultaneously with a spatially resolved gradient in the quantity of each component film that is deposited. Measurement of the PTI's over a wide temperature range allows for the parallel determination of the enthalpies and entropies of hydrogen (de)/absorption for all the compositions present in the deposited thin film. This enables the

investigation of full metal-hydrogen binary, ternary or quaternary systems and allows the identification of the most suitable compositional region and/or alloy for practical application in a matter of days. This has been successfully probed with the ternary Mg-Ni-Ti system, where a thermodynamically favorable composition of $Mg_{0.69}Ti_{0.05}Ni_{0.26}$ with an enthalpy of hydride formation of -40 kJ/mol H_2 was found [3].

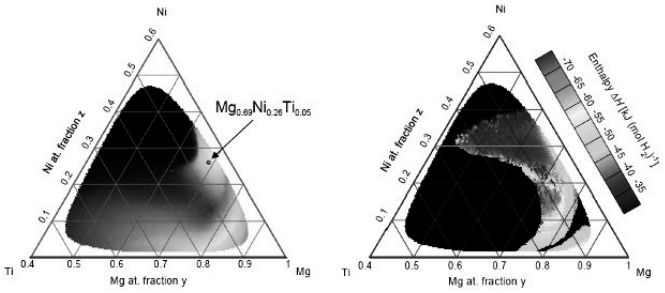

Fig. 1.6. Ternary composition diagram (left) showing the final optical transmission state and the enthalpy map (right) of the Mg-Ni-Ti system, estimated using the optically determined hydrogenation plateaus. Black region on the right-hand picture represents chemical compositions that do not have a well defined plateau on the PTI's.

1.5 Thin film substrate clamping and its effect on the thermodynamics

A critical issue in *Hydrogenography* is the impact of the substrate. The hydrogenation of metal hydrides is accompanied by a large volume expansion varying from 11% to as much as 32%. Bulk materials can expand in all three directions, while in general a rigid substrate does not allow for the free expansion of the film parallel to the surface during hydrogen uptake. Hydrogen causes the host metal lattice to expand, whereas adhesion forces act in the opposite direction, preventing thin film expansion in the basal plane (x-y direction). This clamping creates considerable in-plane compressive stresses that can be of the order of several GPa (Fig. 1.7). These stresses may influence the equilibrium plateau pressures of metal hydride films and, consequently, alter the thermodynamics of the system as compared to the corresponding bulk materials.

If the volumetric expansion on hydrogenation is prevented by stress this causes a shift of the equilibrium pressure plateau and a change of the thermodynamics of thin films

as compared to bulk materials. This is a direct consequence of the H-H interaction in the material. The nature of the hydrogen-hydrogen interaction is of elastic origin [5]. When hydrogen is dissolved into the metal, the host lattice expands. This creates a long-range strain field around the solute atom, making more favorable the absorption of next hydrogen. However, the sign of this interaction depends on the boundary conditions [6]. In thin films with an external boundary, represented by the substrate, the absorbed hydrogen actually compresses the lattice, changing the sign of the H-H interaction from attractive to repulsive. This means that the next hydrogen needs a higher energy or a higher chemical potential to dissolve into the metal and nucleate the β-phase, shifting the equilibrium plateau to a higher hydrogen pressures.

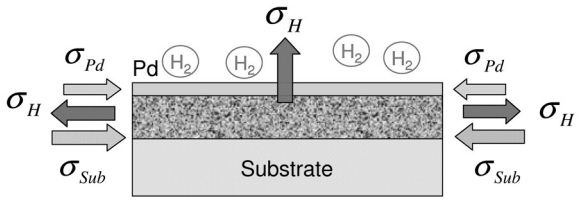

Fig. 1.7. Schematic representation of the substrate clamping effect during hydrogen absorption of the metal hydride thin film with a protective Pd layer. Red arrows represent tensile stresses in the film due to absorbed hydrogen, gray arrows represent compressive stresses due to the substrate and yellow arrows are due to compressive stresses coming from a Pd capping layer.

1.6 Hysteresis phenomena

Up to now, we only discussed hydrogen absorption. In an ideal case, the hydrogenation and dehydrogenation isotherm should follow the same path. This is not observed experimentally. In reality, there is a difference between absorption and desorption pressure plateaus, termed as hysteresis (Fig. 1.8).

There are two different explanations of the hysteresis phenomena, but both of them attribute hysteresis to stresses, arising in material during the phase transformation on (de-)hydrogenation. Hysteresis are related to *elastic* or/and *plastic* deformations.

In the first case, *plastic* deformations are not considered at all and the material behaves purely as an elastic body. When hydrogen incorporates in the metal lattice, it creates strain and consequently, stress, when it is below the Yield stress of the material. Hydrogen absorption, therefore, is characterized by the elastic strain energy. Based on the elastic strain energy effects, associated with the occupancy of hydrogen atoms in the lattice,

Sinha et al. [7, 8] developed a model to explain the difference between measured absorption and desorption equilibrium pressures. According to them, during absorption the hydrogen atoms occupy smaller (than the hydrogen atoms) interstitial sites. Thus, there is a strain energy barrier to overcome, resulting in a higher absorption equilibrium pressure. Since there is no strain energy barrier to be overcome during the desorption, i.e. no extra energy should be applied to take out the hydrogen atoms from the interstitial position, the dehydrogenation reaction occurs at a lower desorption pressure as compared to absorption.

A somewhat different approach was introduced by Schwarz and Khachaturyan [9]. They consider (de-)hydrogenation process not in terms of individual hydrogen atoms, but in terms of metal (α–phase) and hydride (β–phase) phases in a material. The formation of the expanded β-phase occurs under the compressive forces of the α–phase during hydrogenation, leading to the so-called coherency stresses. The opposite situation takes place during desorption, where nucleation of α–phase happens under a tensile stresses of the β-phase matrix. Therefore, during hydrogen adsorption more energy should be supplied to expand the metal lattice during absorption; the dehydrogenation benefits from the expanded lattice and therefore takes place at higher pressures. The model quantitatively predicts the hysteresis in a coherent MH (metal hydride) in which an iso-structural transformation takes place on hydrogenation (such is the case in Pd-H). The hysteresis depends on the mechanical properties of the metal hydride (Shear modulus, G_s and Poisson's ratio, ν), lattice expansion (ε_o), width of the a-b plateau ($c_\beta - c_\alpha$) and temperature:

$$\ln\left(\frac{P_{abs}}{P_{des}}\right) = \frac{8\upsilon_o G_s \frac{(1-\nu)}{(1+\nu)} \varepsilon_o^2 (c_\beta - c_\alpha)}{kT} \tag{1.2}$$

Both elastic theories predict that the real equilibrium pressure plateau is in-between absorption and desorption (Fig. 1.8). Another consequence of these theories is that there is no way to prevent the hysteresis in the coexistence region.

Now let us discuss the possible role of plastic deformations in the occurrence of the hysteresis.

Initially, a material deforms elastically, but, as the stresses become higher than the yield stress, the material deforms plastically. This involves formation of dislocations during hydrogen formation and decomposition. Elastic deformations represent a reversible process, whereas plastic deformations are irreversible changes (work) in the material which lead, according to Flanagan et al. [9], to a shift of the plateaus to higher and lower pressures, respectively. The overall hysteresis, which is directly proportional to the total irreversible

work, is then equal to the energy involved in formation and movement of dislocations accompanying hydride formation and decomposition.

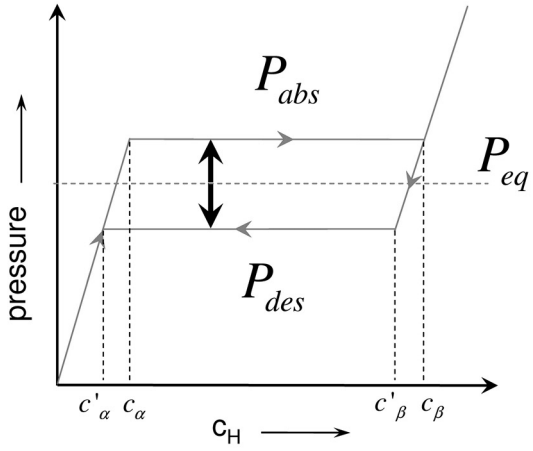

Fig. 1.8. Typical absorption and desorption isotherm of a metal hydride. The difference between the upper and the lower branch, shown by the black arrow, is called hysteresis. P_{eq} is the hypothetical equilibrium plateau, $c_{\alpha,\beta}$ and $c'_{\alpha,\beta}$ are the boundaries of the α- and β-phase during hydrogen loading and unloading, respectively.

Alternatively, the hysteresis, which is associated with a loss of energy, can be expressed as a change of the Gibbs free energy, i.e. ΔG. Birnbaun et al. [11] assumed that the change of the free energy during hydride formation, ΔG_{abs}, originates from different contributions:

$$\Delta G_{abs} = \Delta G_{abs}^{chem} + \Delta G_{abs}^{el} + \Delta G_{abs}^{pl} + \Delta G_{abs}^{surf} \tag{1.3}$$

where the first term corresponds to the free energy change on forming the unconstrained hydride (β) phase from the metal (α) phase, where ΔG_{abs}^{el} and ΔG_{abs}^{pl} are the free energies associated with the elastic and plastic deformation due to the volume increase on forming the β phase, and ΔG_{abs}^{surf} is a surface free energy term. Similarly, the change of the Gibbs free energy during hydride decomposition, ΔG_{des}, is:

$$\Delta G_{des} = \Delta G_{des}^{chem} + \Delta G_{des}^{el} + \Delta G_{des}^{pl} + \Delta G_{des}^{surf} \tag{1.4}$$

They argued that the chemical terms (ΔG^{chem}), elastic accommodation terms (ΔG^{el}) and the surface free energy change (ΔG_{abs}^{surf}) have the same value upon α to β and β to α

transformations. The overall change of the Gibbs free energy then reflects the total amount of plastic accommodation work done during absorption and desorption of hydrogen since the other terms ($\Delta G^{chem}, \Delta G^{el}, \Delta G_{abs}^{surf}$) will be removed from the equation by reversion:

$$\Delta G = \Delta G_{abs} - \Delta G_{des} = \Delta G_{abs}^{pl} - \Delta G_{des}^{pl} \quad (1.5)$$

Thus, their model suggests that the appearance of the hysteresis is caused only by the plastic deformations.

A lot of work has been done to get insight of the hysteresis phenomenon in metal hydrides. Still, in spite of the presence of several theories and qualitative models, there is no general theory able to answer the question: "*Why there is a difference between hydride formation and hydride decomposition plateaus?*" and which could be applied to various metal hydrides systems, interstitial or complex ones.

1.7 This Thesis

In this thesis we investigate whether thin films provide reliable data on the thermodynamics of bulk metal hydrides for hydrogen storage.

Various experimental approaches of how thermodynamic properties of films and bulk materials can be measured are given in ***Chapter 2***, where the basic working principles of the Sievert's and Hydrogenography method to study the thermodynamics of the hydrogen formation and hydrogen decomposition reactions are presented.

To validate our thin film approach, in ***Chapter 3*** we study the (de-)hydrogenation behavior of Pd films with and without substrate by means of *Hydrogenography* and the Sievert's technique, respectively. Additionally, we verify the influence of the crystallinity, chemical nature and surface roughness of the substrate on the thermodynamic properties of thin film metal hydrides as compared to bulk materials. We deposit Pd films on glass, quartz and sapphire substrates and compare the Pressure-Transmission-Isotherms (PTI's) in a wide temperature range. Because of the weak adhesion of the Pd films, in the course of the cycling procedure the films start to delaminate (buckle) from the substrate and after an appropriate number of hydrogenation cycles the plateau pressure becomes identical for all substrates. We find almost no difference in the thermodynamics properties or critical temperature between Pd films on different substrates and also compared to the free-standing Pd films, as studied by means of both, *Hydrogenography* and the Sievert's technique. We conclude that buckling is a very effective method to release the stress. The similarity between the *Hydrogenography* results on buckled films and the Sievert's result on free-standing films proves that hydrogenography is comparable to conventional

methods. It has, however, the great advantage to provide a mean to measure a large number samples under exactly the same experimental conditions.

While delaminated films exhibit thermodynamic properties essentially equal to that of bulk materials, metal hydride thin films in general show a strong interaction with the substrate and, in this case, some influence on the thermodynamic properties is expected. In ***chapter 4*** we model the situation of non-buckled films. We again use Pd, but add Ti as an intermediate sticking layer to increase the interaction with the substrate. *Hydrogenography* measurements indeed reveal a change of the thermodynamic properties: the enthalpy of hydride formation and decomposition decreases and increases by about 2.7 and 1.3 kJ/mol H_2 respectively, as compared to buckled Pd films. The change in thermodynamics comes from a different stress relaxation mechanism in the clamped Pd films during the (de-)hydrogenation cycle involving much more plastic deformation. Based on a stress and strain analysis of the films during a hydrogenation cycle, we develop a simple model which is able to explain the thermodynamic behavior and quantitatively predict the hysteresis change in the Pd/Ti samples.

The developed stress-strain model allows to understand both qualitatively and quantitatively the influence of the substrate on the thermodynamics and hysteresis behavior of thin films with an iso-structural transformation, as in the case of Pd. However, structural transformations accompany the phase transition from the metallic to hydride phase in many metal hydride systems, including MgH_2 and Mg_2NiH_4, which are of particular interest for this thesis. In addition, on volume expansion is relatively small (11%) and its mechanical properties barely change on going from metal to hydride state, which is not the case for the Mg-based materials. In ***Chapter 5*** we focus our attention on $La_{1-z}Y_z$ thin films, where the amount of volume change and the presence of a structure transformation vary with the Y concentration. By investigating their structural properties, (de-)hydrogenation behavior and hysteresis we estimate the effect of the structural transformations on the thermodynamic properties of metal hydride thin films. We find an enormous increase in the hysteresis when the hydrogenation is accompanied by a structure transformation. We suggest that this is due to the fact that the film has to switch between two preferential orientations of different symmetry.

In the last chapter an attempt will be made to destabilize magnesium hydride, a promising high gravimetric density hydrogen storage material. However, beforehand, a careful investigation of MgH_2 thin films was conducted to investigate the effects connected with the clamping phenomenon in this system. In ***Chapter 6*** we measure pressure-transmission isotherms of MgH_2 films in a wide temperature range (313 K – 533 K) and deduce the enthalpy and entropy of hydrogen (de-)absorption. We find that the stress-strain model can be successfully applied to qualitatively explain hysteresis behavior in MgH_2

films. While there is a structure transformation involved, albeit without any signs of a preferential orientation, we do not observe an additional component in the hysteresis, which can be fully explained on the basis of the plastic deformation due to the volumetric change.

Mg_2NiH_4 belongs to a completely different class of hydrogen storage materials – complex hydrides. The formation of the Mg_2NiH_4 phase involves the reaction between various solid phases and the transition to totally different crystal systems. In ***Chapter 7*** we study (de-)hydrogenation behavior of complex Mg_2NiH_4 hydride thin films, which act as a model system for other complex hydrides, such as, for instance, alanates. Our stress-strain analysis, applied to qualitatively predict a very large difference between absorption and desorption branches of the isotherm in Mg_2NiH_4 films, is able to explain the hysteresis increase in Mg_2NiH_4 thin films as compared to bulk when the energy of the monoclinic-hcp structure transformation is taking into account. Again the metal and hydride phase have different symmetries and retain their preferential orientation on cycling (similar to the case of YH_x). With the proper ΔG_{str} term, the stress-strain model, initially developed to quantitatively describe the difference between the hysteresis behavior in buckled and clamped Pd films, can be also used to predict the clamping effect in complex hydride thin films, provided that this term can be independently measured by calorimetry or calculated using first principles.

Concluding, the Hydrogenography results should be properly analyzed before drawing conclusions on the corresponding bulk materials. Important is to verify whether the film remains clamped to the substrate or has a tendency to delaminate. Second, one needs to be aware of an expanded hysteresis, especially when one cycles between preferentially oriented crystalline metal and metal hydride states.

With the knowledge gained we then turn to investigate the Mg-Ti-Al system by means of *Hydrogenogprahy* (***Chapter 8***). In order to estimate the bulk enthalpies of hydrogen formation, the *Hydrogeography* results of Mg-Ti-Al films should first be corrected for the influence of the substrate. According to the *Hydrogenography* data on $Mg_{0.8}Ti_{0.2}$, the clamping effect lowers (make it more negative) the enthalpy of hydrogenation by about 13 kJ/mol H_2, as compared to MgH_2 bulk The experimentally obtained enthalpies of hydride formation were found as low as -53 kJ/mol H_2, even taking into account the substrate effect, confirming that indeed we have a destabilization effect in the Mg-Ti-Al-H. However, in contrast to computational predictions, equilibrium pressures did not change substantially as compared to Mg-Ti due a phenomenon known as the enthalpy-entropy compensation.

1.8 References

[1] A. Züttel, A. Borgschulte, L. Schlapbach (Eds.), Hydrogen as a Future Energy Carrier, Wiley-VCH Verlag GmbH & Co. KGaA, Weinheim, 2008, pp. 275-334.

[2] A. Baldi, D.M. Borsa, H. Schreuders, J.H. Rector, T. Atmakidis, M. Bakker, H.A. Zondag, W.G.J. van Helden, B. Dam R. Griessen, Mg-Ti-H films as switchable solar absorbers, Int. J. Hydrogen Energy 33 (2008) 3188.

[3] R. Gremaud, C. Broedersz, D. Brosa, A. Borgschulte, P. Mauron, H. Schreuders, B. Dam and R. Griessen, Hydrogenography: an optical combinatorial method to find new light-weigth hydrogen storage materials, Adv. Mater. 19 (2007) 2813.

[4] A. Baldi, M. Gonzalez-Silveira, V. Palmisano, B. Dam, and R. Griessen, Destabilization of the Mg-H System through Elastic Constraints, Phys. Rev. Lett. 102 (2009) 226102.

[5] G. Alefeld, Phase transitions of hydrogen in metals due to elastic interaction, Ber.Bunsenges. Phys. Chem. 76 (1972) 746.

[6] H. Zabel and H. Peisl, Sample-Shape-Dependent Phase Transition of Hydrogen in Niobium, Phys. Lett. 42 (1979) 511.

[7] V.K. Sinha and W.E. Wallace, Strain-energy model for solid-solution limits in Zr+H system, J. Less-Common Metals 91 (1983) 239.

[8] A.Y. Esayed and D.O. Northwood, Hysteresis in $(Nb_{1-x}Fe_x)_{1-y}Cr_y$-H systems: Effect of composition, temperature and cycling, Int. J. Hydrogen Energy 18(4) (1993) 301.

[9] R.B. Schwartz, A.G. Khachaturyan, Thermodynamics of open two-phase systems with coherent interfaces: Application to metal-hydrogen systems, Acta Mater. 54(2006) 313.

[10] T.B. Flanagan and J.D. Clewley, Hysteresis in metal hydrides, J. Less-Common Metals 83 (1982) 127.

[11] H.K. Birnbaum, M.L. Grossbeck and M. Amano, Hydride precipitation in Nb and some properties of NbH, J. Less-Common Metals 49 (1976) 357.

Chapter 2

2.1 Introduction

Chapter 2 will give a brief introduction to the basic working concepts of two techniques, Volumetry and Hydrogenography, their similarities and inequalities. The Volumetric (Sieverts) method is one of the two primary methods for the determination of equilibrium sorption and desorption isotherms in bulk materials. Hydrogenography is an attractive technique having as a goal the investigation of the thermodynamic properties of hydrogen storage materials using a thin film optical approach.

The following chapter will be published in: K. Gross (Ed.), *Recommended Best Practices for the Characterization of Storage Properties of Hydrogen Storage Materials.*

2.2 Sieverts method

Volumetry, also known as the Manometric or Sieverts method is used to characterize hydrogen sorption and desorption properties of a material at thermodynamic equilibrium and the kinetic evolution of the reaction. The equilibrium measurements, which are the main focus of this chapter, are based on a stepwise hydrogen uptake/release by the material recorded in Pressure-Concentration-Isotherms (PCI). The hydrogen sorption is measured by monitoring the drop in hydrogen pressure in a bulk sample place in a system with a fixed, known volume, with desorption being monitored by an increase in pressure.

We distinguish the absorption (chemisorption) and adsorption (physisorption) of hydrogen. The former indicates that hydrogen atoms are chemically bound to the interior (bulk) of the material, whereas the latter denotes a physical bonding between hydrogen molecules and the materials' surface. The physisorption interaction, described by relatively week van der Waals forces is explored in porous hydrogen storage materials like ZIFs or MOFs (explain acronyms), which are mostly active at low temperatures, i.e. 77 K – 293 K. This type of interaction is not relevant for the purposes of this thesis, which is focused on interstitial and complex metal hydrides and, therefore, only the chemisorption of hydrogen will be considered in the following.

A simplified version of our Volumetric setup (PCTPro-2000, Fig. 2.1) is schematically shown in Fig. 2.2. The major parts are the sample reservoir, where the hydrogen absorbing media is placed, the reference reservoir and a valve S between them (Fig. 2.2). There is a gas line used to supply hydrogen and a pump line, used to evacuate/clean the reference/sample reservoir. The pressure transducer, P measures hydrogen pressure in the system, P_{sys} when the valve S is open and measure the reservoir pressure, P_{ref} when the valve S is closed.

When a dose (aliquot) of hydrogen is provided via the valve in the gas line, a certain pressure, P_{ref} sets in the reference volume. The connecting valve, S, is closed to isolate the sample reservoir, which has a cell pressure, P_{cell} (in the case this is not the first step, otherwise $P_{cell}=0$) and an empty volume V_{cell}, where V_{cell} is a difference between the sample volume reservoir, V_{sample} and the volume of hydrogen storage material, V_{mat}=(m)mass/ρ(density). When S opens, a new value of P_{sys} is established. The number of moles of hydrogen atoms absorbed by the sample can then be calculated from the change in pressure measured when S is opened.

Fig. 2.1. PCTPro-2000 Sieverts apparatus (Hy-Energy LLC) with MicroDoser attachment and the sample holder.

Assuming an ideal gas behavior and equality of temperatures of the hydrogen gas in the reference (T_{ref}) and sample (T_{cell}) reservoirs, the quantity of gas absorbed by the sample during an aliquot (step) is equal to:

$$\Delta n_{H_2} = \frac{P_{sys}(V_{ref} + V_{cell})}{RT} - \frac{P_{ref}V_{ref} + P_{cell}V_{cell}}{RT} \tag{2.1}$$

As the hydrogen loading process is composed of a number of steps, k, expressed by eq. (2.1), the total quantity of hydrogen absorbed by the sample in N-steps are given:

$$n_H = \sum_{k=1}^{N} \Delta n_H^k \tag{2.2}$$

Although eq. (2.1) gives a clear picture of the working principal of the Sieverts technique, it is oversimplified. It does note take into account the change of density of the material during the hydrogen uptake and the difference between T_{ref} and T_{cell}. Besides that, due to a non-ideal gas behavior the compressibility of the gas should be taken into account during the sorption/desorption measurements at high pressures. However, all of the above mentioned effects are implemented in the software (HyData) of the PCTPro-2000 setup and automatically corrected, providing an accurate analysis of the results.

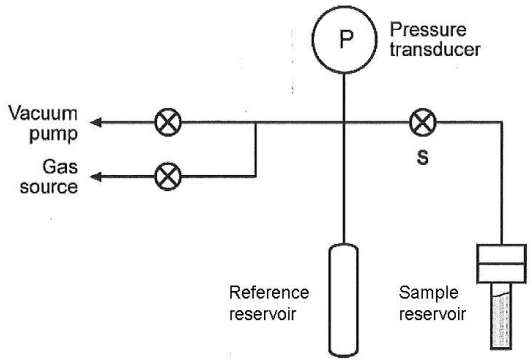

Fig. 2.2. Simplified representation of Sieverts apparatus for determining the uptake of hydrogen gas atoms or molecules by the samples.

The main control panel of the HyData software, which controls the PCTPro instrument, performs experimental measurements, data collections, and system processes is presented in Fig. 2.3.

It can be noticed that the layout of the setup is much more complicated as compared to Fig. 2.2. There are 11 air-operated valves (circular buttons), which are totally controlled by the software and which are used to separate different compartments of the setup. Valve 1 is the main valve that delivers aliquots of gas to and from the sample (analogue of the S valve in Fig. 2.2). There are several choices of the sample holder (reservoir), depending on the amount of the material available. The Autoclave (see Fig. 2.3) is used for samples in the gram/kilogram range, whereas the MicroDoser attachment provides the possibility to analyze samples of tens of milligrams; the minimum weigh that MicroDoser is able to measure is 10 mg.

Sample holders are specially designed to transfer samples without air contact from an inert atmosphere glove box to the instrument. They are developed for ease of handling, cleaning, loading and closing in a glove box environment. Autoclave and MicroDoser attachments include thermocouples, which measure temperature of the sample, while the gas handling enclosure maintains a constant gas temperature (±1 K). The maximum temperature for both sample holders is 673 K.

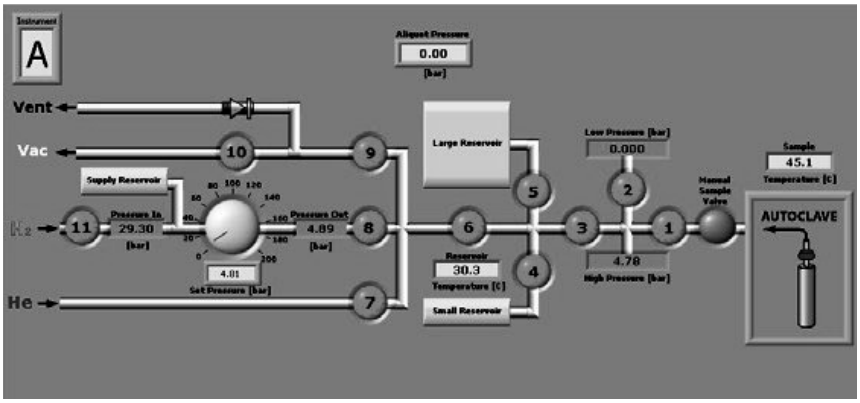

Fig. 2.3. Master control panel of the HyData software of the PCTPro-2000 Sieverts setup. Circular buttons are the air-operated automatic valves. He and H_2 denote helium and hydrogen gas supply line, used for cell volume calibration and sorption measurements, respectively. The setup is equipped with a roughening pump (Vac) for evacuation of the sample/reservoir volume and cleaning of the lines. There is a ventilation line (Vent), which takes all the excess pressure from the system that the vacuum pump cannot handle.

There are two pressure transducers, namely a low pressure and a high pressure. The latter one, which is the main measurement transducer, allows to measure pressure in the range from 0.5 to 200 bars; 200 bars is the highest achievable hydrogen pressure for Autoclave, while the maximum allowed pressure with the MicroDoser sample holder is only 30 bars. The low pressure transducer is used for making gas sorption measurement in the low-pressure regime, generally 0.01 to 5 bars. Depending on the experimental pressures used during the measurement, only one of the pressure transducers is working.

The combination of two pressure transducers in PCTPro-2000 allows to have pressure readings in a wide pressure range, i.e. 0.01-200 bars H_2, which is very advantageous for the analysis of hydrogen storage materials. However, it is still impossible to investigate (de-)/hydrogenation of samples with equilibrium pressures in the millibar range at near room temperatures. This problem can be easily overcome by increasing the temperature and, accordingly, shifting the equilibrium plateaus upwards. For certain materials, like Mg nanoparticles, an increase of temperature is highly undesirable because of a pronounced particle growth and/or evaporation at elevated temperatures, implying the necessity of a different measuring technique to study the influence of the grain size (size effect) on the thermodynamic properties.

The ability to measure Pressure-Concentration-Isotherms of samples of various sizes and weights is ensured by a number of small and large reservoirs. The PCTPro-2000

instrument actually includes 5 built-in and calibrated reservoir volumes (approximate ranges 3, 20, 150, 1000, and 1150 ccm). The choice of an appropriate one depends on cell volume, V_{cell} and the amount of experimental points (aliquots) you want to record during sorption or desorption measurement. Some knowledge of the sample's equilibrium plateau, pressure and capacity is helpful in determining the appropriate aliquot size (reservoir volume) and applied pressure (reservoir pressure). For PCI measurements, the reservoir volume and a gas pressure is selected in a way that it produces an aliquot containing a fraction of the total potential gas that can be absorbed or desorbed by the sample. This determines the number of data points measured on the PCI plot. For example: an aliquot of 1/10th, the total sample concentration should give about 10 data points along the PCI. A number of aliquot of about 15-50 may be sufficient for a good PCI curve.

The accuracy of the volumetric measurement strongly depends on several factors, like cell volume calibration, sample quantity and its weighing.

The calibration of cell volume is a crucial step for obtaining good and reliable results in the sorption and desorption measurements. The calibration procedure involves filling/evacuating of the sample holder with an inert gas (helium in this case) and measuring sample volume in the absorbed and desorbed state. An inert gas is chosen so as to have no absorption by the material and, therefore, have no influence on the sample volume; this, however, only works if the sample does not significantly adsorb helium at the temperature being measured. Although the process is fully automated, accuracy of cell volume calibration depends on the amount of cycles and time per each cycle. To obtain the best results it is necessary to do at least 10 consecutive loading and unloading with helium with sufficiently long time (usually a few hours). However, the process time, which largely depends on settings, might take from tens of minutes to tens of hours. Due to volume expansion of the sample on heating, which can affect the total empty volume of the sample holder, V_{cell}, the calibration procedure should be performed at each temperature before the equilibrium experiment.

The effect of the sample quantity on the result is not straightforward. Small amounts of sample give less of an error on cell volume, V_{cell} determination, but pressure changes due to sorption are consequently smaller, leading to larger errors in the final result. Larger quantities of sample give more accurate and reliable reading on the pressure change, but introduce more error on the dead volume determination. Since the higher accuracy in the pressure measurement is significantly more important than the cell volume measurement (using helium gas), larger amounts of sample are almost always preferred.

Precise knowledge of the sample amount is another critical parameter along with the sample quantity in the volumetric experiments. The sample mass is used to determine the gas concentration in units of weight %, H/M, H/formula unit, or standard cubic centimeters

per gram of sample. The higher the degree of accuracy of sample quantity (and thereby also of sample purity), the more accurate the hydrogen concentration will be estimated. Therefore, it is very important to pack the same amount of sample into the sample holder after the sample weighing.

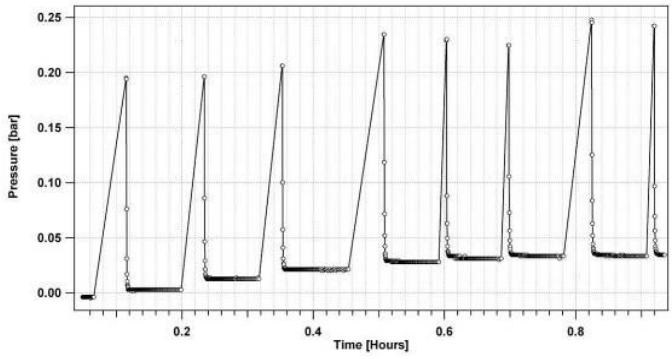

Fig. 2.4. Pressure vs. time data in the beginning of the plateau region of the absorption PCI measurement of the free-standing Pd film at 311 K.

The volumetric measurement technique is advantageous for measuring pressure-concentration isotherms and, consequently, for Van 't Hoff analyses. This method is very accurate in identifying plateau pressures at exact hydrogen concentrations. At those concentrations the pressure time profile can be observed to ensure that the reaction has reached equilibrium. In fact, for materials with poor kinetics, it may be possible to use the pressure / time profile to extrapolate to a theoretical plateau pressure without waiting an unreasonable amount of time (more than a few days) to reach equilibrium for each gas dose. The issue, however, is that even for materials with relatively good absorption and desorption kinetics (e.g. $LaNi_5$ in the example), collecting a series of PCT measurements may take from several days to weeks. Even worse, materials with moderate to poor kinetics may take many weeks to months to perform a proper series of equilibrium thermodynamic PCT measurement.

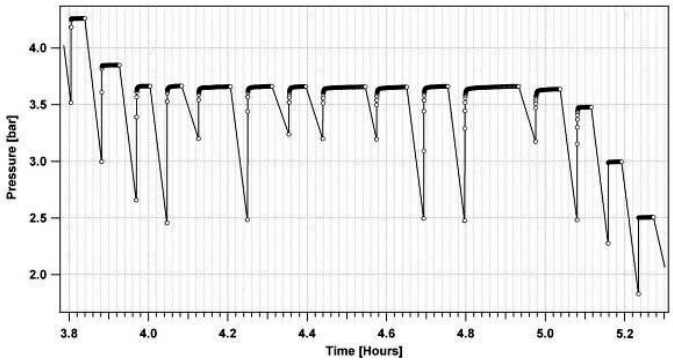

Fig. 2.5. Pressure vs. time data for the plateau region of the desorption PCI measurement of the free-standing Pd film at 473 K.

In order to reduce the experimental time during the PCI measurement, an equilibrium test function was implemented in the software of the PCTPro-2000 setup. The equilibrium test function is an efficient data collection operation, which checks whether equilibrium has been achieved. This function requires the instrument to stay within a given dose until sufficient time has passed and a test of equilibrium conditions has been met. The test criteria for the equilibrium condition is rate-limit, which is an average change in the rate of absorption or desorption over the last ten readings. When the rate limit falls below a selected value, the software allows the instrument to automatically move on to the next aliquot, which maximizes the efficient use of the instrument. Rather than waiting a fixed amount of time between aliquots (which may be significantly longer than the time it takes to reach equilibrium) the routine will cut the aliquot short when equilibrium is achieved.

Fig. 2.4 and 2.5 show the pressure time data for a segment of dosing collected in the beginning of the absorption PCI at 311 K and similar pressure vs. time data across the plateau region of the desorption PCT at 473. The data demonstrates that the absorption and desorption at each dose has reached a sufficiently steady pressure. This means that the sample's hydride phase can be considered to be in equilibrium with the gas phase at the final pressure reading of each dose (equilibrium pressure). It is this final pressure reading of each aliquot that corresponds to the pressure point in the corresponding PCI plot at the measured hydrogen concentration.

2.3 Hydrogenography

Hydrogenography, which is an alternative technique to Sieverts method, is used to measure absorption and desorption properties of hydrogen storage materials, by exploiting the change in optical properties of metal hydride thin films. The hydrogen absorption and desorption is monitored by measuring the optical transmission of the films while cycling the hydrogen pressure. Equilibrium measurements are recorded in so-called Pressure-Transmission-isotherms (Fig. 1.5).

A *Hydrogenography* setup is represented schematically in Fig. 2.7. The main component is the (de)/hydrogenation gas cell, where the samples are placed. The whole cell is located in an oven with a temperature controller. The maximum temperature that cell components including transparent sapphire windows can withstand is limited to 573 K, which restricts the operating temperature range to 293 K - 573 K. The complete thermal equilibration of the setup is verified by comparing the output of two PT-100 resistors placed at different locations in the oven, one of them being in contact with the sample holder. A 150 W diffuse white light source (the projector) illuminates the sample from the substrate side, and a 3-channel (RGB) SONY XC-003 Charged-Coupled Device (CCD) camera continuously monitors the transmitted light as a function of hydrogen pressure. To avoid any disturbance from a stray light entering the setup, a blanket is used to cover the camera and vacuum cell. The 3-channel transmission intensities are added together, resulting in a 1.1 to 3.3 eV photon energy bandwidth. The use of a camera allows for the recording of the transmission for all compositions simultaneously.

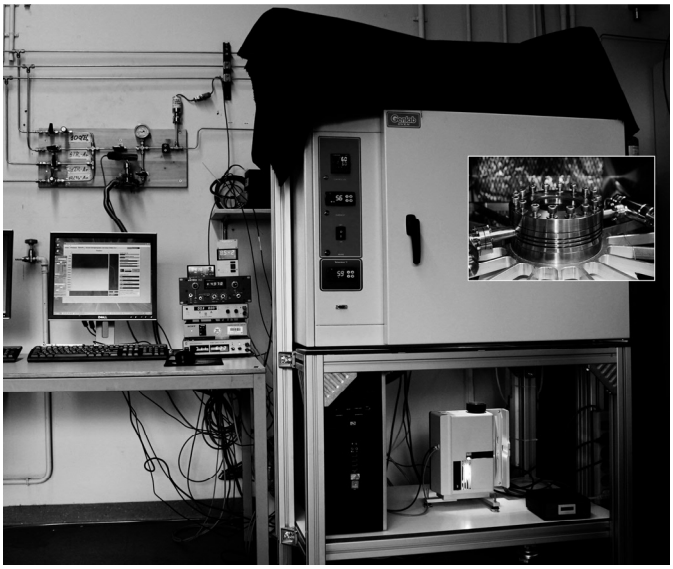

Fig. 2.6. Hydrogenography setup. The inset shows an enlarged picture of the hydrogenation cell placed in the oven and used in the hydrogenography experiments.

Unlike the standard Sieverts setup, where the pressure-composition-isotherms are determined on a discrete or nearly static basis, i.e. aliquot by aliquot, *Hydrogenography* operates in a dynamic mode, meaning that a certain constant flow rate of a gas through the hydrogenation cell is maintained during the absorption and desorption reactions. The gas pressure in the cell is controlled by the inlet and the outlet electronic valves and a flow meter. The amount of gas entering the cell is regulated by the a forward Proportional-Integral-Differential (PID) system that controls the opening of the input valve depending on the desired pressure and the reading of the actual pressure by the baratron pressure gauge. The type of the electronic valve allows a pressure ramp up from vacuum to a maximum of 10 bar H_2, which is the maximum pressure that a typical single crystal sapphire windows of the gas cell with a UHV compatible metal-glass seal can withstand.

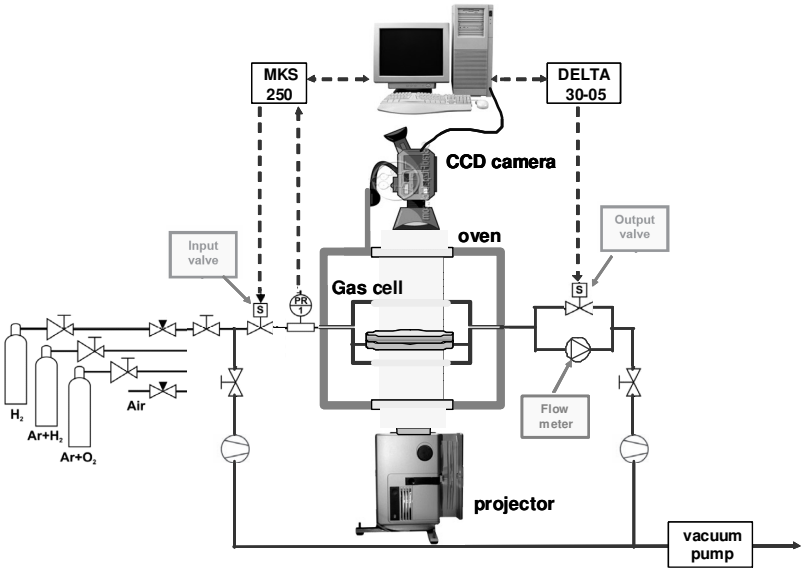

Fig. 2.8. Schematic representation of the Hydrogenography setup.

The output valve and the flow meter control the pumping speed at the output of the cell to have a constant gas flow of 20 sccm. The opening of the output valve is regulated by the PC via a Delta 0-30 volt power supply. The flow meter, connected in parallel to the valve is used to set the gas flow. When the pressure in the cell is below 150 mbar, the pressure difference is insufficient to maintain a constant flow of 20 sccm and the pumping rate is controlled by the electronic valve only. At higher pressures the output valve becomes essentially closed and the outlet flow from the cell to the vacuum pump is controlled solely through the flow meter.

A selection of bottles with $Ar+H_2$ mixtures and pure H_2, connected to the inlet of the gas cell allows one to measure the hydrogenation behavior of the metal hydride samples over a wide pressure range between 10^{-6} bar and 10 bar. For desorption, a flow of an $Ar+O_2$ mixture or air is used to enhance the dehydrogenation of metal hydrides of metal hydrides with slow kinetic, such as Mg. Otherwise, unloading experiments are performed in vacuum.

As *Hydrogenography* is an optical technique, there are several requirements for the samples. First of all, thin films should be deposited on a transparent substrate, usually glass, sapphire or quartz to have no influence on the measured signal. Typically, sample sizes used in *Hydrogenography* experiments range up to 3 inch diameter wafers. It is basically

determined by the sample holder of the deposition system and the diameter of the sapphire windows of the gas cell.

Secondly, samples should have a measureable optical transmission in the as-deposited state, meaning that an initial optical transmission, T_o should be higher than the dark signal (signal with no illumination). To satisfy this demand the thickness of thin films is restricted to 50-100 nm.

Another important point is the optical contrast, i.e. the difference between optical transmission in the metallic and hydrided state. *Hydrogenography* is capable of monitoring the change in the optical transmission to the order of 0.5%-1% for the above mentioned thicknesses, which makes it possible to measure thin films remaining in the metallic state on hydrogenation such as Pd. For other materials, such as Mg, Y or Gd the optical contrast is not an issue as they experience a metal-to-semiconductor transition on hydrogen loading and their optical transmission changes substantially. In this case, however, the maximum optical transmission might be a problem as it can exceed the saturation level of the camera. To prevent the saturation a light filter should be used to decrease the light intensity.

As most metal hydrides are highly oxidizing materials, all films are covered with thin layer of Pd (10-20 nm) to protect them against oxidation. Additionally, this Pd layer serves as a catalyst for the dissociation of the H_2 molecule to atoms.

After deposition, fresh samples are either stored in a glove box to prevent any possible contamination or directly transferred to the *Hydrogenography* setup, where the optical transmission is measured as a function of time, hydrogen pressure, or temperature.

Before a real equilibrium measurement can be done, the thin films need to be cycled. Cycling is a common procedure for many metal hydride systems and consists of a few relatively fast loading/unloading cycles. This is needed to (i) stabilize the system behavior by the release of stress and modification of the microstructure. It is also important, (ii) to optimize the signal to noise ratio of the light source and the camera with respect to the thickness (50-120 nm) and the type of the sample (with or without a metal-to-semiconductor transition). The amount of cycles necessary to achieve a reproducible behavior strictly depends on the type of film, i.e. its interaction with the substrate and the stability of the film. The number of cycles needed does not usually exceed 20 cycles. Optimization of the optical signal is needed to ensure that the optical transmissions of a film in the metallic state is higher than the limit of detection and lower than the saturation limit of the camera. If a too large optical change occurs, a gray filter is used to prevent the saturation of the CCD camera signal.

After the cycling procedure, the equilibrium properties are measured. There are two possible ways to record the pressure-transmission-isotherms, namely with a pressure-stepping mode or by continuous pressure ramping. A stepwise mode of pressure change is

needed to check the kinetics of a hydride formation or desorption. This is done by measuring the optical signal ($\ln(T/T_M)$) as a function of time with each pressure step to ensure that equilibrium is reached within the fixed dosing time (Fig. 2.9). If equilibrium is not reached within the time limit of each separate step, the time to reach can be extrapolated for the entire measurement and a new PTI can be recorded for the second time with a more gradual increase or decrease of the hydrogen pressure. Thus the step scan measurement is generally used to determine the time constant needed to obtain a quasi-equilibrium measurement.

During *Hydrogenography* experiments, additional attention should be paid to the kinetics of the (de)/hydrogenation reactions of the clamped metal hydride films. High stresses in these films might cause the kinetics to slow down, which will result in a sloping behavior of the pressure-transmission-isotherms. Therefore, it is very important to measure first the loading/unloading cycle (after the activation procedure) in a step scan mode to insure that equilibrium has been achieved between hydrogen in metal and in gas phase. With this, the time needed for the real equilibrium scan can be determined.

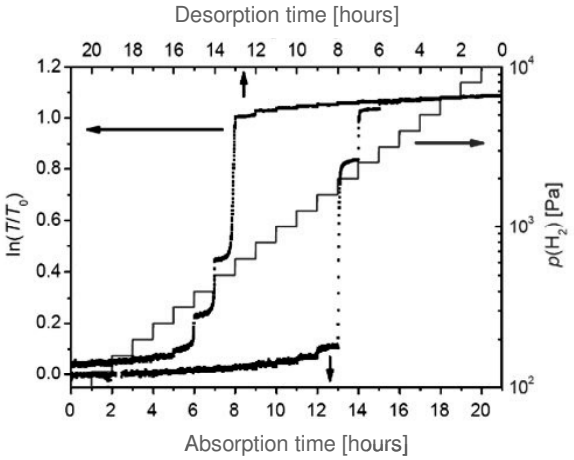

Fig. 2.9. Transmission measurements (black line) of a 65 nm PdH_x thin film as a function of hydrogen pressure during absorption and desorption step scans at 294 K after cycling. Each pressure step (blue line) is maintained one hour to ensure relaxation of the film and equilibrium with the hydrogen environment. The transmission T is normalized by the transmission in the as-deposited metallic state T_M.

Alloying process between Pd-cap layer and a metal hydride film is another difficulty which can affect *Hydrogenography* experiment and the data analysis. An inter-alloying process can change the chemical composition and the stability of the measured film; the experimental results, obtained in this kind of systems will not reflect the thermodynamic properties of the corresponding bulk materials. Alloying can also lead to the formation of a blocking layer, which is not permeable for hydrogen and result in a negligible hydrogen absorption by the sample. For this reason, to insure stability of the film, it is necessary to measure and compare several loading/unloading cycles.

No substantial alloying is expected during *Hydrogenography* experiments below 363 K. However, as the diffusion of metal atoms is a temperature limited process, *Hydrogenography* experiments at elevated temperatures (>363 K) need to be conducted with an additional interlayer between Pd and the film to prevent inter-alloying from occurring. This interlayer should be chemically stable within the measurement temperature range.

Chapter 3

Validation of the Hydrogenography technique using Pd films as a model system

3.1 Introduction

The presence of the substrate is the main 'limiting factor' of the Hydrogenography technique. A transparent substrate acts as a support for thin metal films. Along with this, it prevents thin films to expand freely during hydrogen loading, i.e. films become clamped in the x and y direction. Clamping leads to compressive in-plane stresses of the order of several GPa acting on the film during hydrogenation. This will have some impact on the enthalpy and entropy of hydrogenation as compared to bulk materials.

In this chapter we measure pressure-transmission- and pressure-concentration-isotherms of the Pd films with and without a substrate using Hydrogenography and Sievert's techniques in a wide temperature range and evaluate their thermodynamic properties. In this chapter we show that the influence of clamping on the thermodynamic properties depends strongly on the adhesion forces between film and the substrate and, consequently, on the stress relaxation mechanism. For a weak film-substrate interaction, as in the case of Pd films, the in-plane compressive stresses can be released by means of buckling and partial delamination of the film. Loosely bound to the substrate, these films behave such as elastic bodies with a minor part of plastic deformations. They possess the same desorption behavior as found for Pd bulk [12] and a hysteresis, close to a theoretical prediction made by the elastic theory [21].

The number of cycles needed to achieve a full release of the stress mainly depends on the chemical nature of the substrate, i.e. sapphire, quartz, glass. However, after this activation process, Pd films on various substrates show almost no difference in the

thermodynamics properties. Moreover, the thermodynamics of these films is also quite similar to that of free-standing Pd films, which we studied as a reference by means of both Hydrogenography and Sievert's techniques. Free-standing films have no clamping issues and can be considered as bulk materials, which suggest that buckling is a very effective method to release the stress and proves that hydrogenography is comparable to conventional methods.

The following chapter is published in *Scripta Materialia*, *Volume 60, Issue 5*, *March 2009*, *Pages 348-351.*

3.2 Effect of the substrate on the thermodynamic properties of PdH_x films studied by hydrogenography

Abstract:

We investigated the influence of the substrate on the thermodynamic properties of metal hydride thin films by hydrogenography, using PdH_x as a model system. After appropriate hydrogen cycling, reproducible hydrogenation properties are found at the same equilibrium pressure for all substrates studied. Comparing these thin films with free-standing films -measured both by hydrogenography and by Sievert's method- we find a very similar behavior. Hence, thin films can be used to study the hydrogenation behavior of the corresponding bulk materials.

3.2.1 Introduction

The extensive search for a suitable material for hydrogen storage [1, 2] led to an increasing interest in high-throughput techniques to screen the storage behavior of a large number of chemical compositions simultaneously [3-6]. Recently, an optical method called hydrogenography has been proposed to investigate the thermodynamic properties of metal hydride thin films in a combinatorial way [7,8]. This technique is based on the optical change induced in metal films upon hydrogen loading. As a measure of hydrogen concentration we take the logarithm of the optical transmission, $\ln(T/T_o)$, that, according to Lambert-Beer's law [9] is proportional to the hydrogen concentration in the material. This allows us to record the analogue of the pressure-concentration-isotherms and discover new materials [8, 10].

Although thin films allow for fast screening, a fundamental difference with respect to bulk samples is the presence of a substrate which might alter the hydrogenation properties. Due to clamping thin films cannot expand freely in all three dimensions during hydrogen loading. When hydrogen expands the metal host lattice, adhesion forces act in the opposite direction to prevent the expansion of the film in the x-y directions creating considerable in-plane stresses of the order of several GPa [5, 11]. These stresses may change the equilibrium pressure plateaus of metal hydride films as compared to the corresponding bulk materials. However, if the film-substrate adhesion energy is lower than the stress energy, these stresses can be reduced by the formation of so-called buckles as observed in Pd and Pd-Fe films, respectively [12,13]. The question remains, however, whether the substrate adhesion forces were totally relieved in this way.

In this work we investigate the influence of the roughness and the chemical nature of the substrate on the thermodynamic properties and the hysteresis behavior of Pd thin films. Hydrogenography allows us to record the room temperature (de)/hydrogenation pressure-transmission-isotherms for several Pd films simultaneously and to investigate the dependence of the equilibrium pressure plateau for each of these samples on the cycle number. Repeating the hydrogenation at several temperatures reveals the effect of the substrate on the enthalpy of formation as deduced from the Van 't Hoff plot. We compare these results with those obtained from films which have been detached completely from the substrate. These free-standing Pd films were measured both volumetrically and optically and confirm the validity of our optical method.

3.2.2 Experimental details

Pd thin films with a thickness of 65 nm are prepared at room temperature by dc magnetron sputtering (background pressure 10^{-7} Pa, deposition pressure 0.3 Pa) on polished 1x1 cm^2 sapphire and α-quartz substrates. The surface roughness (rms), as characterized by atomic force microscopy (AFM, Veeco MultiMode SPM) is about 3.5 nm for α-quartz and 0.7 nm for sapphire. In addition, we prepared a substrate from the resonator of a quartz crystal rate monitor, commonly used to measure sputter deposition rates. Before use, its gold electrode was dissolved in hydrochloric acid. The macroscopic roughness of this quartz crystal is too large to be analyzed with an AFM technique. To compare the effect of roughness on sapphire substrates we modified the surface in various ways: namely by sputtering with Ar ions and by grinding with a rough polishing paper P360, yielding a roughness (rms, e.i. root mean square) of 3.5 nm and 100-200 nm, respectively. Prior to deposition, all wafers were cleaned in an ultrasonic bath with isopropanol for 1 hour followed by spin-drying. The typical Pd deposition rate is 1.1 Å/s (50 W dc power). Experimental details on the optical characterization of the hydrogenation process can be found elsewhere [8].

For this research, the hydrogenography experiments are carried out in a continuous mode of pressure ramping, with 17 slow and fast cycles; slow hydrogenations are recorded during the 1^{st}, 6^{th}, 11^{th} and 17^{th} cycle. Loading is done by gradually increasing the hydrogen pressure in the cell from 10^2 to 10^4 Pa; desorption is obtained by evacuating the cell. Slow cycles are measured for 20 h both in absorption and desorption to ensure the equilibrium between the hydrogen in the gas phase and within the film [14]. Fast cycles are done within one hour.

3.2.3 Results and discussion

Pressure-transmission-isotherms (PTIs) at 295 K of the Pd films on α-quartz, rough crystalline quartz and polished sapphire substrates during the 1^{st}, 6^{th}, 11^{th} and 17^{th} cycle are given in Fig. 1. We observe a different ab/desorption behavior during cycling. Already from the first cycle, Pd films on the α-quartz substrate show flat pressure plateaus with a desorption curve which is in a good agreement with the data for the bulk Pd [15] (Fig. 3.1). Until the 6^{th} cycle we observe a steady decrease in the width of the hysteresis. In the following cycles, only small variations in the position of the equilibrium pressure plateaus are observed. A similar activation procedure is found for the Pd films on rough quartz crystal substrates (Fig. 3.1). Apparently, the clamping of these two films is similar in spite of the differences in crystallinity and surface roughness of the substrates. The relatively

small optical contrast observed for Pd on the rough quartz substrate is due to the surface roughness, which diffuses the light and reduces the transmittance in the hydrogenated state. Pd films on sapphire (Fig.1.1) exhibit the largest hysteresis of all films. There is, moreover, an anomalous sloping plateau in the desorption isotherm. Subsequent hydrogenation cycles reveal substantial changes in the shape and slope of the pressure plateaus, along with a reduction of the hysteresis. After 17 cycles, the hydrogenation of Pd on sapphire becomes similar to that of the other Pd films. In this case, the decrease of the normalized transmission is caused by a formation of pinholes and cracks on the surface of the films on cycling.

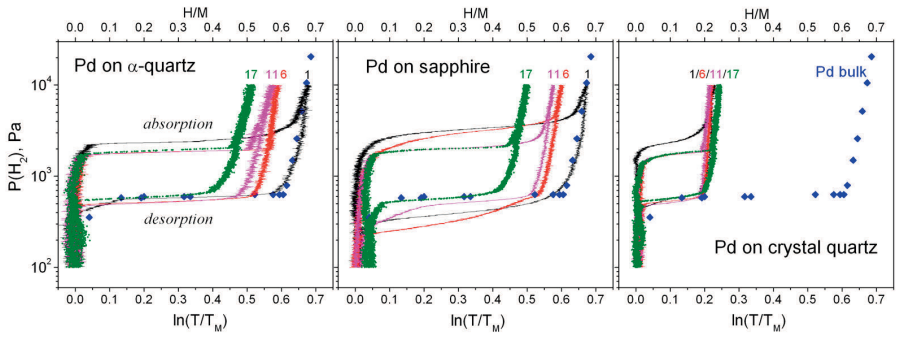

Fig. 3.1. Pressure-transmission-isotherms of Pd films on the α-quartz, sapphire and crystal quartz substrates during 1st, 6th, 11th and 17th slow hydrogenation cycles at 295 K; numbers represent the cycle number. Blue diamonds are the pressure-concentration-isotherm of bulk PdH_x [15] at 293 K. To compare the optical hydrogenography data and the bulk p-c-isotherm data we have chosen the relationship: $ln(T/T_M)=1.3 \times c_H$.

A microstructural study using in-situ laser confocal microscopy demonstrated a considerable correlation between hydrogenation behavior and the evolution of the Pd surface morphology on cycling (Fig. 3.2). Already after the first cycle, the whole surface of the Pd film on α-quartz is covered with round-shape buckles. For Pd films on sapphire, the majority of the film is buckle free up to the 6th six cycle; just a very small number of buckles could be observed at the edge of the sample. Apparently, the adhesion forces of the Pd-sapphire interface are bigger than those on quartz, which is reflected in a higher hysteresis compared to the buckled Pd films during 1-6 loadings. In the absence of an effective stress release hydrogen absorption requires more energy to expand a metal host lattice, i.e. to overcome the potential barrier created by the film-substrate adhesion forces. However, a rapid spreading of the buckle network is observed in the Pd film on sapphire

during the 11-17 cycles. After the 17th cycle the buckle network is entirely formed and, in spite of a completely different behavior during the first cycles, the thermodynamic properties and the hysteresis behavior of the Pd thin films on the various substrates becomes comparable between each other.

The appearance of buckles is known to effectively reduce stresses in thin films [12, 13, 16-18]. The buckles are created due to the lattice expansion during hydrogen absorption, leading to a partial detachment of the film from the substrate (Fig. 3.2) if the adhesion energy of the film is lower than the hydrogenation induced stress energy [17, 18]. Once a complete network of buckles is formed and most of the stress energy is released, the pressure plateaus are expected to remain constant upon cycling. Indeed, we find that the relatively fast transition to a reproducible hysteresis on cycling Pd films on quartz substrates is correlated with the speedy formation of a buckle network in the films.

Remarkably, the roughness of the quartz substrate does not have a large influence on the cycling behavior. Similarly, we find no difference between the PTI's of the Pd films on the polished substrate as compared to those obtained on sapphire substrates roughened in various ways (Fig. 3.3), which suggests that the substrate roughness has no influence on the clamping effect.

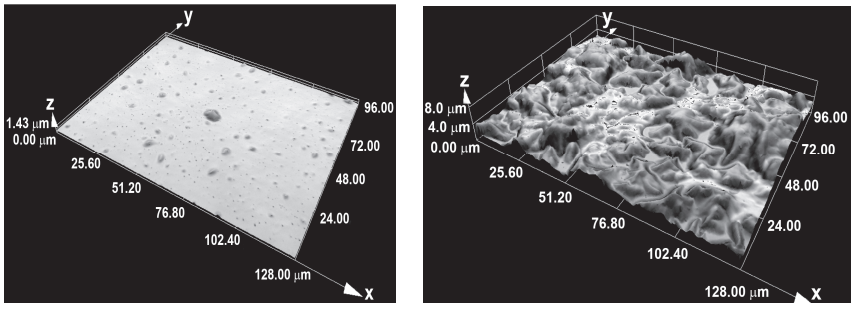

Fig. 3.2. In-situ micrograph of the Pd film on α-quartz after 10 hydrogen loadings in the metallic state (left) and in the fully hydrided state - at 1 bar H_2 (right), taken by an Olympus confocal laser scanning microscope LEXT OLS3100.

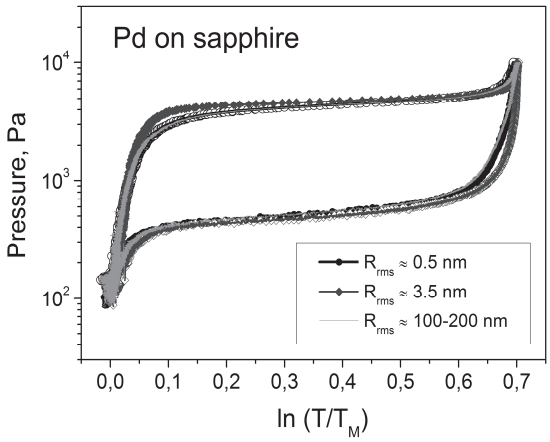

Fig. 3.3. PTI's of the Pd films sapphire substrates with different surface roughness. Black line + symbols – polished sapphire substrate, blue line + symbols - Ar etched and Red line - grinded a rough polishing paper sapphire substrates.

To verify whether the above also holds at higher temperatures, we perform hydrogenation experiments at 393 K and 515 K. The corresponding Van 't Hoff plots are presented in Fig. 3.4. Again, almost no differences are found between α-quartz, crystalline quartz and sapphire substrates, once the films have reached their fully buckled, reproducible state. The results are in a very good agreement with recent more elaborate hydrogenography experiments of Pd films on sapphire (presented as a line in Fig. 3.3) [14] and with desorption experiments on bulk Pd [15] (Fig. 3.4). However, there is a small disagreement between Pd films and bulk Pd in the *absorption* behavior. Hysteresis (P_{abs}/P_{des}) in the Pd films is about 1.7 times larger compared to the Pd nano-clusters [19], which probably represent best 'free' bulk behavior (Fig. 3.4). This discrepancy could either arise from remaining residual stresses in the films or from different intrinsic properties of the films compared to bulk materials. Therefore we compare our Pd thin films to a free-standing Pd film. The latter films also allowed us to test our optical measurement with a volumetric measurement of the hydrogenation using a high sensitive Sievert's apparatus.

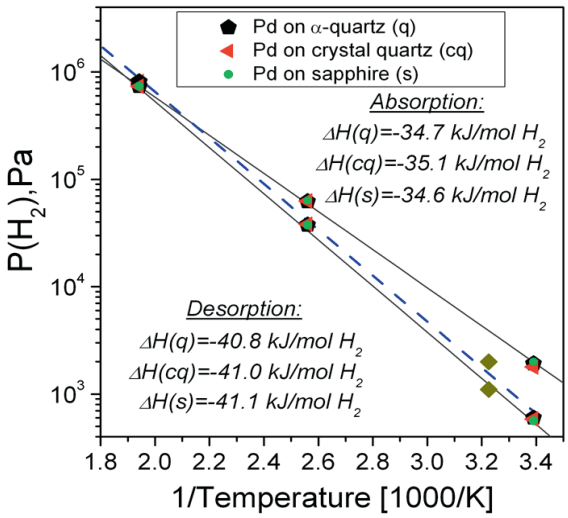

Fig. 3.4. Van 't Hoff plot of Pd films on α-quartz, sapphire and crystal quartz substrates for temperatures between 295 and 515 K measured by hydrogenography. Literature data for Pd films on sapphire (black line) [14], bulk Pd in desorption (blue dashed line) [15] and Pd clusters (yellow diamonds) [19] are presented for comparison. Enthalpies in the absorption and desorption are calculated from the linear fits to the experimental data.

For hydrogenography free-standing Pd films are obtained using a standard lift-off technique [20]. During hydrogenation, the thin film samples are placed between two glass plates to prevent curling of the Pd films. For the volumetric measurements, we deposit 90 nm thick Pd films with a 20 nm Ni bottom layer on a 3 inch silicon wafer. The films are scraped away from the substrate, loaded into a stainless steel MicroDoser sample holder and placed inside a Hy-Energy PCTPro-2000 instrument; the entire mass of the films was about 91.3 mg. Before measurements, the sample holder free gas volume is auto-calibrated with a film in the desorbed state using helium. PCT isotherms were measured at 311 K, 383 K and 473 K in a pressure range from 10^{-2} to 2.2×10^{6} Pa.

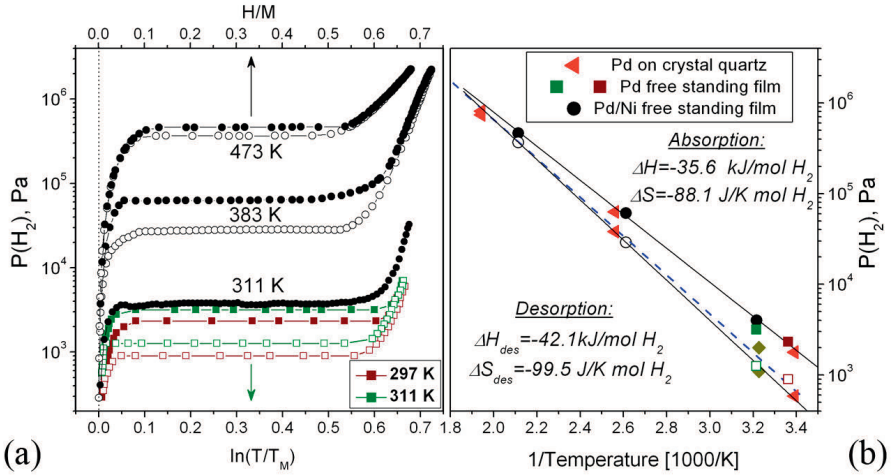

Fig. 3.5. (a) Pressure-concentration-isotherms (circles) and pressure-transmission-isotherms (squares) of the free-standing Pd films with (b) the corresponding Van 't Hoff plot; close and open symbols are the loading and unloading, respectively. For data normalization the relation $ln(T/T_M)=1.3 \times c_H$ is used. In (b) data for Pd films on crystal quartz (red triangles, by hydrogenography), bulk Pd in desorption (blue dotted line, by Sieverts) [15] and Pd clusters (yellow diamonds, by Sieverts) [19] are presented for comparison; values for the enthalpy and entropy of hydride formation/decomposition are obtained from the fit to the data for the free-standing Pd/Ni films, measured volumetrically.

The pressure-concentration and pressure-transmission-isotherms of the free-standing Pd films measured volumetrically and optically are collected in Fig. 3.5 along with the corresponding Van 't Hoff plot. The agreement is remarkable, both in the Van 't Hoff plots and the isotherms measured at 311 K, proving that the hydrogenography technique is completely comparable to the conventional methods. The total reversible capacity of the Pd films measured volumetrically is 0.67H/M at 311 K and 3.5×10^4 Pa. The series of PCT measurements at these three temperatures clearly maps out the α-PdH solid solution to PdH_x phase diagram for this sample; in this regard the behavior is also essentially the same as that of bulk PdH_x. As compared to the supported thin films, the only difference is that the free-standing films exhibit flatter plateaus. The similarity between supported and free-standing Pd films confirms that buckling is a very effective stress release model. However, the hysteresis in the free-standing films is still larger than that of the Pd nano-crystals (Fig. 3.5).

Recently, a so-called coherency theory was proposed to explain and predict the hysteresis (P_{abs}/P_{des}) in the MH bulk materials [21]. The theoretical prediction for the hysteresis in bulk Pd (1.80) is found to be very close to the experimentally obtained hysteresis in Pd nano-clusters (1.86) [19]. Such agreement between theory and Pd clusters is somewhat unexpected, since nano-materials usually exhibit different density modes compare to the bulk samples [22]. This also could be one of the reasons for a small disagreement in the hysteresis behaviour between the free-standing Pd films (2.59) and these nano-clusters. Another reason could be connected to different mechanical properties (Young's/Shear Modulus) of thin films as compared to the bulk, caused by a specific microstructure and defect density. Recent experiments of textured thin Pd films obtain higher values for the Young's modulus (E_s) than that of bulk samples [23]. Taking into account the maximum reported value of the E_s (247 GPa) for the Pd films, sputtered at RT, the coherency theory then would predict a hysteresis, which is comparable to the experimentally obtained in the Pd films. Therefore, we propose that the mechanical properties of the Pd thin films as compared to bulk Pd are responsible for the higher hysteresis in the both the free-standing and the supported Pd samples, since other parameters such as lattice expansion, hydrogen volume in metal and coexistence regions are found comparable to that of the Pd bulk. To validate this, however, an independent measurement of the elastic properties of the Pd films needs to be performed.

3.2.4 Conclusion

Hydrogenography experiments of Pd films show that after an appropriate number of hydrogenation cycles the plateau pressure becomes identical for all substrates investigated. The number of cycles needed for the formation of a complete buckle network depends on the nature of the substrate; the roughness appears irrelevant. The desorption behavior is equal to that of Pd bulk nano-crystals. The larger hysteresis observed in our films is probably due to a difference in the mechanical properties. The similarity between buckled and free-standing Pd films reveals that buckling is a very effective method to release the stress. The very good agreement between the optical and volumetrical measurements of the hydrogenation properties of free-standing Pd films proves that hydrogenography is comparable to conventional methods.

3.2.5 References

[1] A. Züttel, A. Borgshulte and L. Schlapbach, Hydrogen as a Future Energy Carrier, WILEY-VCH Verlag GmbH & C. KGaA, Weinheim, 2008.

[2] L. Schlapbach and A. Züttel, Hydrogen-storage materials for automobile application, Nature 414 (2001) 353.

[3] J.P. Lemmon, Combinatorial techniques and results for hydrogen storage discovery, Presentation at the MH2006 Conference on Metal Hydrides, Maui, Hawaii, 2006.

[4] J.C. Zhao, Combinatorial approaches as effective tools in the study of phase diagrams and composition–structure–property relationships, Prog. Mater. Sci. 51 (2006) 557.

[5] A. Ludwig, J. Cao, A. Savan and M. Ehmann, High-throughput characterization of hydrogen storage materials using thin films on micromachined Si substrates, J. Alloys Comp. 446-447 (2007) 516.

[6] S. Guerin, B.E. Hayden, D.C.A. Smith, High-Throughput Synthesis and Screening of Hydrogen-Storage Alloys J. Comb. Chem. 10 (2008) 37.

[7] B. Dam, R. Gremaud, C. Broedersz and R. Griessen, , Combinatorial thin film methods for the search of new lightweight metal hydrides, Scripta Mater. 56 (2007) 853-858.

[8] R. Gremaud, C. Broedersz, D. Brosa, A. Borgschulte, P. Mauron, H. Schreuders, B. Dam and R. Griessen, Hydrogenography: An optical combinatorial method to find new light-weight hydrogen-storage materials, Adv. Mater. 19 (2007) 2813.

[9] A. Borgschulte, W. Lohstroh, R. Weesterwaal, H. Schreuders, J.H. Rector, B. Dam and R. Griessen, Combinatorial method for the development of a catalyst promoting hydrogen uptake, J. Alloys Comp. 404-406 (2005) 699.

[10] C.P. Broederz, R. Gremaud, B. Dam, R. Griessen and M. Lovvik, Highly destabilized Mg-Ti-Ni-H system investigated by density functional theory and hydrogenography, Phys. Rev. B 77 (2008) 024204.

[11] U. Laudahn, A. Pundt, M. Bicker, U. V. Hulsen, U. Geyer, T. Wagner, R. Kirchheim, Hydrogen-induced stress in Nb single layers, J. Alloys Comp. 293-295 (1999) 490.

[12] R. Gremaud, M. Gonzalez-Silveira, Y. Pivak, S. de Man, M. Slaman, B. Dam and R. Griessen, Hydrogenography of PdH_x thin films: Influence of H-induced stress relaxation processes, Acta Mater. 57(4) (2008) 1209.

[13] S. Wagner and A. Pundt, Mechanical stress impact on thin $Pd_{1-x}Fe_x$ film thermodynamic properties, Appl. Phys. Lett. 92 (2008) 051914.

[14] R. Gremaud, M. Slaman, H. Schreuders, B. Dam, and R. Griessen, An optical method to determine the thermodynamics of hydrogen absorption and desorption in metals, Appl. Phys. Lett. 91 (2006) 213916.
[15] H. Frieske and E. Wicke, Magnetic Susceptibility and Equilibrium Diagram of PdH_n, Ber. Bunsenges. Phys. Chem. 77 (1972) 48.
[16] B. Audoly, Stability of Straight Delamination Blisters, Phys. Rev. Lett. 83 (1999) 4124.
[17] G. Gille, B. Rau, Buckling instability and adhesion of carbon layers, Thin Solid Films 120 (1984) 109.
[18] A. Pundt, E. Nikitin, P. Pekarski, R, Kirchheim, Adhesion energy between metal films and polymers obtained by studying buckling induced by hydrogen, Acta Mater. 52 (2004) 1579.
[19] A. Pundt, C. Sachs, M. Winter, M.T. Reetz, D. Fritsch, R. Kirchheim, Hydrogen sorption in elastically soft stabilized Pd-clusters, J. Alloys Comp. 293-295 (1999) 480.
[20] M. Gonzalez-Silveira, M.T. Clavaguera-Mora, F. Pi, J. Rodriguez-Viejo, Time resolved x-ray reflectivity study of interfacial reactions in Cu/Mg thin films during heat treatment, Phys. Rev. B 75 (2007) 075419.
[21] R.B. Schwartz, A.G. Khachaturyan, Thermodynamics of open two-phase systems with coherent interfaces: Application to metal hydride systems, Acta Mater. 54 (2006) 313.
[22] H, Wagner, in: G. Alefeld and J. Völkl (Eds.), Topics of Applied Physics: Hydrogen in Metals I, Springer-Verlag, Berlin, Heidelberg, New York, 1978, pp. 5-50.
[23] S.U. Jen, T.C. Wu, Young's modulus and hardness of Pd thin films, Thin Solid Films 492 (2005) 166.

Chapter 4

Influence of the substrate on the thermodynamic properties and hysteresis behavior in highly adhesive Pd films

4.1 Introduction

In the chapter 3 we have shown that buckled films have thermodynamic properties essentially equal to that of bulk materials. However, metal hydride thin films in general show a strong interaction with the substrate and thus remain intact during (de-)hydrogenation. In this case, a larger impact of the substrate on the thermodynamics is expected for such clamped films as compared to the buckled ones. The question then arise what the magnitude of this effect is and whether it can be quantified.

A film remains clamped during hydrogen (abs-)desorption when the adhesion forces are larger than the critical force to detach the film from the substrate to form a buckle. In the absence of buckling, there is no substantial stress reduction and the stress relaxation occurs by a different mechanism. By measuring Pd films on a highly adhesive Ti layer we demonstrate that the in-plane compressive stresses reach values up to 1.5 GPa during hydrogenation. The stress release in the clamped films occurs mainly plastically. By the formation and movement of dislocations the total film thickness is increased to accommodate the lattice expansion on hydrogenation. These large plastic deformations lead to an increased mechanical work during hydrogen loading/unloading. This extra work represents an additional barrier which hydrogen should overcome in absorption and in desorption for the α-β and β-α transitions to occur. Therefore, the (de-)hydrogenation reactions in the clamped samples take place at higher and lower equilibrium pressures, respectively, as compared to the non-clamped film, increasing the hysteresis width and changing the thermodynamic properties as inferred from a Van ‘t Hoff analysis.

In this chapter we investigate (de-)hydrogenation behavior and stress relaxation processes in the clamped Pd/Ti films. We discuss the influence and qualitatively model the effect of plastic deformations on the thermodynamic properties and hysteresis behavior in the clamped Pd films. We show that the enthalpy of hydride formation and decomposition of the highly adhesive Pd films decreases and increases by about 2.7 and 1.3 kJ/mol H_2 respectively, as compared to buckled Pd films. We develop a simple 'stress-strain model' which proves that the change in the thermodynamics and the expansion of the hysteresis correlate with the mechanical work needed to accommodate the stress induced plastic deformations in clamped Pd/Ti films during the (de-)hydrogenation cycle.

The 'stress-strain model' is not only practically important, as it allows to recalculate the bulk enthalpies of the hydride formation and decomposition from the corresponding Hydrogenography results, but it also shines light on the nature of the hysteresis. This theory does not take into account coherency of the lattice during the hydride nucleation or structure transformation, but relies mainly on a macroscopic volume strain of the films during hydrogenation and the in-plane compressive stresses, accompanying this expansion. Therefore, the 'stress-strain theory' can, in principal, also be used for the interstitial metal hydrides with both, a phase and structure transformations, for instance MgH_2 and for the complex hydrides, such as Mg_2NiH_4.

The following chapter is published in *International Journal of Hydrogen Energy*, *Volume 36, Issue 6*, *March 2011*, *Pages 4056-4067.*

4.2 Thermodynamics, stress release and hysteresis behavior in highly adhesive Pd films

Abstract:

We investigate the role of clamping on the thermodynamics of highly adhesive metal hydride thin films. Using Pd as a model system, we add Ti as an intermediate adhesion layer to increase the interaction with the substrate. We show that Pd/Ti films remain clamped during (de-)hydrogenation while the stress release occurs by means of rearrangement and pile up of the material. The compressive stress build-up reaches a value of about 1.5 GPa during hydrogen absorption. The enthalpy of hydride formation and decomposition, measured using Hydrogenography is found to decrease and increase by about 2.7 and 1.3 kJ/mol H_2 respectively, as compared to buckled Pd films. A simple model confirms that the change in the thermodynamics and the asymmetric expansion of the hysteresis correlate with the mechanical work needed to accommodate the stress induced plastic deformations in clamped Pd/Ti films during the (de-)hydrogenation cycle.

4.2.1 Introduction

Recently, we developed a new combinatorial technique called *Hydrogenography*, as an alternative to the volumetric and gravimetric methods to study the thermodynamic properties of hydrogen storage materials [1-4]. Unlike these bulk techniques, Hydrogenography uses thin films of metal hydrides. It is an optical method, which is based on the fact that metallic films change their optical properties upon hydrogen loading and unloading. A big advantage of Hydrogenography over the conventional methods is the possibility to measure simultaneously a very large number of compounds, using compositional gradient thin films created by co-deposition from several targets. This was successfully demonstrated in the ternary Mg-Ni-Ti system [3], where a thermodynamically favorable composition of $Mg_{0.69}Ti_{0.05}Ni_{0.26}$ with an enthalpy of hydride formation of -40 kJ/mol H_2 was found.

However, the presence of a substrate raises the question whether thin film experiments are well suited for the thermodynamic behavior of bulk materials. A rigid substrate usually does not allow a free expansion of the film during hydrogen loading, which creates considerable compressive biaxial stresses (of the order of several GPa [5]). The stress state affects the sign and the size of the H-H elastic interaction [6, 7]. In the case of a thin film, we expect that clamping reduces the attractive elastic hydrogen-hydrogen interaction [7, 8] with respect to free bulk material. This consequently leads to higher absorption and desorption pressure plateaus and a lower critical temperature, as long as the behavior is determined by elastic effects only [8]. However, clamping only fully develops when the adhesion forces between film and a substrate are stronger than the hydrogenation stresses. If this is not the case, the in-plane compressive stresses are released by the formation of so-called buckles [9]. Indeed, a considerable reduction of mechanical stresses was observed in buckled Pd and Pd-Fe thin films during hydrogen cycling [10-12]. These films, which are characterized by a relatively week film-substrate interaction possess thermodynamic properties very similar to those of bulk systems. A recent comparative study on buckled and free-standing Pd films by means of Hydrogenography and Sievert's volumetric measurements, confirms that buckling very effectively releases stresses, resulting in almost delaminated films with thermodynamic properties essentially equal to that of bulk materials [4]. However, metal hydride thin films in general show a strong adhesion with the substrate and - in the absence of an effective stress release - plastic in addition to elastic deformations influence their thermodynamic properties.

In this paper we investigate the role of clamping on the thermodynamics of thin film metal hydrides. We use Pd as a model system, but add Ti as an additional adhesion layer to increase the interaction with the substrate. A microstructural analysis shows that the films

do not buckle and remain clamped to the substrate on cycling between the dilute α phase and fully hydrogenated β phase. Using Hydrogenography we follow (de-)hydrogenation at ambient and elevated temperatures and determine the enthalpy and entropy of the hydride formation and decomposition. We show that the hysteresis in the Pd films with Ti adhesive layer asymmetrically expands with respect to the hysteresis in the buckled Pd films. A simple model, based on a stress-strain analysis of the films allows us to discriminate between the role of elastic strain and plastic deformation on the thermodynamic properties as derived from the Van 't Hoff analysis.

4.2.2 Experimental details

Thin Pd films with a Ti adhesive layer are prepared by dc magnetron Ar sputtering (background pressure 10^{-7} Pa, deposition argon pressure 0.3 Pa) on 10×10 mm sapphire (1102) and α-quartz substrates. Before deposition, all wafers are cleaned in an ultrasonic bath with isopropyl alcohol for 1 hour and spin-dried; after the cleaning the substrates were sputtered etched with Ar ions for 2 min. The thicknesses of the Pd and Ti layers, estimated from the tooling prior to the deposition process, are respectively 65 nm and 2 nm. Typical deposition rates are 0.1-0.2 nm/s for Pd (50-110 W dc power) and 0.04 nm/s for Ti (110 W dc power).

After deposition, the metal films were transferred to the hydrogenography setup, to investigate their optical properties as a function of hydrogen pressure at constant temperature. The Hydrogenography setup consists of a diffuse white light source (the projector) with a constant power of 150 W, which illuminates a gas tight and optically transparent cell, located in a furnace with a temperature control up to 573 K [3]. The gas pressure in the cell is controlled by the inlet and the outlet electronic valves and a flow meter. The amount of gas entering the cell is regulated by the MKS 250 forward Proportional-Integral-Differential (PID) system that controls the opening of the input valve depending on the desired pressure and the reading of the actual pressure by a MKS baratron. The electronic valve allows a pressure ramp up from vacuum to a maximum of 1 MPa H_2, which is the maximum pressure that the single crystal sapphire windows of the gas cell can withstand [3].

Hydrogen cycling of the Pd/Ti thin films on α-quartz and sapphire substrates at room temperature (RT) was done during 18 slow and fast cycles in the pressure range from 10 to 10^5 Pa H_2. Slow 1st, 6th and 12th cycles were measured in a continuous mode of pressure ramping for 20 hours both in absorption and desorption, which is enough for the buckled Pd films to be in equilibrium with the gas phase [13]; fast cycles have been conducted within several hours in loading and unloading. The last slow 18th cycle was

carried out in a stepwise mode of pressure change. Allowing the system to relax in each step ensures that equilibrium is reached. After an extrapolation to determine the minimum relaxation time, the pressure-transmission-isotherms were recorded for the second time with a gradual increase/decrease of the hydrogen pressure.

High-temperature hydrogenography experiments were carried between 333 and 483 K at hydrogen pressures up to 1 MPa. As Pd/Ti films showed slower kinetics than buckled films, measurements were repeated twice at each temperature. The first cycle was conducted in a pressure step mode in order to ensure equilibrium between the gas phase and hydrogen in the clamped Pd/Ti films, whereas the second one was performed in a continuous pressure increase mode with a measuring time found by extrapolating a step scan [13]. The absorption/desorption equilibrium pressures, as determined from the Pressure-Transmission-Isotherm's (PTI's) of the last cycle, were plotted in a Van 't Hoff plot, from which the enthalpy and entropy of hydride formation/decomposition were obtained using a linear regression analysis.

The Pd/Ti thin films were characterized ex-situ using an Olympus optical microscope. The structural properties were investigated by means of x-ray diffraction (XRD) using a Bruker D8 Discover diffractometer (Cu K_α radiation, λ =1.5418 Å), equipped with an Euler goniometer and a two-dimensional HI-STAR detector. The 2θ ($23^o - 57^o$) and χ ($60^o - 120^o$) axis denote the two scan directions of the detector. A Beryllium dome is used for the *in situ* x-ray experiments upon (de-)hydrogenation. Absorption experiments are conducted under a constant hydrogen pressure of 1,5 kPa whereas desorption is performed in a vacuum; before each scan of 1 hour there was a waiting time of a few hours to complete the (de-)hydrogenation reaction. The inter-planar distance in the out-of-plane direction of the film was measured at rotational angle $\varphi = 0^o$ (φ is the angle between diffraction plane and the film normal). Rotation of the film by $\varphi = 70^o$ gave information about inter-planar distances in the in-plane direction of the film. Diffraction profiles were analyzed using Pseudo-Voigt functions. The in-plane and out-of-plane lattice expansion of the textured films is calculated from $\varepsilon_x = \varepsilon_y = (d_x^{MH} - d_x^M)/d_x^M$ and $\varepsilon_z = (d_z^{MH} - d_z^M)/d_z^M$ respectively, where d^{MH} and d^M represent the inter-atomic distance between (111) planes in the hydride and metallic state. The overall lattice volume strain is estimated as follows: $\varepsilon_v = 2 \cdot \varepsilon_x + \varepsilon_z$.

4.2.3 Results and discussion

Hydrogenography experiments on clamped Pd/Ti films

Two kinds of substrates, namely sapphire and α-quartz are used in this study. However, the behavior of the Pd appears to be dominated by the Ti adhesive layer and no difference is observed between these two substrates.

The Pressure-Transmission-Isotherms of Pd thin films deposited on sapphire with a Ti adhesive layer are collected in Fig. 4.1, showing the 1st, 6th, 12th and 18th slow cycles at RT; PTI's of Pd thin films without Ti adhesive layer are shown for comparison.

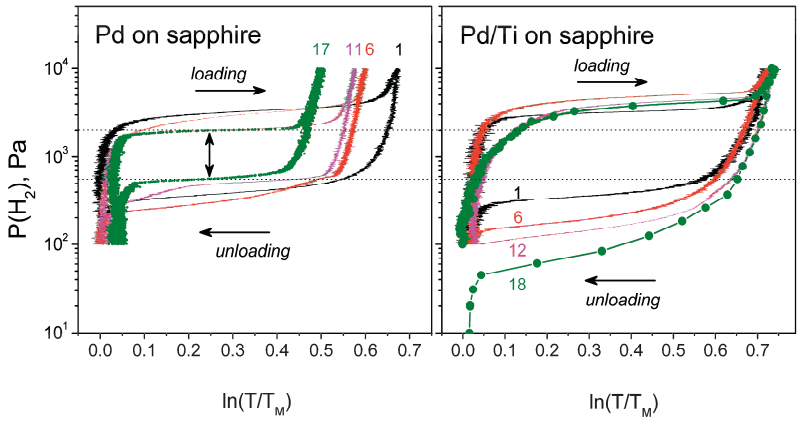

Fig. 4.1. Pressure-transmission-isotherms of the Pd (left) and Pd/Ti (right) thin films during multiple hydrogenation cycles at 295 K; numbers represent the cycle number.

The first loading shows only a marginal difference between Pd films with and without the Ti adhesive layer. In subsequent hydrogenation cycles a large difference between the two samples emerges. In the Pd/Ti samples an expansion of the hysteresis (the difference between the absorption and desorption pressure plateaus, Fig. 4.1) is observed during the 6th cycle. Following 12-18 loadings lead to an even larger hysteresis together with an increase of the slope of the desorption pressure plateau (Fig. 4.1). This behavior contrasts with pure Pd films where, due to formation of a buckle network a substantial lowering of the hysteresis occurs during cycle 11-17, after which the hysteresis cycle remains stable [13]. The appearance of buckles leads to a partial delamination of the film, which becomes loosely bound to the substrate. This effectively reduces the mechanical

stresses created during hydrogen loading [10-12]. The increase of both the hysteresis and the slope of the PTI's on cycling suggest that such a reduction of the in-plane stresses does not take place in the Pd/Ti film.

The formation of buckles in the Pd films is accompanied by the appearance of cracks, which causes the reduction of the width of the plateau (Fig. 4.1) and, therefore, decoupling of the optical transmission from the H concentration with cycling [10]. Pd/Ti films, on the other hand, show no change in the width of the plateau, supporting the assumption that there is no stress reduction due to buckling in the clamped samples.

The increase in hysteresis and in slope on dehydrogenating the clamped film can be both of a thermodynamic or kinetic nature. Evaluating in more detail the 18th cycle in a pressure step scan mode, we find that that the film needs much more time to reach equilibrium than the buckled film. The 20 hours, which is the normal measuring time in absorption and in desorption for the buckled Pd films [13] is not long enough for the Pd/Ti samples to reach equilibrium. Consequently, another (de-)hydrogenation cycle (19th) with a continuous mode of pressure changing has been performed with a longer measuring time, as derived from the pressure step experiment. The slope in the desorption pressure plateau disappears when the (un-)loading time is increased from 40 to 70 hours (Fig. 4.2). We also observe now that, given enough time, the hysteresis remains at approximately the same size as in the first cycle. Obviously, (de-)hydrogenation kinetics of the clamped films is slower than that of the buckled films.

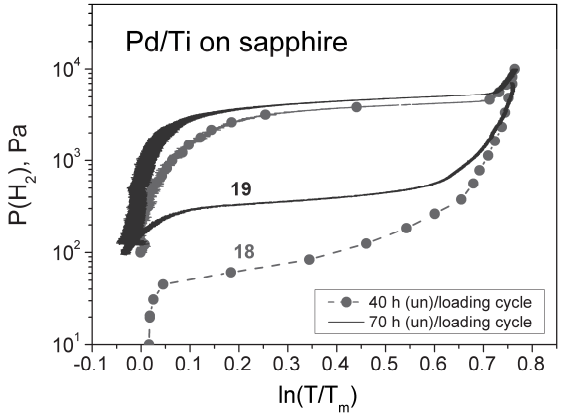

Fig. 4.2. Pressure-transmission-isotherms of Pd/Ti films on sapphire measured within 40 (pressure step scan mode) and 70 (continuous pressure ramp mode) hours at 295 K.

We relate the sloping behavior to unreleased compressive in-plane forces in the clamped Pd films which cause stress gradients within the film and, as a result, gradients in the energies of the sites occupied by H in the Pd lattice. Diffusion of hydrogen in metals is very fast even at room temperature meaning that the limiting step in establishing equilibrium in the clamped films is the diffusion of the host metal. An increase in measuring time allows the metal host lattice to rearrange during hydrogen absorption and desorption and to approach equilibrium conditions.

Hydrogenography experiments at elevated temperatures are conducted in the same way as at RT: first, the required kinetics for equilibrium conditions are defined during a pressure step mode, which is followed by the continuous pressure ramp mode in equilibrium condition. Fig. 4.3 shows two representative examples of the pressure-transmission-isotherms (PTI's) of the clamped Pd films taken at 333 K and 353 K. At 333 K insufficient kinetics require more time for the equilibrium measurement and an additional measurement cycle is performed. By optimizing the pressure ramp settings flat plateaus are obtained during hydrogen absorption and desorption at 353 K.

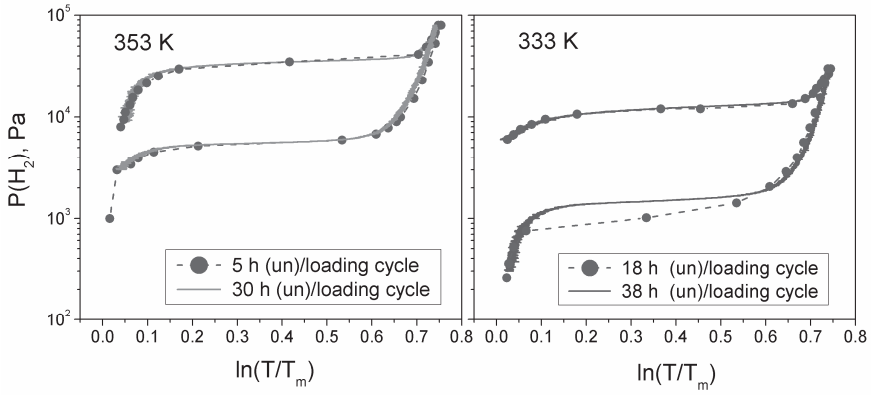

Fig. 4.3. Comparison between pressure step scan mode (dotted line + symbols) and continuous pressure ramp mode (line) PTI's of the Pd/Ti films at 333 K and 353 K.

All PTI's of the clamped Pd films with Ti adhesive layer in the temperature range 298–483 K with the corresponding Van 't Hoff plot are shown in Fig. 4.4. The high-temperature data follow the same trend as observed during RT hydrogenography experiments: absorption and desorption in the clamped Pd films are found at higher and lower pressures, respectively, than that of the buckled one, which, in turn, is very similar to that of bulk Pd [14]. The increase in hysteresis in clamped Pd-Ti samples is not

symmetrical, e.g. in the absorption branch a higher deviation is found than in desorption. Consequently, the enthalpies determined from a Van 't Hoff analysis of the hydride formation and decomposition pressures in the clamped Pd films are increased / decreased by about 2.7 / 1.3 kJ/mol H_2 respectively as compared to the delaminated Pd samples. Moreover, in the extrapolation to high temperatures, we observe a substantial increase of the critical temperature (T_c) from 565 K in the case of Pd bulk [15] to 693 K in the case of the clamped Pd films. Hence we conclude that the clamping produced by adding just 2 nm Ti adhesive layer has clear effect on the thermodynamics of the system. The question to be addressed is whether or not these changes are related to the structural changes during hydrogenation.

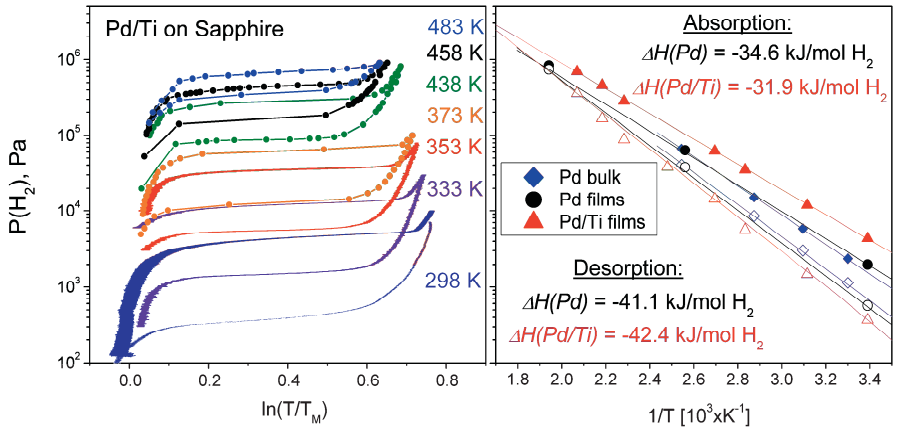

Fig. 4.4. PTI's in the temperature range 298–483 K (left) together with the corresponding Van 't Hoff plot (right) of the Pd/Ti thin films; results for buckled Pd films [4] (black circles) and bulk Pd [14] (blue diamonds) are also presented. The enthalpy of hydride formation and decomposition is calculated from a linear fit to the experimental data.

Structural and morphological analysis

The ex-situ surface characterization of the Pd and Pd/Ti films is presented in Fig. 4.5. Contrary to Pd films, optical microscopy reveals no micro-structural changes in the Pd/Ti samples during 18 (de-)hydrogenation cycles.

The absence of buckles in a fully loaded state in the clamped samples implies that the adhesion forces are higher than the critical stresses for buckling [9]. Due to the in-plane expansion constraints hydrogenation will result in larger in-plane compressive stresses as

compared to buckled Pd. As the film does not extend over the edge of the substrate, volume expansion in clamped Pd can only take place in the vertical direction.

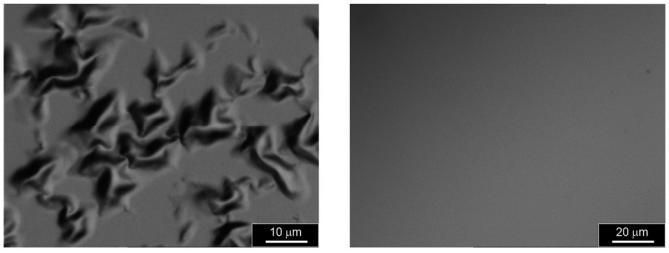

Fig. 4.5. Optical microscopy micrographs of buckled Pd (left) and non-buckled Pd/Ti (right) thin films after 17 and 18 hydrogenation cycles, respectively.

To investigate the lattice change on hydrogenation we performed X-ray analysis. Fig. 4.6 presents room temperature XRD spectra of the clamped film during the last 18^{th} loading cycle of the activation procedure, showing the Pd 111-reflection in the metallic and hydrided state. These patterns, taken at various rotational (φ) angles, namely 0^{o} and 70^{o} degrees, represent the out-of-plane and in-plane expansion of the sample. Remarkably, these X-ray diffraction experiments measure an in-plane expansion of 3.09% in the Pd/Ti thin films during hydrogen absorption, which is much smaller than the lattice change of a free bulk sample. The out-of-plane expansion is higher as compared to Pd bulk, i.e. 4.46% instead of 3.54%. The overall volume strain of the clamped films equals to 10.64%, assuming expansion in the x and y direction to be identical. Surprisingly, this result is quite close to the isotropic volume expansion of the buckled Pd films and bulk Pd, namely 10.95% and 11% respectively. The volume expansion of the buckled Pd samples is calculated from the in-plane and out-of-plane expansion, 3.58% and 3.79% respectively, measured in a similar manner as for clamped Pd films (Fig. 4.6). The bulk data is taken from literature [15].

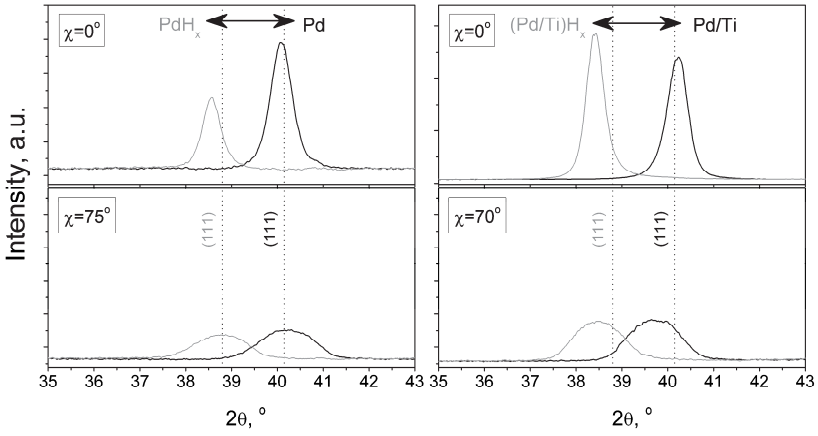

Fig. 4.6. X-ray diffraction spectra of the Pd (left) and Pd/Ti (right) thin films in the metallic (black line) and hydrided state ($p(H_2)=16x10^3$ Pa, red line) at two rotation (χ) angles during $18^{th}/17^{th}$ hydrogenation cycle. Dotted line represents 111 reflection of the Pd bulk in the loaded and unloaded state [16].

The observed in-plane lattice expansion of the 10 mm wide clamped Pd/Ti film should result in a macroscopic elongation of around 0.3 mm in the x/y direction. This is not observed experimentally: the film remains within the boundaries of the substrate. The complete lattice volume strain of 10.64%, measured with XRD then has to occur through rearrangement of the material and macroscopic vertical expansion of the film. This is confirmed by profilometry (not shown here), which measured about 11% thickness change of the Pd/Ti films during hydrogen loading and unloading. A large part of this - ~6% - has to be due to plastic deformation. In the Pd films the stress is released through buckling (see Fig. 4.7).

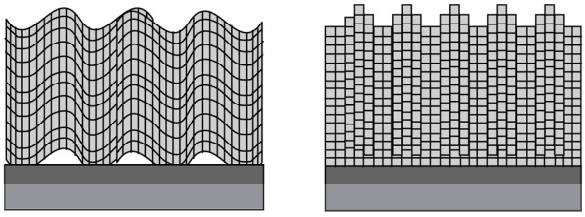

Fig. 4.7. Schematic representation of the buckling and material pile-up stress release models in Pd (left) and Pd/Ti (right) thin films during (de)/hydrogenation.

Relaxation processes usually involve the generation and movement of dislocations. Their diffusion may also lead to a material pile-up on the films surface. This material pile-up, most likely, occurs by means of dislocations glide steps (Fig. 4.7), which were observed previously in clamped Nb and Gd thin films after hydrogenation [17,18]. A substantial material rearrangement in the clamped state can be inferred from the change in texture during (de)/hydrogenation. Figure 4.8 shows two-dimensional X-ray diffraction patterns of the Pd/Ti sample before and after cycling. In the as-deposited state the polycrystalline Pd is represented by smooth and continuous 111 and 200-diffraction rings. However, after 18 hydrogenation cycles considerable material reorientation is evident from the complete disappearance of the 200 reflection and the collaps of the 111 ring to a single broad reflection peak. Similar out-of-plane texturing, i.e. an increase of the intensity of the 111 reflection was also observed during cycling of the Pd films on sapphire substrate [10]. In this case, however, no orientational changes in χ-direction or disappearance of the 200 reflection were observed in the diffraction pattern. It is worth mentioning, that the microstructure of the Pd/Ti thin before the cycling procedure (Fig. 4.8) was found very similar as compared to the Pd films in the as-deposited state (Fig. 2 in ref. [10]).

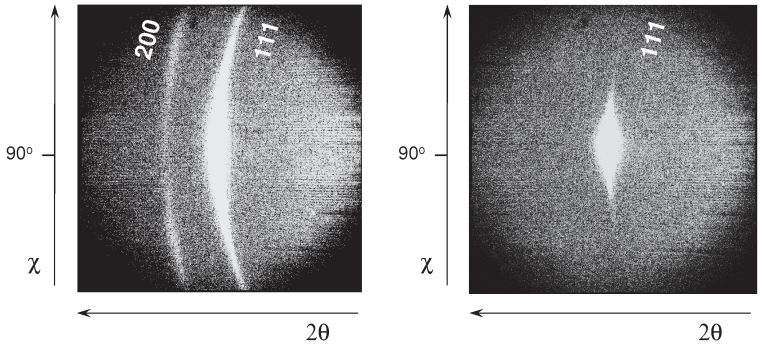

Fig. 4.8. 2D X-ray diffraction pattern ($20^\circ \leq 2\theta \leq 60^\circ$, $60^\circ \leq \chi \leq 120^\circ$) of the Pd/Ti films in the as-deposited state (left) and after 18 hydrogenation cycles (right).

The out-of-plane inter-planar distance, d_{111} for both Pd films in the metallic (α) and the hydrided (β) state as a function of the hydrogenation cycle is presented in Fig. 9; the data for bulk Pd is taken from [16]. First of all, we observe for both cases an expanded lattice in the as-deposited state, which is probably due to the sputter process which often induces lattice strains; this slightly expanded state remains in repeatedly cycled buckled Pd

film. First loading of this film gives an out-of-plane expansion of 3.59% that is only slightly larger than that observed in bulk Pd (3.54%). In clamped films, a somewhat larger out-of-plane expansion is found, i.e. 3.95%. However, the most remarkable difference between the buckled and the clamped film takes place after desorption, where the out-of-plane lattice of the latter sample appears to be contracted relative to the bulk (Fig. 4.9). We attribute this to the rearrangements of the film on hydrogenation. Since the film remains intact during cycling, large plastic deformations are again needed during dehydrogenation. After elastic relaxation and subsequent contraction, the required volume reduction forces material transport back into the film to prevent the formation of cracks and holes. Apparently, this process is not driven to a full completion and a substantial out-of-plane lattice compression accompanied by an in-plane tensile stress remains (Fig. 4.9).

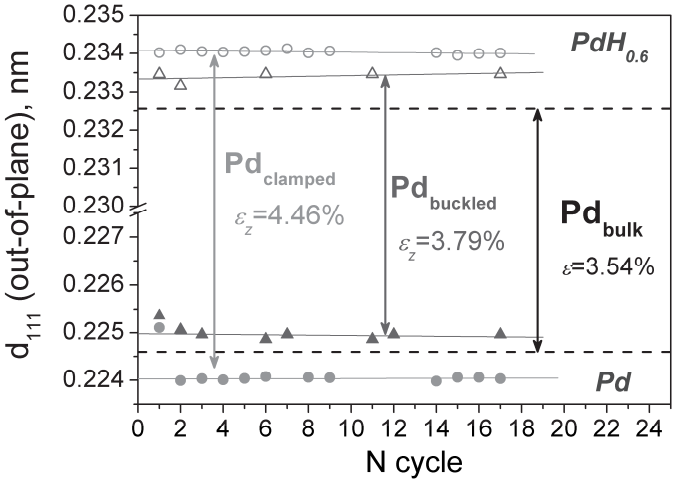

Fig. 4.9. The out-of-plane inter-atomic distance (d_{111}) in the buckled (green triangles) and clamped (red circles) Pd films in the metallic and hydrided state as a function of cycle number. The dotted line is the bulk data [16] and the solid lines are a guide to the eye. The lattice expansion is calculated from the last cycle of the activation procedure.

In pure Pd films during dehydrogenation, the buckled areas simply fall back on the substrate surface by a restoring elastic force, while the film resumes it original shape. This process involves a bit of plastic rearrangement, but no substantial lattice contraction is involved.

The following (de-)hydrogenation cycles 2-18 reveal hardly any changes in the lattice parameters. Cycling of the clamped films involve both compressive and tensile

stresses both in absorption and desorption. The lattice expansion becomes much larger than in bulk Pd, e.g. 4.46%. A similar situation was observed in epitaxial Nb films with a very high adhesion and no morphological changes or delamination during H_2 cycling [19]. The cycling of Pd films without Ti layer involves mainly compressive stresses in addition to relatively small plastic deformations in absorption and desorption. Extensive buckling accommodates the volume change with a minimum amount of plastic deformation. Imagining the film to consist of various sections separated by grain boundaries, one sees that a slight shift of the sections with respect to each other is enough to create or annihilate buckles. As a result, the lattice expansion remains close to that of bulk, e.g. 3.79%, during the subsequent cycles.

Hysteresis behavior

To explain and quantify the difference in the thermodynamic behavior between clamped and buckled Pd films we propose the following simple model.

Incorporation of hydrogen into a host metal generates lattice stresses and, consequently, lattice strains (volume expansion). These stresses, according to Schwarz and Khachaturyan [20], create a macroscopic thermodynamic barrier which splits absorption and desorption plateaus (P_{abs}, P_{des}) apart, creating the so-called *intrinsic* hysteresis (Fig. 4.10, A). Such an *intrinsic* hysteresis is observed in many metal-hydride systems [13, 20-30] and, in the simplest approximation, it is a function of the mechanical properties of material (compressibility), the volume expansion during hydrogenation and the amount of hydrogen that can be absorbed. Based on the elasticity theory, the authors [20] derived an equation that quantitatively explains the hysteresis (P_{abs} / P_{des}) in the Pd-H system. Their theoretical prediction for this ratio, i.e. 1.92, is found to be quite close to the experimentally observed hysteresis for bulk Pd (1.78 ± 2.1 [14,29,30]) suggesting that the *intrinsic* hysteresis is indeed mainly of this elastic origin.

Strictly speaking, the model of Schwarz and Khachaturyan [20] is valid only for an open system with coherent interfaces between metal and hydride phase, i.e. for a coherent nucleation. Even for an iso-structurally transforming Pd this is not the case since the stresses, associated with hydride precipitation are too high to create a coherent or semi-coherent interface. Still, the theory has been successfully applied to predict hysteresis in Pd bulk. This is probably due to the fact that the plastic contribution to the hysteresis is much smaller then the elastic one. Bulk materials are free to expand, which allows them to minimize their plastic work by means of system rearrangement. Moreover, Pd bulk crystal has the fcc structure with 12 slip systems, which facilitates the plastic deformations to proceed.

A similar situation is observed in buckled Pd films, where we found a value of 3.05 for the pressure hysteresis. Dislocations, formed during first few loading-unloading cycles, release the in-plane compressive stresses in the film by means of buckling and reduce the overall plastic deformations. Slightly bonded to the substrate, they possess elasto-plastic behavior during (de-)hydrogenation with the elastic part having the major contribution to the hysteresis; the plastic deformations involved in the buckled samples play quite a small role. Therefore, the hysteresis in these films is also mainly of elastic origin. The relatively small difference in size of hysteresis between bulk and buckled Pd is attributed to a different defect structure and, accordingly, different mechanical properties of the films [4].

This is contrary to clamped Pd films, where plastic deformations remain the same for each loading-unloading cycle. The much larger plastic contribution in the clamped films would then results in a larger hysteresis in this case, i.e. extrinsic. To quantify this we need to analyze the relation between hysteresis and stress/strain in more detail.

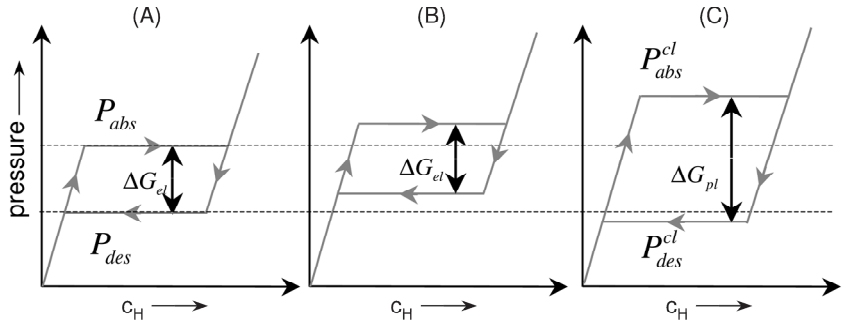

Fig. 4.10. Schematic representation of the intrinsic hysteresis (A) and its shift (B) and widening (C) in the clamped system due to elastic and plastic contributions, respectively; P_{abs}, P_{des} *and* P_{abs}^{cl}, P_{des}^{cl} *denote the absorption and the desorption pressure for the unconstrained (free) and clamped system, respectively.* c_H *is the hydrogen concentration.*

During the hydrogenation of clamped Pd/Ti, the films have to deal with an external boundary, i.e. the substrate, leading to an in-plane compressive stress. Due to lateral expansion constraints, the volume change is characterized by both elastic and plastic contributions. An elastic compression reduces the long-range attractive H-H interaction in the material [19], which results in a reduction of the thermodynamic potential for hydrogenation. Hence, both branches of the hysteresis will be equally affected (see Fig. 4.10 B). The *frictional* energy which characterizes *plastic* deformation reflects an energy

loss both during ab- and desorption and this will therefore *increase* the hysteresis width (see Fig. 4.10 C).

Thus, for the clamped Pd/Ti film we need to add the elastic and plastic contributions to the *intrinsic* hysteresis. This results in an asymmetric expansion of the hysteresis with respect to the non-clamped film. For the absorption pressure plateau the two contributions enhance each other, shifting the plateau to higher pressures, P_{abs}^{cl} (Fig. 4.10 C). During the unloading process both contributions counteract each other. Still, the desorption plateau P_{des}^{cl} shifts to a lower pressure as compared to buckled Pd films, (Fig. 4.4) implying that the plastic deformation is larger than the elastic one [31,32].

Hysteresis is associated with a loss of energy and can be expressed as a change of the Gibbs free energy during the (de-)hydrogenation cycle [24,25,27]. In the case of free and pseudo-free materials such as bulk Pd and buckled Pd films, the difference between absorption and desorption pressure plateaus is given by (Fig. 4.10 A):

$$\frac{1}{2}RT\ln(P_{abs}/P_{des}) = \Delta G_1 \tag{4.1}$$

The plastic deformations in clamped Pd films are reflected in a bigger hysteresis and a larger value of ΔG:

$$\frac{1}{2}RT\ln(P_{abs}^{cl}/P_{des}^{cl}) = \Delta G_2 \tag{4.2}$$

The increase of the hysteresis and the change of the thermodynamic properties in the Pd/Ti sample with respect to buckled Pd films are related to the increase of the Gibbs free energy change associated with the hysteresis:

$$\frac{1}{2}RT\ln\left((P_{abs}^{cl}/P_{des}^{cl})/(P_{abs}/P_{des})\right) = \Delta G_2 - \Delta G_1 = \Delta G_{hyst} \tag{4.3}$$

ΔG_{hyst} is determined by the energy terms due to elastic and plastic deformations of the material considered [24,27,30]. In our case, the Gibbs free energy change (ΔG_{hyst}) and, accordingly, the hysteresis in the buckled and clamped Pd films is equal to the additional mechanical work done during the (de-)hydrogenation cycle. This mechanical work can be estimated from a polygon area on the stress-strain curve [33], representing the change of a material deformation as a function of the applied stress. Taking this into account, the increase of the hysteresis during absorption and desorption can be rewritten as:

$$\frac{1}{2}RT\ln\left((P_{abs}^{cl}/P_{des}^{cl})/(P_{abs}/P_{des})\right) = \left(V_M/(c_\beta - c_\alpha)\right)\cdot\left[\int_o^{\varepsilon_{(\max)_2}} \sigma_2 d\varepsilon_{V_2} - \int_o^{\varepsilon_{(\max)_1}} \sigma_1 d\varepsilon_{V_1}\right] \tag{4.4}$$

where R is the gas constant, V_M is the molar volume of Pd, $c_{\beta,\alpha}$ is the maximum hydrogen concentration in the β and α phase and $\sigma_{2,1}$ and $\varepsilon_{2,1}$ correspond to the stresses and volume strains in the $(Pd/Ti)_2$ and Pd_1 thin films, respectively.

It is worth mentioning, that eq. (4.4) implies a similar width of the equilibrium pressure plateaus between clamped and buckled Pd films. In the case of substantially different values of $(c_\beta - c_\alpha)$ due to, for instance, a completely different microstructure of compared films [34], this equation would change by opening the brackets and dividing each of the integrals by the α→β solid solution.

Here we assume that the difference in the width of the plateau is relatively small between Pd and Pd/Ti films [35]. So, to validate our theory all we need is to calculate the right-side of eq. (4.4) by constructing the stress-strain curve for buckled and clamped Pd samples and compare the calculated increase in hysteresis with the experimental results, obtained by means of hydrogenography.

Stress evaluation

The phase transformation from the α- to β-phase in the unconstrained Pd bulk is accompanied by an isotropic lattice expansion ε. Thin films, on the other hand, are clamped and the α→β transformation occurs under in-plane compressive forces (Fig. 4.11). As a result, the out-of-plane strain in Pd films becomes larger by $\Delta\varepsilon_z$ as compared to bulk. Here, we define $\Delta\varepsilon_z$ as an additional expansion of the film in the vertical direction due to the elasticity of material (Poisson's factor). The value of $\Delta\varepsilon_z$ depends on the in-plane forces acting on the film, meaning that the out-of-plane lattice expansion can be used to evaluate mechanical stresses in Pd and Pd/Ti films during the hydrogenation.

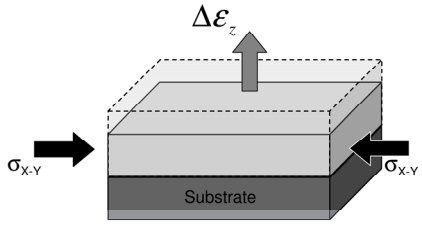

Fig. 4.11. Schematic illustration of an additional out-of-plane expansion, $\Delta\varepsilon_z$, (shaded area) in thin films due to the in-plane compressive stresses (σ_{x-y}) during hydrogenation.

Assuming that the volume expansion due to the hydrogenation of the clamped film results in a uniaxial stress exerted by the substrate, we can apply Hooke's law for an isotropic media, namely:

$$\varepsilon_z = 1/E \cdot (\sigma_z - \nu(\sigma_x + \sigma_y)) \tag{4.5}$$

where ε_z is the lattice expansion in z direction, σ_z and σ_x, σ_y are the out-of-plane and the in-plane stresses, respectively and E and ν are the Young modulus and Poison's ratio of the media. Since the surface of the film is free, there is no stress build up in the z direction, i.e. σ_z=0. Hence, the hydrogenation stresses in the buckled and clamped Pd films can be estimated as follows:

$$\sigma_x = \Delta\varepsilon_z E / 2\nu \tag{4.6}$$

Thus the stress in the hydrogenated film is related to $\Delta\varepsilon_z$, which is the difference between the observed lattice expansion in the out-of-plane direction of the Pd film and bulk Pd: $\Delta\varepsilon_z = \varepsilon_z - \varepsilon$.

For the calculation we use the mechanical properties of Pd assuming that the Young modulus and the Poisson's ratio do not change significantly during the hydrogenation. Substituting the literature values for the elastic constants of bulk Pd (E=126 GPa and ν=0.39 [36]) and the measured out-of-plane lattice strains (see Fig. 4.9) into eq. (6) , we obtain the in-plane compressive stresses acting on the clamped and buckled Pd films during hydrogenation to be 1.49 GPa and 0.40 GPa, respectively. There is a substantially more stress build-up in the Pd-Ti sample, than in the Pd film, where mechanical stresses are released by means of buckling. The values are in reasonable agreement with the hydrogenation stresses, measured in similar films by the curvature method [37, 38]. This bending technique gives maximum compressive stresses of about 1 GPa and 0.35 GPa for clamped Pd film on Ti adhesive layer and a 200 nm thick Pd film, respectively.

Stress-strain analysis

To quantify the mechanical work done by the system during the absorption/desorption cycle we analyze the strain-stress relation during the loading and unloading process of thin films. Here we present a sketch of the strain-stress curves of the buckled and clamped Pd films during the corresponding hydrogenation and dehydrogenation steps in Fig. 4.12. We show the situation for a sample after the activation procedure, i.e. after a number of hydrogenation cycles.

In the metallic state of the Pd film- point 1- the film is loosely bonded to the substrate. Since the buckled film has relaxed on the substrate the in-plane compressive

stress in the metallic phase is very small [10] and is taken, for simplicity, as zero. By absorbing a small amount of hydrogen the Pd film expands elastically, until it reaches the so-called Elastic limit or Yield point, point 2, beyond which the nature of the strain changes from elastic to plastic, causing it to deform permanently. Up to this point the volume change occurs mostly by the elongation of the lattice in the out-of-plane direction. We assume here that the α-phase coincides with the elastic limit [5]. Considering the fact that the coexistence of the α- and β-phases gives rise to hydrogenation stresses in the material, this is quite a realistic assumption [5]. As the buckled Pd is considered as nearly free from the influence of the substrate [4] and it resembles the bulk behavior, the maximum hydrogen concentration in the α-phases is taken to be similar to that of Pd bulk, $\alpha^{H}_{\max} = 0.008\ \ H/M$ [39]. It was measured experimentally [35] that the solid solution in the α-phase of the polycrystalline Pd films is about an order of magnitude higher, i.e. i.e. 0.02 as compared to Pd bulk. This is due to larger grain boundary concentration, which influences hydrogen solubility in both, alpha and beta phases [34]. However, the assumption that the $\alpha^{H}_{\max}$ in buckled Pd and Pd bulk is similar still valid for the qualitative analysis made here and would have a minor influence on the calculated results.

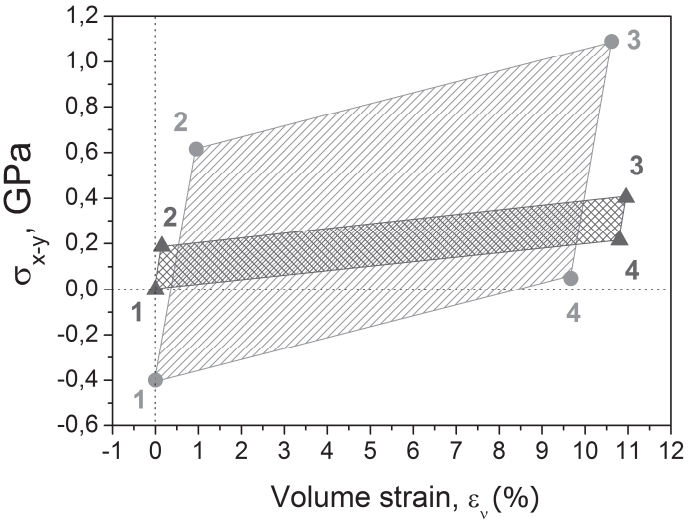

Fig. 4.12. Stress-strain curve of the buckled (green) and clamped (red) Pd films during loading/unloading cycle; numbers represent different hydrogenation and dehydrogenation steps, namely elastic expansion of the films (1-2), plastic deformations (2-3), elastic recovery (3-4) and plastic deformations (4-1), returning the films to its initial state (1).

According to [39], the bulk volume expansion in Pd depends linearly on hydrogen concentration:

$$(\Delta V / V)_H = 0.19 \times c_H \tag{4.7}$$

Substituting $\alpha_{\max}^H$ into eq. (4.7) gives the volume expansion of bulk Pd and, hence, the buckled Pd film in the elastic region: ε_{el}=0.15%. During the elastic regime the stress is proportional to the strain via Young's modulus, $E : \sigma_{el} = E \cdot \varepsilon_{el}$.

Similarly, assuming that the elastic constants are the same for bulk and thin free films, the slope of the line between points 1 and 2 is simply the modulus of elasticity and the Yield point, e.g. point 2, is then equal to 0.19 GPa (Fig. 4.12).

An increase of the hydrogen concentration leads to buckling, i.e. plastic deformation. These buckles involve only a relatively small amount of dislocations therefore the lattice expansion in this material is close to the isotropic case. The in-plane lattice change in the delaminated Pd film during (de)/hydrogenation, measured with XRD is very close to that of the out-of-plane expansion, 3.58% and 3.79% respectively. The complete volume expansion of 10.95% (Fig. 4.6) and the maximum in-plane compressive stress (see paragraph on stress evaluation) of about 0.4 GPa result in point 3 (Fig. 4.12).

The unloading procedure takes place in the opposite direction. First, buckled Pd films experience an elastic recovery up to $\beta_{\min}^H$ (point 4) which is minimum hydrogen concentration in the hydride phase. The amount of the volume change during this step and the slope of the 3-4 line are kept the same as during the loading process in the elastic region (1-2). Afterwards, the film shrinks plastically by deformation of buckles, going to its initial state (point 1).

Let us now compare this with the clamped Pd/Ti films. In the first place we observe that in the alpha phase the *cycled* films experience a tensile in-plane stress of 0.4 GPa (point 1) as derived from the out-of-plane lattice compression. Absorption of hydrogen in this α-phase leads to an elastic expansion of the Pd-Ti film (point 2), occurring solely in the vertical direction. This one-dimensional lattice change, which was also observed for clamped Nb films [40], is possible only up to a certain critical hydrogen concentration $\alpha_{\max}^H$ [41]. However, the $\alpha_{\max}^H$ in the clamped Pd sample is different from that of the buckled Pd film. It was observed by the thin film curvature stress measurement [34], that the elasticity region in the clamped sample holds up to about 0.05 H/M before in-plane lattice relaxation starts, which, according to eq. (4.7), lead to the elastic volume expansion of 0.95% (point 2, Fig. 12). The out-of-plane volume change of 0.95% is composed of the expansion of the stress-free sample, which is 1/3 of the corresponding volume increase and an additional expansion due to Poisson's factor, $\Delta\varepsilon_z$ (Fig. 11). By simple calculation the extra out-of-

plane expansion of 0.63% is found. Using a similar approach for the in-plane stress evaluation as was described in paragraph 3.4 and substituting $\Delta\varepsilon_z$ into eq. (6) gives the Elastic limit (point 2) in the clamped Pd/Ti film, i.e. 1.02 GPa (Fig. 4.12). The slope of the strain-stress curve in the elastic region, i.e. 107 GPa is found quite similar to that of bulk Pd, supporting the assumption that the mechanical constants are barely affected by nano-sizing effects. Please note, that in the buckled Pd a similar stress build-up takes place in the film during first hydrogenation. However, as the delamination of the film releases hydrogenation stresses very effectively, following hydrogenation cycles result in a decrease of the in-plane compressive stresses down to 0.19 GPa.

After the Yield point, the volume expansion of the clamped Pd film occurs by means of plastic deformation. In the fully expanded state (10.64%) (point 3) the maximum estimated stress reaches 1.49 GPa (Fig. 4.12). On hydrogen desorption, first elastic relaxation will set in until point 4. Note, that at this point, due to the previous plastic deformation, the substrate already exerts a stress on the film. As a result, on further dehydrogenation plastic deformations are needed to return the film to its primary state (point 1). Again, the elastic recovery involves the same amount of stress decrease and the same amount of volume change as during the loading process (1-2).

The mechanical work, performed by buckled and clamped Pd films upon (de-)hydrogenation cycle is represented as a shaded area in Fig. 4.12 and can be estimated from the area of the corresponding polygons, i.e. $\int_{o}^{\varepsilon_{\max}} \sigma d\varepsilon_V$. A considerable difference in the calculated mechanical work is found between clamped and "free" Pd samples, namely 0.158 GJ/m^3 and 0.044 GJ/m^3, which scales with the maximum evaluated compressive stresses in these materials, e.g. 1.5 GPa and 0.4 GPa, respectively. Taking a difference between calculated mechanical work in clamped and buckled Pd films and substituting it into the left side of eq. (4.4) along with the molar volume of Pd, V_M=8.9×10^{-6} m^3/mol and the bulk phase boundaries, (c_β–c_α)=0.6 [15] yields the Gibbs free energy change, ΔG_{hyst} of about 1.69 kJ/(mol H). This value will change slightly up to 2.54 kJ/(mol H) if take into account the measured phase boundaries in buckled and clamped Pd films, 0.4 H/M (the averaged value for both films). A substitution of the hydrogenography data for the experimentally observed hysteresis (P_{abs} / P_{des}) in clamped (11.9) and buckled (3.05) Pd films (Fig. 4.4) at room temperature (295 K) with the gas constant, R=8.314 J/(K·mol) into the right hand side of eq. (4.4) leads to 1.67 kJ/(mol H). This reasonable agreement between experiment and theory confirms that the hysteresis increase in the clamped Pd film is essentially due to a larger expansion work during (abs)/desorption cycle, due to the significant contribution of the plastic deformation.

The same theory can be applied to relate the hysteresis in bulk Pd to the results of hydrogenography on buckled Pd films. With the same procedure an increase of ΔG_{hyst} in buckled Pd with respect to bulk material can be calculated (0.653 kJ/(mol H)) using the mechanical work in the delaminated Pd sample as estimated from Fig. 4.12. Here the ΔG of Pd bulk is taken as zero as there is no expansion constraint and, consequently, no increase of the plastic contribution to the intrinsic hysteresis. A simple reorganization of the eq. (4) and a substitution of ΔG_{hyst} along with the pressure ratio, P_{abs} / P_{des} measured in buckled sample at RT gives a value for the hysteresis in Pd bulk of about 1.8, which fits well with the literature data, 1.78 ±2.1 [14,29,30]. This example again shows the importance of plastic deformations on the hysteresis in metal hydride thin films.

From the extrapolation of the Van 't Hoff plots for desorption and absorption we find that the plastic deformations also influence the critical point, T_c in the clamped Pd films. The elastic H-H interaction is usually attractive and should reduce due to clamping effect [7]. This consequently should lead to a decrease of the critical point, as was observed in the buckled Pd films [4]. To verify whether the increase in T_c is due an incorrect extrapolation of the Van 't Hoff plot from low to high temperatures (close to T_c), a direct measurement of T_c is required. Unfortunately, this point remains unresolved as the maximum temperature that hydrogenography set up can reach is 573 K, which is lower than the extrapolated critical point, i.e. 693 K.

4.2.4 Conclusion

Highly adhesive Pd thin films exhibit a much larger hysteresis on hydrogen cycling than weakly adhesive films. Using Pd thin film with Ti adhesive layer as a model system, we show that hydrogen absorption and desorption induces a rearrangement and pile up of the material. The volume strain of the clamped Pd, measured by XRD is found to be very similar to that of bulk Pd and buckled Pd films, meaning that the macroscopic volume expansion in Pd/Ti thin films takes place mainly plastically and only in the vertical direction. The adhesion of this film is higher than the critical stresses to detach the film from the substrate to form buckles, leading to compressive stresses of the order of 1.5 GPa. As a result the hydrogenation hysteresis is expanded. Using the hydrogenography technique we have determined that the enthalpy of hydride formation and decomposition of Ti buffered Pd films respectively increase by 2.7 kJ/mol H_2 and decrease by 1.3 kJ/mol H_2 as compared with the values for buckled Pd films: ΔH_{abs}= - 31.9 kJ/mol H_2 and ΔH_{des}= - 42.4 kJ/mol H_2. A stress-strain analysis comparing the buckled and clamped Pd materials show that the hysteresis increase and the change of the thermodynamics correlate with the mechanical work on cycling.

There are two possible ways for stress release in thin films during hydrogen cycling, namely buckle formation and material pile up. In the first case in-plane mechanical compressive stresses are released by the delamination of the film. Loosely bound to the substrate, these samples show a thermodynamic behavior similar to that of the corresponding bulk materials. In the second case, larger expansion constraint and higher plastic deformations indeed change the thermodynamics of the system. However, the influence of the stress energy on the thermodynamic properties in the case of clamped Pd films is rather small - the change in the thermodynamics of the system is only 2.7 and 1.3 kJ/mol H_2 respectively in the absorption and in the desorption. In other materials the difference in elastic constants between metallic and hydrided state and a volume expansion might be larger, which would results in a stronger influence of the stress energy on the thermodynamics behavior of thin films. However, a simple stress-strain analysis would allow to recalculate the bulk enthalpies of the hydride formation and decomposition from the corresponding films results, obtained with the Hydrogenography. We therefore conclude that thin films, buckled or clamped can be used as a model system to probe thermodynamic properties of metal hydride storage materials.

4.2.5 References

[1] A. Remhof, B. Hjörvarsson, R. Griessen, I. Giebels, and B. Dam, Hydrogen Functionalized Materials, in : A. Züttel, A. Borgschulte, L. Schlapbach (Eds.), Hydrogen as a Future Energy Carrier, Wiley-VCH Verlag GmbH & Co. KGaA, Weinheim, 2008, pp. 275-334.

[2] B. Dam, R. Gremaud, C. Broedersz and R. Griessen, Combinatorial thin film methods for the search of new lightweight metal hydrides, Scripta Mater. 56 (2007) 853-858.

[3] R. Gremaud, C. Broedersz, D. Borsa, A. Borgschulte, P. Mauron, H. Schreuders, B. Dam and R. Griessen, Hydrogenography: An optical combinatorial method to find new light-weight hydrogen-storage materials, Adv. Mater. 19 (2007) 2813.

[4] Y. Pivak, R. Gremaud, K. Gross, M. Gonzalez-Silveira, A. Walton, D. Book, H. Schreuders, B. Dam and R. Griessen, Effect of the substrate on the thermodynamic properties of PdH_x films studied by hydrogenography, Scripta Mater. 60 (2008) 348.

[5] U. Laudahn, A. Pundt, M. Biker, U.V. Hulsen, U. Geyer, T. Wagner, R. Kirchheim, Hydrogen-induced stress in Nb single layers, J. Alloys Comp. 293-295 (1999) 490.

[6] B. Hjørvarsson, G. Andersson, E. Karlsson, Metallic superlattices: quasi two-dimensional playground for hydrogen, J. Alloys Comp. 253-254 (1997) 51.
[7] A. Baldi, M. Gonzalez-Silveira, V. Plamisano, B. Dam and R. Griessen, Destabilization of the Mg-H system through Elastic constrains, Phys. Rev. Lett. 102 (2009) 226102.
[8] G. Song, M. Geitz, A. Abromeit, and H. Zabel, Solubility isotherms of hydrogen in epitaxial Nb(110) films, Phys. Rev. B 54 (19) (1996) 14093.
[9] A. Pundt, E. Nikitin, P. Pekarski, R. Kirchheim, Adhesion energy between metal films and polymers obtained by studying buckling induced by hydrogen, Acta Mater. 52 (2004) 1579.
[10] R. Gremaud, M. Gonzalez-Silveira, Y. Pivak, S. de Man, M. Slaman, B. Dam and R. Griessen, Hydrogenography of PdH_x thin films: Influence of H-induced stress relaxation processes, Acta Mater. 57(4) (2008) 1209.
[11] M.W. Lee and R. Glosser, Pressure concentration isotherms of thin films of the palladium-hydrogen system as modified by film thickness, hydrogen cycling, and stress, J. Appl. Phys. 57 (12) (1985) 5236.
[12] S. Wagner, A. Pundt, Mechanical stress impact on thin $Pd_{1-x}Fe_x$ film thermodynamic properties, Appl. Phys. Lett. 92 (2008) 051914.
[13] R. Gremaud, M. Slaman, H. Schreuders, B. Dam, and R. Griessen, An optical method to determine the thermodynamics of hydrogen absorption and desorption in metals, Appl. Phys. Let. 91 (2006) 213916.
[14] S. Qian and D.O. Northwood, Hysteresis in metal-hydrogen systems: a critical review of the experimental observations and theoretical models, Int. J. Hydrogen Energy 13(1) (1988) 25.
[15] F.A. Lewis, The Palladium-Hydrogen System, Academic Press, London, 1967.
[16] F.D. Manchester, Phase diagrams of binary hydrogen alloys, ASM International, Materials Park, 2000.
[17] K. Northemann, R. Kirchheim, A. Pundt, Surface modification of Nb-films during hydrogen loading, J. Alloys and Comp. 356-357 (2003) 541.
[18] A. Pundt, M. Getzlaff, M. Bode, R. Kirchheim, R. Wiesendanger, H-induced plastic deformation of Gd thin films studied by STM, Phys. Rev. B 61 (2000) 9964.
[19] H. Zabel and H. Peisl, Sample-Shape-Dependent Phase Transition of Hydrogen in Niobium, Phys. Lett. 42 (1979) 511.
[20] R.B. Schwartz, A.G. Khachaturyan, Thermodynamics of open two-phase systems with coherent interfaces: Application to metal-hydrogen systems, Acta Mater. 54(2006) 313.

[21] A.R. Ubbelhode, Some properties of the metallic state. I. Metallic hydrogen and its alloys, Proc. R. Soc. A 159 (1937).
[22] D.W. Everett and P. Nordon, Hysteresis in the Palladium + Hydrogen System, Proc. R. Soc. A 259 (1960) 341.
[23] N.A. Scholtus and W.K. Hall, Hysteresis in the Palladium-Hydrogen System, J. Chem. Phys. 39 (1963) 868.
[24] H.K. Birnbaum, M.L. Grossbeck and M. Amano, Hydride precipitation in Nb and some properties of NbH, J. Less-Common Metals 49 (1976) 357.
[25] T.B. Flanagan and J.D. Clewley, Hysteresis in metal hydrides, J. Less-Common Metals 83 (1982) 127.
[26] V.K. Sinha and W.E. Wallace, Strain-energy model for solid-solution limits in Zr+H system, J. Less-Common Metals 91 (1983) 239.
[27] S. Tanaka, Hysteresis of hydrogen absorption (and desorption) isotherms in the α-β two-phase region of $LaNi_5$, J. Less-Common Metals 89 (1983) 169.
[28] A.Y. Esayed and D.O. Northwood, Hysteresis in $(Nb_{1-x}Fe_x)_{1-y}Cr_y$-H systems: Effect of composition, temperature and cycling, Int. J. Hydrogen Energy 18(4) (1993) 301.
[29] E. Wicke nad G, Nenrst, Ber. Bunsenges Physik. Chem. 68 (1964) 224.
[30] T.B. Flanagan, J.D. Clewly, T. Kuji, C.-N. Park and D.H. Everett, Isobaric and isothermal hysteresis in metal hydrides and oxides J. CheM. Soc., Faraday Trans. 1 82 (1986) 2589.
[31] S. Qian and D.O. Northwood, Elastic and plastic accommodation effects on hysteresis during hydride formation and decomposition, Int. J. Hydrogen Energy 15(9) (1990) 649.
[32] R. Balasubramanian, Hysteresis in metal-hydrogen systems, J. Alloys Comp. 253-254 (1997) 203.
[33] T.H. Courtney, Mechanical Behavior of Materials, McGraw-Hill, New York, 1990.
[34] A. Pundt, Hydrogen in Nano-sized Metals, Adv. Mater. 6 (2004) 11.
[35] S. Wagner, A. Pundt, Acta Materialia 58 (2010) 1387.
[36] G. Simmons, H. Wang, Single Crystal Elastic Constants, 2nd ed., MIT Press, Cambridge, 1971.
[37] A. Pundt and R. Kircheim, Hydrogen in metals: Microstructural aspects, Annu. Rev. Mater. 36 (2006) 555.
[38] A. Ludwig, J. Cao, A. Savan, M. Ehmann, High-throughput characterization of hydrogen storage materials using thin films on micromachined Si substrates, J. Alloys Comp. 446-447 (2007) 516.

[39] J. Peisl, Hydrogen in Metals I, in: G. Alefeld and J. Volkl (Eds.), Topics in Applied Physics, Vol .28 (Springer-Verlag), 1978.

[40] Ch. Rehm, H. Fritzsche, H. Maletta and F. Klose, Hydrogen concentration and its relation to interplanar spacing and layer thickness of 1000-Å Nb(110) films during in-situ hydrogen charging experiments, Phys. Rev. B 59 (1999) 3142.

[41] H. Zabel and B. Hjørvarsson, Hydrogen in thin films and multilayers, in: Goltsov V.A. (Ed.), Progress in Hydrogen Treatment of Materials, Donetsk-Coral Gables, Kassiopeya, Donestk, 2001.

Chapter 5

Effect of the structure transformation on the hysteresis behavior of $La_{1-z}Y_z$ films

5.1 Introduction

The stress-strain model we developed allows us to understand both qualitatively and quantitatively, the influence of the substrate on the thermodynamics and hysteresis behavior of thin Pd films with an iso-structural transformation. However, Pd is rather an exception than a common representative, since for many metal hydrides, such as MgH_2 and Mg_2NiH_4, the phase transition from the metallic to hydrided state is accompanied by a structural transformation. Additionally, the mechanical properties of Pd barely change on going from the metal to the hydride phase, which is not the case for the Mg-based materials, having metal-to-insulator transition. All these parameters may have an additional impact on the plastic deformations and, consequently, on the thermodynamic properties of thin film metal hydrides with respect to the corresponding bulk materials.

In this chapter we study the effect of a structural transformation on the (de-)hydrogenation properties of metal hydride thin films using the La-Y system as an example. This system is characterized by a metal to semiconductor transition, while the structural and volumetric change depends on the Y/La ratio. Using hydrogenography we measured pressure-transmission-isotherms of the $La_{1-z}Y_z$ films in a wide temperature range (333 K–523 K), which revealed a considerable difference in hysteresis behavior between LaH_x, $La_{0.6}Y_{0.4}H_x$ and YH_x films. The hysteresis in La-containing films is found essentially the same as in bulk materials, while the hysteresis in YH_x films is about 2-3 orders of magnitude (473–523 K), much higher than in bulk. The stress-strain theory, applied to explain the huge hysteresis in YH_x films, quantitatively confirms that this is caused by a

combined effect of both the mechanical work done by the film during (de-)hydrogenation and the fcc-hex structure transformation in these preferentially oriented thin films. Hence, when applying the stress-strain model, in addition to volumetric changes has to take structural issues into account, especially in preferentially oriented thin films.

5.2 Hysteresis behavior and stress-strain analysis of $La_{1-z}Y_zH_x$ films, studied by means of Hydrogenography

Abstract:

The (de-)hydrogenation properties of $La_{1-z}Y_zH_x$ (z= 0, 0.4, 1) thin films during dihydride-trihydride transition were investigated by means of Hydrogenography. We show that La-rich films, i.e. LaH_x and $La_{0.6}Y_{0.4}H_x$, are almost hysteresis free in the temperature range 423–523 K. This appears to be due to a small and/or negative volume expansion and the absence of the structure transformation on hydrogenation. The presence of the small difference between absorption and desorption sloping plateaus in these films, is assigned to minor plastic deformations due to the substrate clamping. On the contrary, YH_x films, expand by about 12 % between the dihydride and the trihydride. They moreover exhibit an fcc-hex structure transformation, show a huge (2-3 orders of magnitude) hysteresis. This giant hysteresis is caused, according to our stress-strain analysis, by the clamping induced mechanical work done by the film during (de-)hydrogenation and the reorientation required to maintain the preferential orientation during the fcc-hex structure transformation. Using our stress-strain model, improved by an additional structural parameter ($\Delta G_{fcc-hex}$,), we were able to predict the increase of the hysteresis in both, thin and thick YH_x films measured at 523 K and at 295 K, respectively.

5.2.1 Introduction

The discovery of the switchable mirror effect in YH_x and LaH_x films [1, 2] has led to substantial technological interest in these rare-earth (RE) metals as well as their alloys. RE films exhibit a drastic change of their optical properties when hydrogen concentration, x, increases from 2 H/M to 3 H/M [3]. This change from the reflective (metallic) into the transparent (insulating) state on hydrogenation is reversible and can be induced via the gas phase or, which is more important, electrochemically [4, 5]. Along with a possibility to tune the optical properties by the level of doping in RE-based alloys [2, 3], it makes these materials very interesting for a practical application in smart windows [6] and hydrogen sensors [7].

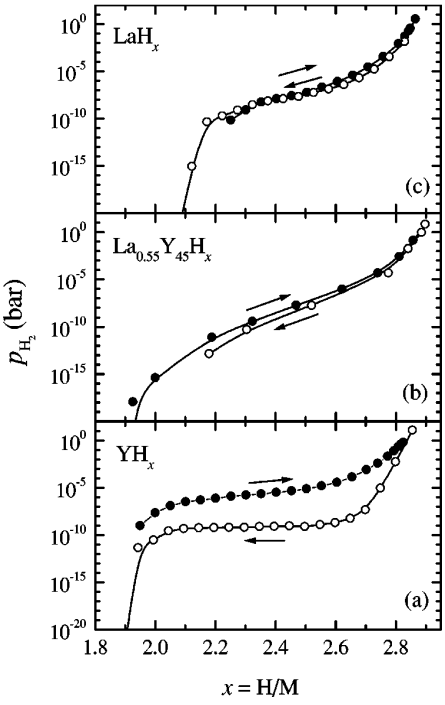

Fig. 5.1. Pressure-composition-isotherms for YH_x (a), $La_{0.55}Y_{0.45}H_x$ (b), and LaH_x (c) at 295 K, determined electrochemically (Figure is taken from [8]).

The $La_{1-z}Y_zH_x$ (z=0-1) system, which has been studied already in thin films before, has very interesting and peculiar properties. Both yttrium and lanthanum are chemically very similar and form a solid solution over almost the whole composition range [9]. For $z \leq 0.4$ and for $z \geq 0.6$ the alloys have a La double hexagonal closed packed (dhcp) and hexagonal close packed (hcp) structures, respectively; in the small concentration region, $0.4<z<0.6$, the alloys form the Sm-type structure [9]. On hydrogenation from x=0 H/M till x=2 H/M, all alloys transform to an fcc dihydride (β) phase. However, they start to behave differently for x between 2 H/M and 3 H/M. During the transition from the dihydride (β), to the trihydride (γ), YH_x films change their structure from fcc to hexagonal, which is accompanied by a large increase in cell volume. Oppositely, the structure of LaH_x films remains fcc and the volume is actually slightly decreasing on hydrogen absorption. Besides structural discrepancies, also the (de-)hydrogenation behavior substantially differs between LaH_x and YH_x films. Electrochemical experiments at 295 K (Fig. 5.1) reveal a negligible difference between absorption and desorption equilibrium pressures for La-rich films, while YH_x films show a very large hysteresis [8, 10, 11].

There are several papers dedicated to explain the presence of the huge hysteresis in YH_x films. Based on structural, electrochemical and optical experiments of YH_x films, Kooij et al. [10] concluded that the origin of the large hysteresis is the fcc-hex structure transformation, which occurs in a very narrow concentration range: he suggests that a two-phase region of face centered cubic and hexagonal structures exists for only $1.9<x<2.1$ (Fig. 5.2 (a)), which is in contrast with the bulk behavior [12]. The authors claim, that due to the internal (clamping induced) stress the enthalpy of hydrogenation is increased by about 14-22 kJ/mol H_2 as compared to YH_x bulk, whereas the enthalpy of decomposition was found essentially the same as in bulk. From the (de-)hydrogenation pressure-concentration-isotherms measured at 293 K these authors calculated that the energy involved in the fcc-hex transformation is $\delta(\Delta H)=9$ kJ/molH_2. This difference is of the same order of magnitude as the value $\delta(\Delta H)=9.64$ and 17.76 kJ/molH_2 calculated from the hysteresis in the equilibrium potential for hydrogen intercalation in NiO_2H_x (0.050 and 0.092 V for electrodes with and without cobalt hydroxide, respectively) in the work of Ta and Newman [13]. Later, in order to explain structural and optical behavior of YH_x film on (de-)hydrogenation, van Gogh et al. [11] developed a more descriptive qualitative model using the loading sequence proposed by Kooij et al. [10]. According to this model, the nucleus of the hex-$YH_{2.7}$, which is formed during hydrogen absorption from the dihydride phase, expands by about 10% along the c axis while remaining in tight lateral mechanical contact, due to clamping, with the neighboring fcc-$YH_{1.9}$. The local c-axis expansion of the hex-$YH_{2.7}$ nuclei is then able to expand the surrounding fcc-$YH_{1.9}$ nuclei along the c axis to such an extent that they are mechanically transformed into hexagonal $YH_{1.9}$ (See Fig. 4 in

[11]). Subsequently, hydrogen diffuses from the initial hex-$YH_{2.7}$ to the neighboring hex-$YH_{1.9}$ until diffusive equilibrium is reached, resulting in a fully hexagonal film with an overall hydrogen concentration x=2.1 (Fig. 5.2 (a)) and the in-plane compressive stress state. During desorption the opposite situation is taking place. When the first fcc-$YH_{2.0}$ nucleus is formed within the hex-$YH_{2.7}$ matrix it shrinks, but, instead of transforming the surrounding hex-$YH_{2.7}$ into fcc, it releases the compressive stresses, resulting in a broad two-phase region ($2<x<2.7$) consisting of fcc-$YH_{2.0}$ and hex-$YH_{2.7}$, as in bulk. Therefore, the authors argued that the huge hysteresis found in YH_x films is caused by a large uniaxial lattice expansion that accompanies the fcc to hexagonal phase transition in combination with the lateral clamping.

In an attempt to solve the mystery of the enormous hysteresis of YH_x films, another set of experiments were performed by Remhof and co-workers [12]. Simultaneous in-situ optical, resistivity and structural measurements on YH_x films led to the conclusion that the phase boundaries reported earlier by Kooij et al. [10] are not correct. The biggest difference with respect to the previous data [10] is in the loading phase diagram, where, according to the new results, the β-phase exists only until x=2.1 H/M while the coexistence region between cubic and hexagonal phase extends till x=2.7 H/M (Fig. 5.2 (b)); note that these thin film results are in line with the bulk phase diagram (Fig. 5.2 (a)). On desorption, nucleation of the β-phase starts at 2.65 and continues until 1.9, which is smaller as compared to loading boundaries (Fig. 5.2 (b)). It is important to point out that the phase boundaries were not determined using PCI's and that the optical/structural/electrical experiments were conducted in a dynamic mode which is in contrast with the measurements of Kooij et al. [10]. The authors also confirmed the presence of a large hysteresis in the optical and electrical results, which, however, was assigned to intrinsic concentration dependent properties of the cubic β-phase [12]. They argued that the fcc-hex phase transformation plays a major role in the hysteresis behavior, though no elaborate explanation was provided.

Hence, in spite of all this work, there is no quantitative model to explain the hysteresis behavior in YH_x.

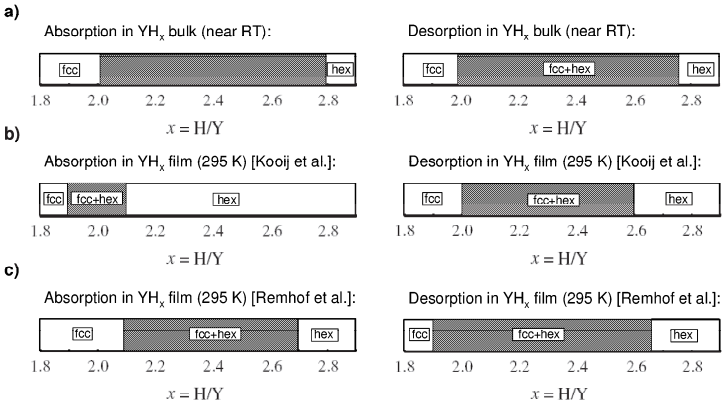

Fig. 5.2. Phase boundaries during absorption and desorption in bulk (a) [14] (top), YH_x films (middle) [Kooij et al., 10] and YH_x films (bottom) [Remhof et al., 12].

Therefore, we investigate the (de-)hydrogenation behavior of La, $La_{0.6}Y_{0.4}$ and Y thin films in more detail and for the first time using Hydrogenography, allowing us to directly compare various compositions. We show that the phase transition from LaH_2 to LaH_3, taking place without a structure transformation, is almost hysteresis free (P_{abs}/P_{des}=2) and does not depend on the temperature within the studied temperature range 423–523 K. On the other hand, the formation of yttrium trihydride, accompanied by the fcc-hex phase transformation, shows an enormous hysteresis of several orders of magnitude (P_{abs}/P_{des}=6200 at 423 K). At 523 K the hysteresis in YH_x thin films is still 74 times larger as compared to bulk. A stress-strain analysis, modified by an additional parameter related to the fcc-hex structure transformation between two preferentially oriented phases quantitatively explains the large difference between hydride formation and decomposition in Y hydride films.

5.2.2 Experimental details

Thin $La_{1-z}Y_z$ (z=0, 0.4, 1) films with a thickness of 40 nm were prepared by co-sputtering the parent metals in a dc/rf magnetron deposition system (background pressure 10^{-7} Pa, argon deposition pressure 0.3 Pa). Due to the highly reactive nature of rare-earth metals with respect to oxygen and water, a buffer layer of Ta of 10 nm was sputtered on the glass substrate before the deposition of the La-Y films. Another layer of Ta (10 nm) was sputtered on top of the film, which, except for the oxidation protection, is used to prevent

alloying between La-Y and the Pd capping layer deposited on top of the layer stack. The Pd cap layer with a thickness of 20 nm, which also acts as a barrier for oxygen diffusion into the film, is necessary as a catalyst for H_2 dissociation during the (de-)hydrogenation experiments.

After deposition, the metallic La-Y films were directly transferred to the hydrogenography setup [15] to minimize exposure to air. Hydrogenography experiments were conducted in the temperature range 333–523 K and the pressure range 0.1 Pa – 10^5 Pa. At first, La-Y films were subjected to approximately 6-8 fast loading and unloading cycles at the measurement temperature. The fast absorption was performed in hydrogen atmosphere within one hour, whereas desorption was carried in vacuum within 1-2 hours. Then the equilibrium Pressure-Transmission-Isotherms (PTI's) were measured using both, step and continuous scans of pressure changing, where the first option was used to check the kinetics of the studied films [15]. Typical loading/unloading times of the $La_{1-z}Y_z$ films are 40 hours/70 hours and 24 hours/24 hours at 423 K and 523 K respectively. The absorption/desorption pressures determined from the midpoint of the corresponding PTI's, were used to construct Van 't Hoff plots and to estimate the enthalpy and entropy of hydride formation/decomposition.

The structural properties of La-Y films were studied ex-situ using a Bruker AXS D-8 diffractometer equipped with a LynxEye detector at room temperature. XRD scans were collected using Co-K_α radiation (λ=1.78897 Å) and a Bragg-Brentano geometry in the angle range 20^o-80^o with a step of 0.02^o and a collecting time of 0.2 seconds per step. The phase analysis and lattice parameter calculations of the La-Y films in the as-deposited and cycled state were performed using ICDD (PDF) database and DIFFRAC^{plus} EVA package program, respectively.

5.2.3 Results and discussion

Structural characterization of $La_{1-z}Y_z$ films

All the films in the as-deposited state show similar diffraction patterns, containing 4 reflections coming from the La-Y film itself and two additional peaks around 38.4^o and 47.0^o, coming from the capping Pd and protective Ta layers, respectively (Fig. 5.3). Based on the position of the observed peaks, La and Y films have been indexed on the basis of the dhcp ($P6_3/mmc$) and hcp ($P6_3/mmc$) lattices, respectively, in agreement with literature [8, 16, 17]. The structure of the $La_{0.6}Y_{0.4}$ film was more difficult to identify, as it could be indexed on the basis of both a dhcp and a Sm (R-3m) type lattice [9]. The Sm structure is very similar to that of dhcp but with an extended c lattice parameter, i.e. $c_{dhcp}=c_{Sm}/9$, which

should lead to extra reflections in the diffraction pattern. The absence of additional reflections in the XRD spectra of $La_{0.6}Y_{0.4}$ films, caused by the preferential growth, complicates the analysis. In fact, all films exhibit a preferred orientation in the (00l) direction perpendicular to the surface.

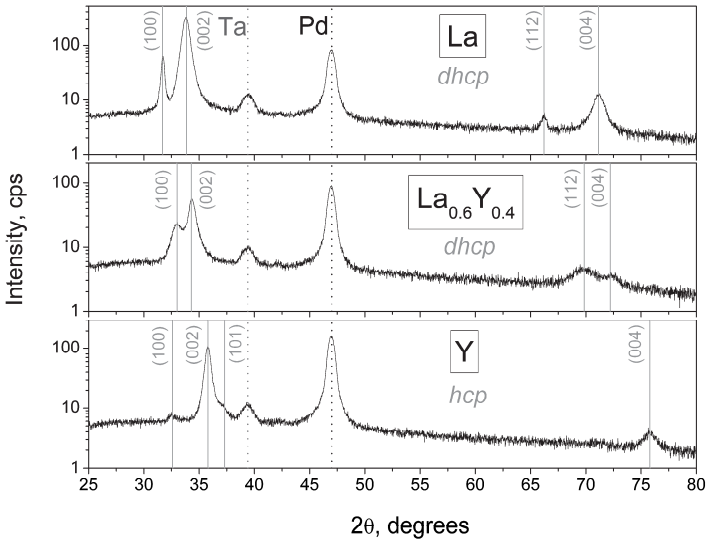

Fig. 5.3. XRD spectra of La, $La_{0.6}Y_{0.4}$ and Y films in the as-deposited state. Solid vertical lines represent the peak position of the $La_{1-z}Y_z$ phases; dotted vertical lines show reflections from Ta and Pd layers. Vertical numbers represent reflection indices of the dhcp (La, $La_{0.6}Y_{0.4}$) and hcp (Y) structures.

To clarify the structure type one might consider the *c*/*a* ratio, which is found to have a strong correlation with the observed crystal structure [18]. According to the calculated lattice parameters, the *c*/*a* ratio of La (1.627) and Y (1.580) films are in good agreement with the reported values for the dhcp (1.619) and hcp (1.580) structures, respectively [8]. The *c*/*a* ratio of $La_{0.6}Y_{0.4}$ film, which is hardly affected by the chosen structure type, i.e. dhcp or Sm, is close to 1.664. This value is substantially larger as compared to the reported ratio for Sm structure in $La_{0.54}Y_{0.46}$ films, i.e. 1.604 [8]. Oppositely, the calculated value (1.664) is relatively close to the *c*/*a* ratios of $La_{1-x}Y_z$ films (z=0–0.3) that form the dhcp structure, e.g. 1.619-1.639. Thus we conclude that $La_{0.6}Y_{0.4}$ films crystallize in the dhcp structure in the as-deposited state, which is in agreement with the La-Y bulk phase diagram

[9]. The somewhat larger *c/a* ratio in $La_{0.6}Y_{0.4}$ films is probably caused by the clamping, coming from the substrate [8].

To check the structural stability of $La_{1-z}Y_z$ films during (de-)hydrogenation, they were subjected to several slow loading/unloading cycles in the temperature range 423 K-523 K. The measuring time and the temperature were chosen the same used during the Hydrogenography experiments. After hydrogenation cycling, the structural changes of the La-Y films were monitored again. The XRD spectra of the cycled films (Fig. 5.4) were recorded at room temperature with exactly the same conditions as for as-deposited films. Because of the extremely low enthalpies of desorption of the La-Y dihydrides ($\Delta H \approx -220$ kJ/molH_2 [19, 20]) and, thus, the extremely low equilibrium pressures ($P_{eq} \approx 10^{-10}$ Pa at 523 K), it was impossible to completely desorb La-Y films by unloading in vacuum using Hydrogenography. Therefore, the diffraction patterns in Fig. 5.4 represent partially loaded $La_{1-z}Y_zH_x$ films (x=2 H/M).

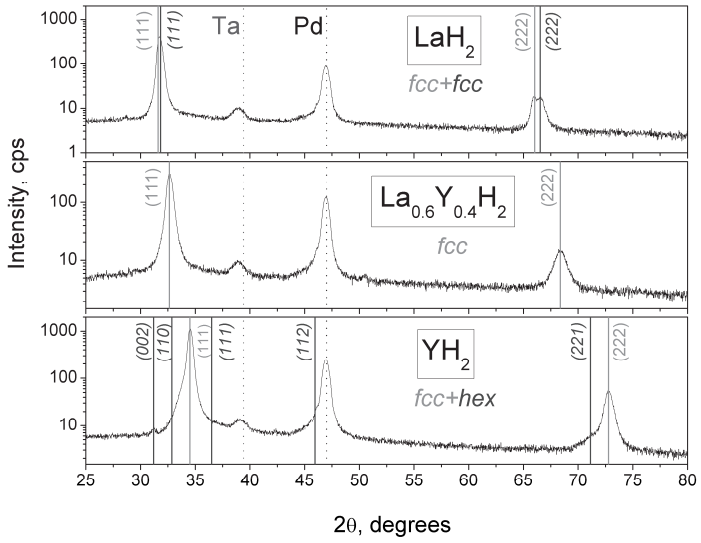

Fig. 5.4. XRD spectra of La, $La_{0.6}Y_{0.4}$ and Y films in the dihydride state after cycling (5-6 times) and hydrogenography measurements at 423 K. Solid vertical red and blue lines represent the peak position of the fcc and hex phases in YH_2 films, respectively; in the case of LaH_2 films these lines represent two fcc phases with different lattice parameters. Normal (red) and italic (blue) vertical numbers indicate reflection indices corresponding to the major and additional phases, respectively. Dotted vertical lines show reflections from Ta and Pd layers.

After the cycling, all films retained their long-range crystallinity and even improved it, as visible from an order magnitude increase (Y) in peak intensities (Fig. 5.4). The structure of cycled La-Y films is fcc with a preferred orientation in the (111) direction. While $La_{0.6}Y_{0.4}H_2$ is single-phase, LaH_2 and YH_2 show additional reflections in the diffraction pattern (blue lines in Fig. 5.2). A closer look reveals a presence of a second fcc and hexagonal (P-3c1) phase [8, 21] in LaH_x and YH_x films, respectively. Remarkably, the molar volumes of these second phases are found close to that of the fully hydrided states, Re-$H_{3-\delta}$ (filled diamonds in Fig. 5.5). Therefore, we conclude that the appearance of the trihydride phases in the XRD scans is caused by an incomplete desorption of La and Y films during (de-)hydrogenation cycling.

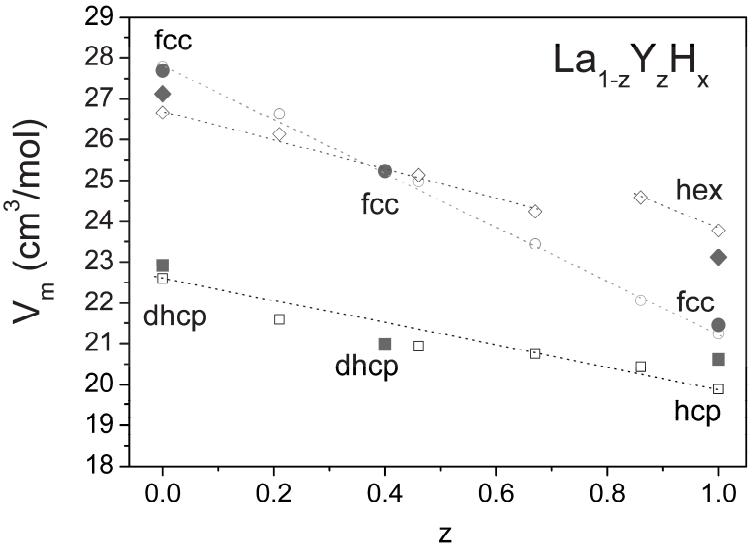

Fig. 5.5. Molar volume of $La_{1-z}Y_zH_x$ films as a function of z in the metal state (x=0, filled squares), dihydride (x=2, filled circles) and trihydride (x=3, filled diamonds). Open symbols are literature values for $La_{1-z}Y_zH_x$ films, measured by van Gogh [8]. Dotted lines are guides to the eye.

The molar volume, V_M, of metal and dihydride phases of $La_{1-z}Y_z$ films, calculated from the lattice parameters is shown in Fig. 5.5 along with the literature results on the same system. The agreement is good between the current and the previous measurements for the dihydride phases, though the results for the as-deposited state are somewhat deviating. For YH_x the volume expansion during dihydride-trihydride transformation, as calculated by van Gogh [8], is used in the stress-strain analysis of our YH_x films.

(De-)hydrogenation behavior of LaH_x and YH_x thin films

As mentioned previously, La-Y films remain in the dihydride state after desorption once they have loaded to the trihydride state. Therefore, the current chapter is focused on the (de-)hydrogenation properties of La-Y films during dihydride to trihydride transformation.

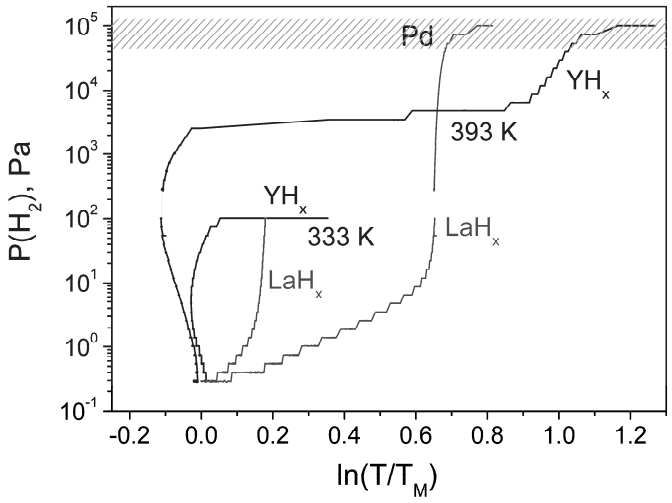

Fig. 5.6. Loading pressure-transmission-isotherms of YH_x (black line) and LaH_x (blue line) films at 333 K and 393 K. The second plateau at around 10^5 Pa on the PTI's measured at 393 K corresponds to the hydrogenation of the Pd capping layer.

At first, a few exploratory loading isotherms are measured simultaneously for Y and La at 333 K and 393 K, in order to verify the pressure range and the kinetics of hydrogenation reaction. Well-defined steps in Fig. 5.6 suggest that the hydrogen loading process occurs under quasi-equilibrium conditions in both films. From this we choose a pressure ramp of 2.34×10^{-5} log(Pa)/sec for the continuous measurements. Due to the difference in the thermodynamic properties between YH_3 and LaH_3, the loading of the YH_x film at 333 K is incomplete in the chosen pressure range, just showing the beginning of the flat plateau, while for the LaH_x film only the final part of the isotherm is visible (Fig. 5.6). At 393 K, the pressure-transmission-isotherm of LaH_x is almost complete but with a sloping plateau, typical for LaH_x system [8]. On the other hand, YH_x shows a well-defined equilibrium plateau at this temperature. The second plateau, exhibited in the PTI's of both

LaH_x and YH_x films at higher pressures, (~10^5 Pa), corresponds to the Pd capping layer. It is worth mentioning that the change of the sign of the $\ln(T/T_M)$ in the beginning of the loading isotherms at 333 K and 393 K is caused by the darkening of YH_x films during hydrogen absorption from x=2 H/M to x=2.1 H/M [8, 10].

For a complete isotherm of LaH_x, we have to raise the experimental temperature to 423 K (Fig. 5.7). We observe that the absorption as well as the desorption plateau remains sloping in the LaH_x films. It is important to stress that the slope is not connected to the kinetics of (de-)hydrogenation reaction (see Fig. 5.6), but has a different origin. The results shown in Fig. 5.7 also reveal that there is a minor difference between the loading and unloading branches of the isotherm ($P_{abs}/P_{des} \approx 2$) in LaH_x films. The YH_x films, on the other hand, exhibit very flat equilibrium plateaus with an enormous difference between absorption and desorption pressures ($P_{abs}/P_{des} \approx 6200$). The same experimental results, namely giant hysteresis (more than 3 orders of magnitude) and small hysteresis, were previously observed in YH_x and LaH_x films at room temperature [8] using electrochemical loading and a resistive measurement of the hydrogenation. The huge difference in hysteresis behavior between YH_x and LaH_x films, was attributed by Van Gogh [8], to the fcc-hex structure transformation taking place in Y during (de-)hydrogenation, which is absent in the La system [19, 24, 25].

A further increase of the temperature leads to some changes in the pressure-transmission-isotherms of LaH_x and YH_x films (see fig. 5.8). Thus, the whole plateau region of LaH_x isotherm flattens and becomes well-defined The possible reasons for this behavior might be connected to (i) the microstructure rearrangement, releasing stresses in this way in LaH_x films, and/or (ii) hydrogen ordering in the lattice. It is worth mentioning that the presence of the plateau in LaH_x films at 523 K is in a fair agreement with the pressure-concentration-isotherm of bulk LaH_x recently measured by means of neutron diffraction at 573 K [27] (see inset in Fig. 5.8). In the case of YH_x films, an anomalously large decrease in plateau width is taking place from 423 K to 523 K. This behavior is attributed to the formation of a secondary plateau, which, however, can not been seen because of the limited pressure range used at 523 K. Nevertheless, the presence of the second plateau was verified by subsequent (de-)hydrogenation (2^{nd}, 3^{d}) cycling at 423 K (not shown here). The appearance of a second plateau in the PTI's suggests the formation of a second phase in YH_x films, which is believed to originate from the high stress gradients in the films upon hydrogen cycling at elevated temperatures.

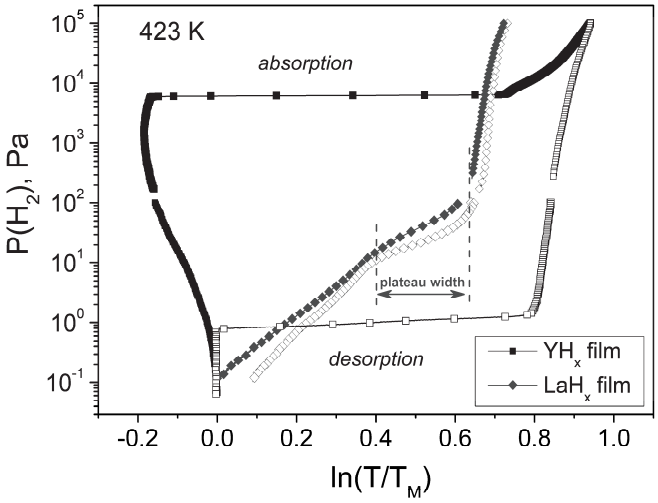

Fig. 5.7. Pressure-Transmission-Isotherms of YH_x (black line) and LaH_x (blue line) at 423 K. Vertical dotted lines represent the phase boundaries and the width of the plateau in LaH_x films measured at 423 K.

Although the shape of the plateaus have changed for PTI's, recorded at 523 K (Fig. 5.8), the hysteresis behavior of La-Y films exhibits the same characteristics. The hysteresis of the YH_x films becomes much smaller at 523 K, i.e. $P_{abs}/P_{des} \approx 224$, however, it is still considerably larger as compared to the essentially hysteresis free LaH_x films ($P_{abs}/P_{des} \approx 1.36$).

Unfortunately, we are not aware of any bulk hysteresis data for the La-H system. However, the small size of the hysteresis observed in LaH_x films both within and outside the plateau region (Fig. 5.8, 5.9) resembles that of many bulk metal hydrides (Pd, $LaNi_5$, Mg, etc.) [28-30]. We attribute the small influence of the substrate on the hysteresis of LaH_x films mainly to the fact that LaH_x does not show a structure transformation. The effect of structure transformation is nicely illustrated by the case of Y-H.

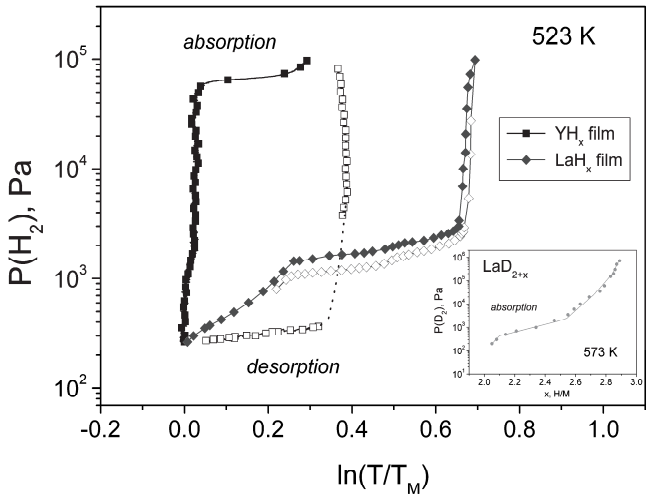

Fig. 5.8. Pressure-Transmission-Isotherms of YH_x (black line) and LaH_x (blue line) at 523 K. Dotted line represents a region of the unloading PTI of YH_x film, where no experimental data are available. The inset shows a pressure-concentration-isotherm of LaD_{2+x} bulk sample, measured at 573 K by means of neutron diffraction [27]; the solid line in the inset is a guide to the eye.

YH_x films expand by about 11.9 % [8] upon the dihydride-trihydride transition and go through a structure transformation. As compared to bulk YH_x the hysteresis in YH_x films is 75 times larger at 523 K (Fig. 5.9), where, similarly to clamped PdH_x films (Chapter 4), the absorption isotherm is affected more strongly than the desorption isotherm. As a result, the enthalpies of hydride formation and decomposition of YH_x films are found larger and smaller by 40.7 kJ/molH_2 and 15.2 kJ/molH_2, respectively as compared to the bulk data; the bulk thermodynamics is estimated from the equilibrium pressures, measured by Yanapopoulos et al. [32] using volumetry in the range 523–600 K. It is, however, interesting to note that the critical temperature (T_{crit}) appears to be not lowered in YH_x films, which would be expected considering only a change in the elastic H-H interaction in clamped thin films (lattice gas model): an extrapolation of the linear fit to absorption and desorption data to high temperatures (dotted lines in Fig. 5.9) gives the critical temperature of 923 K for YH_x films, which is somewhat larger as compared to the approximated T_{crit} of the fcc-hex coexistence region in the YH_x bulk phase diagram, i.e. 800 K [20]. A similar situation was observed for the clamped Pd films [31], where the extrapolated critical temperature was found to be only slightly higher than in bulk Pd.

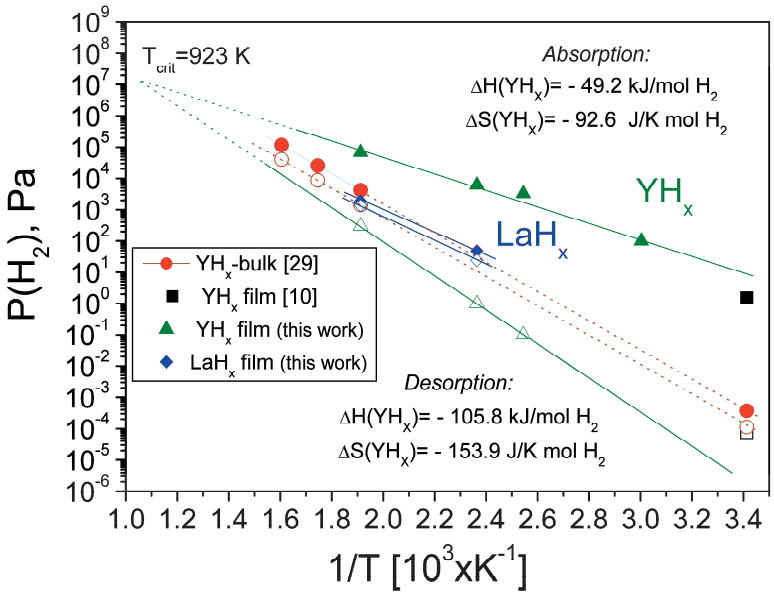

Fig. 5.9. Van 't Hoff plot of LaH_x (blue diamonds) and YH_x (green triangles) films. Red circles are the YH_x bulk data [32]; points at 295 K are extrapolated equilibrium pressures from the measured high temperature data. Black squares are the YH_x thin films results, measured at 295 K by electrochemistry [10]. Filled and open symbols represent absorption and desorption, respectively. Enthalpies and entropies for YH_x films are calculated from the linear fit to the experimental data; the dotted line is an extrapolation to high temperatures, showing the critical temperature, T_{crit}.

Similarly to YH_x, PdH_x films also have a volume expansion of about 11% during hydrogenation but without a structure transformation. Since the hysteresis in clamped Pd films is about 2 at 483 K [31], which is very close to that of Pd bulk, it is logically to assume that the influence of the substrate in YH_x films should be of the same order of magnitude at high temperatures (T>473 K), assuming that the elasticity constants are not too different. As this is not the case, we propose that the fcc-hex structure transformation rather than the clamping effect is responsible for the huge hysteresis observed in YH_x films [10]. To quantitatively model the clamping effect and to study the influence of the structure transformation on the hysteresis behavior in YH_x films, a stress-strain analysis, similar to one done for PdH_x films, is performed.

Hysteresis and stress-strain analysis of YH_X films

There exist several theories, based on elastic [35] and plastic [36, 37] deformations, explaining the presence of the hysteresis in bulk metal hydrides. These theories, however, are not fully applicable to thin films because of an additional plastic deformation, caused by the presence of the substrate [31]. This modifies the thermodynamic equilibrium condition in thin films with respect to bulk, leading to an upwards and downwards shift of the absorption and desorption plateaus, respectively [31]. As a result, the hysteresis in thin films will be expanded as compared to the intrinsic hysteresis, observed in bulk metal hydrides (Chapter 4).

To quantify the influence of the substrate on the hysteresis behavior of thin films (clamping effect), a simple stress-strain model was developed. The model, which was successfully applied for Pd films (Chapter 4), postulates that the increase of the hysteresis in thin films correlates with the extra mechanical work during a single (de-)hydrogenation cycle. This extra mechanical energy represents the expansion and contraction work performed by the film as a result of the in-plane compressive and tensile stresses during absorption and desorption, respectively [31, 38-40]. The stronger the in-plane stresses and the larger the film needs to expand/contract, the bigger the mechanical work will be and the more substantial the increase of the hysteresis in thin films as compared to bulk will appear to be.

By changing clamped and buckled subscripts in eq. (4.4) (Chapter 4) for film and bulk, respectively, the increase of the hysteresis in thin films as compared to bulk due to clamping is:

$$\frac{1}{2}RT\ln\left((P_{abs}/P_{des})_{film}/(P_{abs}/P_{des})_{bulk}\right)=\left(V_M/(c_\beta-c_\alpha)\right)\times$$

$$\times\left[\left(\int_0^{\varepsilon_{(\max)2}}\sigma_2 d\varepsilon_{V_2}\right)_{film}-\left(\int_0^{\varepsilon_{(\max)1}}\sigma_1 d\varepsilon_{V_1}\right)_{bulk}\right] \qquad (5.1)$$

where R is the gas constant, T is the absolute temperature, P_{abs} and P_{des} is the equilibrium absorption and desorption pressures, respectively, V_M is the molar volume, $c_{\beta,\alpha}$ is the maximum hydrogen concentration in the hexagonal γ–$YH_{2.7}$ (β) and cubic $YH_{2.1}$ (α) phase, respectively and σ_2, σ_1 and $\varepsilon_2, \varepsilon_1$ correspond to the stresses and volume strains in the film and bulk, respectively. Since we assume that there is no external compressive/tensile stresses acting on bulk materials during (de-)hydrogenation, i.e. σ_2=0, equation (5.1) can be rewritten as:

$$\frac{1}{2}RT\ln\left(\left(P_{abs}/P_{des}\right)_{film}/\left(P_{abs}/P_{des}\right)_{bulk}\right)=V_M/(c_\beta-c_\alpha)\cdot\int_0^{\varepsilon_{\max}}\sigma\,d\varepsilon_V=\Delta G_{hyst} \qquad (5.2)$$

Upon the development of the model it was assumed that any possible influence of the substrate on the hysteresis behavior of thin films should and will be reflected in the stress-strain curve; irrelevant to the class of the metal hydride; later we will show this does not hold for every metal hydride system. Therefore, it was concluded that the stress-strain theory can potentially be applied to any thin film metal hydride, including YH_x films. In the case of YH_x films, however, a small adjustment to eq. (5.2) as well as additional explanation should be made.

As was mentioned in the introduction, the exact reason for the huge difference between the absorption and desorption branches of the isotherm in YH films is unknown, while all existing experiments point to a relation to the fcc-hex structure transformation. Indeed, we also observe that in films without a structure transformation such as LaH_x, the hysteresis is negligible. We also observe that the widening is highly asymmetrical. The reason why the structure transformation matters for YH_x films and does not have any visible effect on bulk Y is apparently connected to the fact that the thin films are forced to maintain their (preferential) geometry due to presence of the substrate.

Our YH_x films are polycrystalline with a preferred orientation in the $(111)_{fcc}$ direction (Fig. 5.4) perpendicular to the surface normal. During the transformation, the (111) plane of the fcc structure becomes the (0001) plane of hexagonal structure, which is the only possible choice from the structural point of view (these are the planes with the highest atomic packing factor). Since almost the entire volume expansion upon YH_2-YH_3 transition takes place in the *c*-direction of the hex lattice (parallel to the film's normal) [10, 11], structure transformation of the grains, which are vertically oriented, progresses without any substantial in-plane stresses. For the grains which form an angle with the film's normal (misaligned), the volume expansion components in the in-plane direction is impeded by the in-plane compressive stresses; the larger the angle of misalignment, the bigger the opposing forces will be. This will cause part of the plastic deformation responsible for the increased hysteresis in thin films. However, we believe there is a second, even larger component. Given the symmetry of the cubic dihydride structure we have eight equivalent (111) directions. That implies that the hexagonal c-axis may form along each of them. The six axes which have an in-plane component are highly unfavorably oriented. Hexagonal nuclei formed along these directions therefore have to rearrange to minimize the stress. The plastic deformation needed for the rearrangement will further increase the hysteresis of the thin films.

Upon desorption, the hex-fcc structure transformation is taking place. In this case the $(0001)_{hex}$ grains will transform into (111) oriented grains in a unique way, since there is only one unique hexagonal c-axis. Thus upon absorption the only structural factor contributing to the hysteresis is the misorientation of the grains: we have not a perfect alignment. This is the main reason, which causes the asymmetry in the structure transformation in YH_x films.

After the desorption is complete, the film the film is back in its (111) oriented fcc state. On the following re-hydrogenation, due to the multiplicity of (111) directions again large plastic deformations need to occur to transform again the textured β-YH_2 film into the textured γ-YH_3 one, resulting in a virtually stable size of the hysteresis loop. Indeed, (de-)hydrogenation cycling of YH_x films at 423 K reveal only a small variation in the hysteresis width (averaged between two plateaus), despite appearance of the second plateau in the PTI.

Since our stress-strain model is taking into a consideration all possible effects related to the substrate interaction as compared to YH_x bulk, we include an additional structurally related parameter, $\Delta G_{fcc-hex}$ in the equation (5.2):

$$\frac{1}{2}RT\ln\left((P_{abs}/P_{des})_{film}/(P_{abs}/P_{des})_{bulk}\right)=V_M/(c_\beta-c_\alpha)\cdot\int_0^{\varepsilon_{\max}}\sigma\,d\varepsilon_V+\Delta G_{fcc-hex} \quad (5.3)$$

The additional term $\Delta G_{fcc-hex}$ represents an activation energy for the fcc-hex transformation. We assume here that the energy needed to rotate the orientation of an hcp-trihydride grain is roughly equal to the the activation energy for the fcc-hex transformation $\Delta G_{fcc-hex}$, was estimated by van Gogh et al. [8] to be 9.0 kJ/molH_2 at RT. We also consider a negligible temperature dependence of the $\Delta G_{fcc-hex}$, meaning that the same energy is involved in the fcc-hex transformation at 523 K. This temperature is chosen for the stress-strain analysis of YH_x films, as there exists an overlap between thin film and bulk experimental results, making it possible to calculate of the left side of the equation (5.3). By substituting the experimentally observed hysteresis (P_{abs} / P_{des}) in YH_x films (223.5) and in YH_x bulk (3.04) [32] at 523 K with the gas constant, R=8.314 J/(K·mol) into the left-side of eq. (5.3) along with the $\Delta G_{fcc-hex}$, we have the following equality:

$$9.34\ \text{kJ/molH}=V_M/(c_\beta-c_\alpha)\cdot\int_0^{\varepsilon_{\max}}\sigma\,d\varepsilon_V+4.50\ \text{kJ/molH} \quad (5.4)$$

To validate our stress-strain model and to prove that it can be applied to YH_x films as well, all we need is to calculate the mechanical work done by the film during the loading and unloading process.

In the previous chapter, mechanical work was calculated from the stress-strain curve, constructed on the basis of hydrogenation stresses and volume expansion. Stresses and strains of Pd films during (de-)hydrogenation were calculated and measured, respectively by means of X-ray diffraction experiments. Using these results it was possible to precisely depict elastic and plastic deformations of the studied films during hydrogen absorption and desorption. Unavailability of the XRD data for YH_x films at 523 K makes it complicated to draw a detailed stress-strain curve, similar to one drawn for clamped Pd clamped films in the Chapter 4 (shown also in Fig. 5.9). Instead, an approximated stress-strain curve is used to calculate the mechanical energy in YH_x films (Fig. 5.10). This stress-strain curve does not include a change from the compressive to tensile stresses on going from absorption to desorption. Moreover, it is constructed based on only two points: point 1, which is an initial non-expanded state of the film with a zero-stress and point 2, which represents an expanded by 11.9% and compressed by 1 GPa YH_x film; the strain and stress values, assumed to be weakly dependent on temperature, are the literature data on YH_x films measured at RT [8, 42]. The area of the rectangular, which reflects the total mechanical energy involved in the (de-)hydrogenation, obviously presents an overestimated value. Still, in the first approximation, this approach is considered to be valid to calculate mechanical work in the system.

The mechanical work, estimated from the area of the stress-strain curve (Fig. 5.10) is about 0.119 GJ/m^3. By substituting it into the right side of eq. (5.4) along with the experimentally measured molar volume for YH_2 films (Fig. 5.5), V_M=21.45×10^{-6} m^3/mol, and phase boundaries, (c_β–c_α)=0.5 gives the Gibbs free energy change, ΔG_{hyst} of about 5.11 kJ/(mol H). The phase boundaries of YH_x films are taken slightly smaller as compared to bulk values (approximately 0.6 H/M at 523 K [20]) due to a higher amount of grain boundaries, known to reduce solubility limits in the former samples [42]. Adding two terms in the right side of the eq. (5.4), namely ΔG_{hyst} and $\Delta G_{fcc–hex}$, attributed to the additional mechanical work done by the film and the extra energy paid by the system to transform fcc into hex phase, respectively, yields a value of 9.61 kJ/(mol H), which is in a very good agreement with the left side of eq. (5.4), i.e. ratio of the experimentally measured hysteresis in thin films and bulk at 523 K, i.e. 9.34 kJ/(mol H). This supports our assumption that the hysteresis increase in YH_x films as compared to YH_x bulk is caused by a combined clamping effect: mechanical work during (abs)/desorption cycle due to volumetric effects and mechanical work due to the reorientation of crystallites due to the multiplicity of symmetry axes in the fcc to hcp structure transformation. Thus we still can apply our stress-

strain model, but in the case of preferably oriented films, we have to take into account additional terms due to the required preferential orientation in the various phases.

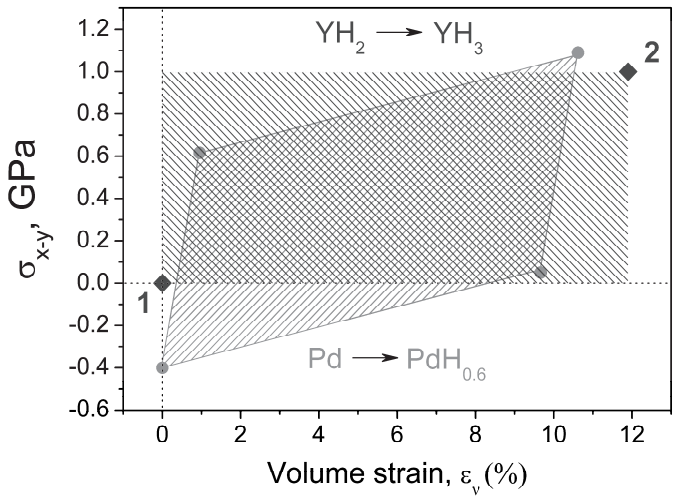

Fig. 5.10. The stress-strain curve of YH_x thin films (in blue) during (de-)hydrogenation; numbers represent points, based on which the stress-strain curve is constructed (see text). The stress-strain curve for PdH_x films (in red) is presented for comparison.

A similar approach can be applied to describe the presence of the huge hysteresis in thick (300 nm) YH_x films, measured by means of electrochemistry at 295 K (black squares, Fig. 5.9). Following the same procedure, an increase of ΔG_{hyst} in the films as a result of clamping is estimated using the mechanical work, evaluated form the stress-strain curve (0.119 GJ/m^3), the molar volume, V_M=21.45×10^{-6} m^3/mol [8] and YH_x films phase boundaries, (c_β–c_α)=0.6 [10]. The stress-strain curves for thick YH_x films at 295 K are taken identical to that one of thin YH_x films used at 523 K, meaning the same maximum stress and strain values, i.e. 1 GPa and 11.9%, respectively. A summation of the ΔG_{hyst} (4.25 kJ/(mol H)) and a stress-induced fcc-hex transformation term, $\Delta G_{fcc–hex}$(4.50 kJ/(mol H)) gives a value of 8.97 kJ/(mol H), which is the overall Gibbs free energy change in thick YH_x films due to the substrate influence. A substitution of the measured absorption, P_{abs}=1.5 Pa (at x=2.55 H/M) and desorption, P_{des}=1.5x10^{-5} Pa equilibrium pressures for YH_x films at 295 K [8] along with the Y bulk pressures (P_{abs} / P_{des}=3.33) at the same temperature into the left side of eq. (5.4) yields value of 10.67 kJ/(mol H). Bulk pressures at RT are extrapolated from high temperature measurements (Fig. 5.9), which result in a

higher error of estimation. Nevertheless, the agreement between both sides of equation (5.4) is very satisfactory. It is worth mentioning, however, that the electrochemically determined equilibrium pressures at 295 K are somewhat shifted as compared to an extrapolated hydrogenography results around RT (see green lines, Fig. 5.9). This might be related to an insufficient amount of experimental points in the Van 't Hoff plot, necessary to make a good fit or to a difference in the films thicknesses, i.e. 40 nm versus 300 nm for hydrogenography and electrochemistry, respectively. The exact reason for a discrepancy between these two techniques remains unclear and requires a more detailed study.

(De-)hydrogenation behavior of $La_{0.6}Y_{0.4}H_x$ thin films

Pressure-transmission-isotherms of $La_{0.6}Y_{0.4}H_x$ films, measured simultaneously with LaH_x and YH_x at 423 K and 523 K, are presented in Fig. 5.11.

The (de-)hydrogenation behavior of $La_{0.6}Y_{0.4}H_x$ films at 423 K agrees well with the electrochemistry results at RT (Fig. 5.1) and shows similar features with lanthanum hydride. Loading and unloading isotherm of $La_{0.6}Y_{0.4}H_x$ also exhibit a sloping plateau, which, however, extends for a much wider range of pressures. Remarkably, the linear dependence of the $\ln(T/T_M)$ on hydrogen pressure is almost 4 orders of magnitude, 10^0–10^4 Pa, which makes this material a perfect candidate for a linear hydrogen sensor, if the long-term oxidation of the RE's during operation can be prevented [44]. The difference between absorption and desorption branch of the isotherm in $La_{0.6}Y_{0.4}H_x$, having no structure transformation, is small ($P_{abs}/P_{des} \approx 5.4$) but a few times larger as compared to LaH_x films (Fig. 5.11). Similar behavior was also observed by electrochemistry (Fig. 5.1), where the hysteresis in LaH_x samples with a small negative expansion was found slightly smaller with respect to $La_{0.6}Y_{0.4}H_x$ having approximately zero volume expansion (see Fig. 5.4); because of a much larger pressure scale used in Fig. 5.1, it is difficult to quantify this difference.

It is very astonishing to observe even a small hysteresis in $La_{0.6}Y_{0.4}H_x$ films, since, according to the elastic theory of Schwarts and Khachaturyan [35], a material with no volume expansion upon hydrogenation should exhibit no hysteresis; here it is assumed that the zero volume expansion, measured at 293 K, remains unchanged at higher temperature. Apparently, the zero volume change in $La_{0.6}Y_{0.4}H_x$ films does not imply the absence of the plastic deformations, known to expand the hysteresis in the films [31]. Atomic displacements, which are responsible for the volume decrease in LaH_{x+2} hydrides [27], are most likely to take place in the (de-)hydrogenation process of $La_{0.6}Y_{0.4}H_x$ films as well. These atomic displacements and relaxations, taking place during hydrogen absorption from x=2 H/M to 3 H/M, probably lead to a minor plastic deformations, which are the origin of the hysteresis in $La_{0.6}Y_{0.4}H_x$ films; same reasoning also applies to LaH_x films.

The fact that the hysteresis in $La_{0.6}Y_{0.4}H_x$ is slightly bigger as compared to LaH_x can be easily understood on the basis of the difference in the plateau width, $\ln(T/T_M)$. Considering that the width of the sloping plateau is proportional to the displacement work and, consequently, to the plastic deformations, an increase of the hysteresis in $La_{0.6}Y_{0.4}H_x$ films as compared to LaH_x films should be of the same order as the ratio of the experimentally observed $\ln(T/T_M)$ in these films. Indeed, a ratio of the optical determined plateau width in $La_{0.6}Y_{0.4}H_x$ ($\ln(T/T_M)$=0.84, Fig. 5.11) and LaH_x ($\ln(T/T_M)$=0.24, Fig. 5.7) films at 423 K, i.e. 3.5, corresponds well with the measured hysteresis ratio, i.e. 2.5, proving our assumption. It is worth mentioning that the hysteresis is calculated using the equilibrium pressures taken from the midpoint of the sloping plateaus (Fig. 5.7, 5.11).

An increase of the temperature to 523 K leads to a further decrease of the hysteresis in $La_{0.6}Y_{0.4}H_x$ films. However, it also changes the appearance of the isotherm. Unlike a continuous filling of the hydrogen interstitial sites, having a range of different energies, which resulted in a linear relation between hydrogen pressure and the normalized optical transmission in the plateau region at 423 K, hydrogen loading at 523 K becomes more discrete (Fig. 5.10). PTI's of the $La_{0.6}Y_{0.4}H_x$ films exhibit two distinctive plateaus, meaning occupation of the octahedral interstitial sites [23] with only two different energy levels. Disordered $La_{0.6}Y_{0.4}H_x$ alloy at 423 K becomes an ordered structure with increasing temperature: the ordering process of hydrogen atoms in the subsystem of octahedral positions, known to occur in superstoichiometric LaH_{2+x} [23, 45] depending on hydrogen concentration, x, is amplified by the temperature and, presumably, clamping. Similarly to LaH_x films, a combination of the stress release, caused by microstructural reorganization, and the hydrogen ordering leads to a formation of two non-coherent lattices with similar structures. These different structures could not be observed in the XRD spectrum of the cycled $La_{0.6}Y_{0.4}H_x$ films, but they are clearly visible in the XRD scan of LaH_x films (Fig. 5.3). It is worth mentioning that the processes, taking place at 523 K in $La_{0.6}Y_{0.4}H_x$ and LaH_x films are irreversible, since after the complete dehydrogenation the second phase is still present in the XRD profile of LaH_x films.

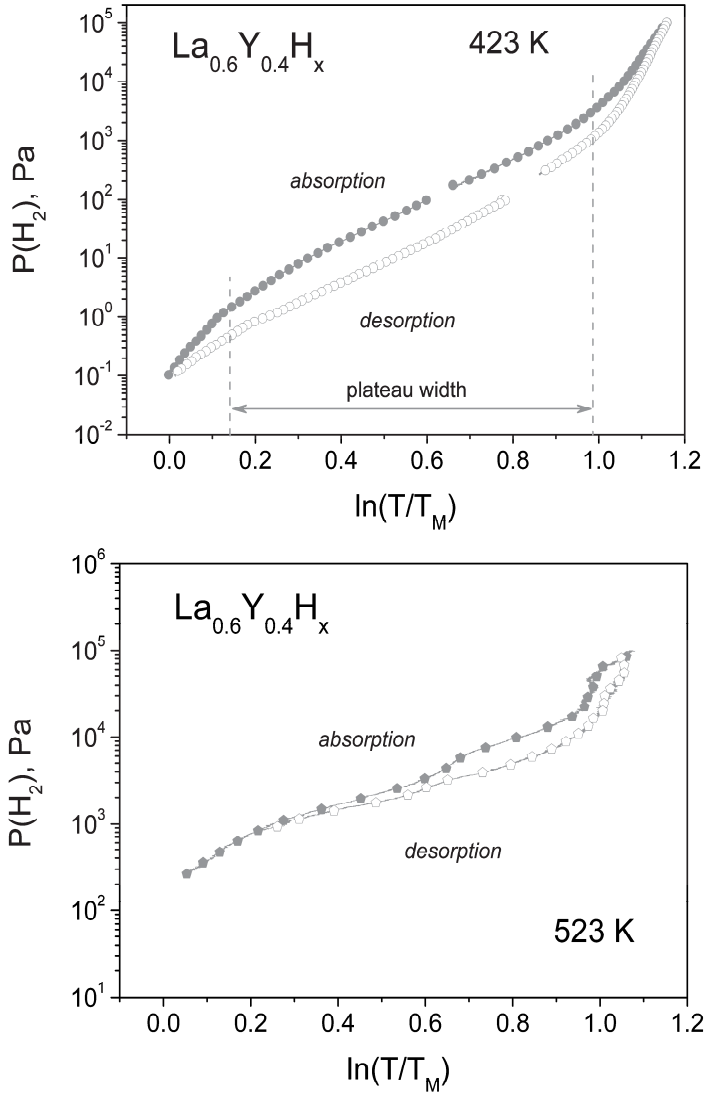

Fig. 5.11. Pressure-Transmission-Isotherms of $La_{0.6}Y_{0.4}H_x$ measured at 423 K (top) and 523 K (bottom). Vertical dotted lines represent the phase boundaries and the width of the plateau in $La_{0.6}Y_{0.4}H_x$ films measured at 423 K.

5.2.4 Conclusion

The (de-)hydrogenation properties and hysteresis behavior of $La_{1-z}Y_zH_x$ (z= 0, 0.4, 1) films were studied by means of the hydrogenography. According to the experimental results, these films can be divided into two categories: (i) films with essentially no hysteresis and (ii) films with a huge hysteresis.

La-rich films, namely LaH_x and $La_{0.6}Y_{0.4}H_x$, belong to the first category. They do not possess a structure transformation during hydrogen loading from x=2 H/M to 3 H/M and their volume expansion close or smaller than zero, which lead to a bulk-like hysteresis behavior (P_{abs}/P_{des}= 2−6) in the temperature range 423–523 K. The small difference between the sloping absorption and desorption plateaus in these films, which violates the elastic theory for hysteresis, is believed to originate from a minor plastic deformations occurring due to atomic rearrangements during (de-)hydrogenation, though no additional XRD measurements were performed to check whether La-rich films indeed possess zero or negative volume expansion. This finding suggests that even above the critical point, where no coexistence region is present, the clamping effect would still cause a difference between loading and unloading in metal hydride thin films. A change of the slope (flattening) of the equilibrium plateaus, taking place in LaH_x and $La_{0.6}Y_{0.4}H_x$ films at 523 K, is, most likely, a result of a combined effect of stress gradients, induced by the clamping effect and hydrogen ordering in the octahedral interstitial sites.

YH_x films, which expand by about 12 % at the dihydride-trihydride transition and exhibit fcc-hex structure transformation during dihydride-trihydride transition, belong to the second category. Their hysteresis is enormous, i.e. 2-3 orders of magnitude at 423–523 K, which is substantially larger as compared to La-rich films. A comparison with the YH_x bulk data at 523 K revealed a 74 times bigger hysteresis in YH_x films ($P_{abs}/P_{des} \approx 224$). In this case, an additional parameter, which is associated with the energy involved in the fcc-hex transition, was included in the stress-strain model. This parameter takes into account the rearrangement of the hexagonal grains on hydrogenation. This rearrangement is necessary to assure a preferential orientation and thereby to assure a minimum of plastic deformation. In this way, our stress-stain model is able to reasonably predict an expansion of the hysteresis in both, thin and thick YH_x films at 523 K and at 295 K, respectively. To further validate our approach it would be interesting to try to reduce the crystallinity of the films to such an extent that the preferential orientation is suppressed.

5.2.5 References

[1] J.N. Huiberts, R. Griessen, J.H. Rector, R.J. Wijngaarden, J.P. Dekker, D.G. de Groot and N.J. Koeman, Nature 380 (1996) 231.

[2] R. Griessen, J.N. Huiberts, M. Kremers, A.T.M. van Gohg, N.J. Koeman, J.P. Dekker, P.H.L. Notten, J. Alloys Comp. 253-254 (1997) 44.

[3] P. van der Sluis, M. Ouwerkerk, and P. A. Duine, Appl. Phys. Lett. 70 (1997) 3356.

[4] P. H. L. Notten, M. Kremers, and R. Griessen, J. Electrochem. Soc. 143 (1996) 3348.

[5] E. S. Kooij, A. T. M. van Gogh, and R. Griessen, J. Electrochem. Soc. 146 (1996) 2990.

[6] T.J. Richardson, J.L. Slack, R.D. Armitage, R. Kostecki, B. Farangis, and M.D. Rubin, Switchable mirrors basedon nickel-magnesium films, Appl. Phys. Lett. 78 (20) (2001) 3047.

[7] M. Slaman, B. Dam, H. Schreuders, R. Griessen. Fiber optic hydrogen detectors containing Mg-based metal hydrides, Sens Actuators B 123 (2007) 538.

[8] A. T. M. van Gogh, D. G. Nagengast, E. S. Kooij, N. J. Koeman, J. H. Rector, and R. Griessen, Structural, electrical, and optical properties of $La_{1-z}Y_zH_x$ switchable mirrors, Phys. Rev. B 63 (2001) 195105.

[9] K.A. Gschneidner, Jr. and F.W. Calderwood, La-Y phase diagram, Bull. Alloy Phase Diagram 3 (1982) 1.

[10] E. S. Kooij, A. T. M. van Gogh, D. G. Nagengast, N. J. Koeman, and R. Griessen, Hysteresis and the single-phase metal-insulator transition in switchable YH*x* films, Phys. Rev. B 62 (2000) 10088.

[11] A. T. M. van Gogh, D. G. Nagengast, E. S. Kooij, N. J. Koeman, and R. Griessen, Quenching of Giant Hysteresis Effects in $La_{1-z}Y_zH_x$ Switchable Mirrors, Phys. Rev. Let. 85 (2000) 2156.

[12] A. Remhof, J.W.J. Kerssemakers, S.J. van der Molen, and R. Griessen, E.S. Kooij, Hysteresis in YHx films observed with *in situ* measurements, Phys. Rev. B 65 (2002) 054110.

[13] K.P. Ta and J. Newman, Proton Intercalation Hysteresis in Charging and Discharging Nickel Hydroxide Electrodes, J. Electrochem. Soc. 146 (1999) 2769.

[14] C.E. Lundin and J.P. Blackledge, Pressure-temperature-composition relationships of the Yttrium-Hydrogen system, J. Electrochem. Soc. 109 (1962) 838.

[15] R. Gremaud, M. Slaman, H. Schreuders, B. Dam and R. Griessen, Appl. Phys. Lett. 91 (2007) 231916.

[16] BJ. Beaudry and F.H. Spedding, The Solubility of RH_{2-x} in Gd, Er, Tm and Y from Ambient to 850°C, Metall. Trans. B. 6 (1975) 419.
[17] T.B. Massalski, P.R. Subramanian, H. Okamoto, and L. Kacprzak, Binary Alloy Phase Diagrams, 2nd ed., Vol. 1,2, and 3, ASM International, Materials Park, OH, 1990.
[18] F. H. Spedding, R. M. Valetta, and A. H. Daane, Trans. Am. Soc. Met. 55 (1962) 483.
[19] Y. Fukai, The metal-hydrogen system: basic bulk properties. Springer series in Material Science, edited by U. Gonser, Springer, Berlin, 1993.
[20] F.D. Manchester, Phase diagrams of binary hydrogen alloys, ASM International, Materials Park, 2000.
[21] Y. Wang and M.Y. Chou, Structural and electronic properties of hexagonal yttrium trihydride, phys. Rev B 51 (2) (1995) 7500.
[22] P. Vajda, Hydrogen ordering and metal-semiconductor transitions in superstoichiometric rare earth hydrides, J. Alloys Comp. 231 (1995) 170.
[23] P. Vajda, in Handbook on the Physics and Chemistry of Rare Earths, edited by K. A. Gschneidner, Jr. and L. Eyring, Elsevier, Amsterdam, Vol. 20 (1995) 207.
[24] R. Bischof, E. Kaldis and M. Tellefsen, Crystal growth and phase diagram of lanthanum trihydride, LaH_{3-x}, Journal of Crystal Growth 70 (1984) 491.
[25] E. Boroch, K. Conder, Cai Ru-Xiu and E. Kaldis, An X-ray investigation of the phase relationships in the system LaH_2-LaH_3, Journal of the Less-Common Metals 156 (1989) 259.
[26] C.E. Messer and G.W.-H. Hung, Dissociation pressures in the System LaH_2-LaH_3, 250-450°C, The Journal of Physical Chemistry XX (1968) 3958.
[27] G. Renaudin, K. Yvon, W. Wolf, P. Herzig, Atom relaxations around hydrogen defects in lanthanum hydride, J. Alloys Comp. 404-406 (2005) 55.
[28] H. Frieske and E. Wicke, Ber. Bunsenges. Phys. Chem. 77 (1972) 48.
[29] S. Tanaka, Hysteresis of hydrogen absorption (and desorption) isotherms in the α-β two-phase region of $LaNi_5$, J. Less-Common Metals 89 (1983) 169.
[30] T. Klassen, W. Oelerich, R. Bormann, Nanocrystalline Mg-based hydrides: hydrogen storage for the zero-emission vehicle, Journal of Metastable and Nanocrystalline Mat. 10 (2001) 603.
[31] Y. Pivak, H. Schreuders, M. Slaman, R. Griessen, B. Dam, Thermodynamics, stress release and hysteresis behavior in highly adhesive Pd–H films, Int. J. Hydrogen Energy 36 (2011) 4056.
[32] L.N. Yannopoulos, R.K. Edwards, and P.G. Wahlbeck, The thermodynamics of the Yttrium-Hydrogen System, The Journal of Physical Chemistry XX (1964) 251.

[33] R. Feenstra, G. J. de Bruin-Hordijk, H. L. M. Bakker, R. Griessen and D. G. de Groot, J. Phys. F 13 (1983) L13.
[34] E. M. Salomons, R. Feenstra, D. G. DE Groot, J. H. Rector and R. Griessen, Ppressure-composition Isotherms of thin PdH, films, J. Less-Com. Metals, 130 (1987) 415.
[35] R.B. Schwartz, A.G. Khachaturyan, Thermodynamics of open two-phase systems with coherent interfaces: Application to metal-hydrogen systems, Acta Mater. 54(2006) 313.
[36] S. Qian and D.O. Northwood, Elastic and plastic accommodation effects on hysteresis during hydride formation and decomposition, Int. J. Hydrogen Energy 15(9) (1990) 649.
[37] T.B. Flanagan and J.D. Clewley, Hysteresis in metal hydrides, J. Less-Common Metals 83 (1982) 127.
[38] U. Laudahn, A. Pundt, M. Biker, U.V. Hulsen, U. Geyer, T. Wagner, R. Kirchheim, Hydrogen-induced stress in Nb single layers, J. Alloys Comp. 293-295 (1999) 490.
[39] A. Ludwig, J. Cao, A. Savan, M. Ehmann, High-throughput characterization of hydrogen storage materials using thin films on micromachined Si substrates, J. Alloys Comp. 446-447 (2007) 516.
[40] T. P. Leervad, C. Salinga, H. Weis, M. Wuttig, Mechanical stresses upon hydrogen induced optical switching in thin films, J. Appl. Phys. 93 (2003) 6034.
[41] T.H. Courtney, Mechanical Behavior of Materials, McGraw-Hill, New York, 1990.
[42] M. Dornheim, A. Pundt, R. Kirchheim, S.J. v.d. Molen, E.S. Kooij, J. Kerssemakers, R. Griessen, H. Harms and U. Geyer, Journal of Applied Physics 93 (2003) 8958.
[43] A. Pundt and R. Kircheim, Hydrogen in metals: Microstructural aspects, Annu. Rev. Mater. 36 (2006) 555.
[44] Palmisano, V., M. Filippi, A. Baldi, M. Slaman, H. Schreuders, B. Dam, An optical hydrogen sensor based on a Pd-capped Mg thin film wedge, Int. J. Hydrogen Energy 35 (2010) 12574.
[45] I.G. Ratishvili, P. Vajda, The phase diagrams of β-RH_{2+x} system (R=La, Ce, Tb). Results of mean-field calculations, J. Alloys and Comp. 253-254 (1997) 171.

Chapter 6

Thermodynamics and hysteresis behavior of MgH_2 films as studied by Hydrogenography

6.1 Introduction

MgH_2 is considered as a promising hydrogen storage material because of its high gravimetric capacity, availability and low price. However, the high thermodynamic stability of MgH_2 (low enthalpy of formation, -74 kJ/mol H_2) results in equilibrium pressures in the millibar range at room temperature, which limits its practical application.

In the coming chapters we will show various approaches to destabilize magnesium hydride. However, beforehand, a careful investigation of MgH_2 needs to be conducted to be able to separate intrinsic effects from those connected to the clamping phenomenon. The fact that a structure transformation and a metal-to-semiconductor transition take place in magnesium upon hydrogenation distinguishes MgH_2 from the Pd case we discussed in the previous chapters.

In the next paragraph we thoroughly measure pressure-transmission-isotherms of MgH_2 films up to 545 K. To prevent interalloying between Mg and the protective catalytic Pd coating, an intermediate layer M (M=Ta, Ti, Fe) of 10 nm was deposited. We show that the thermodynamic parameters of hydrogen desorption are in a very good agreement with bulk MgH_2 reference data. Absorption of hydrogen, on the other hand, is substantially influenced by the clamping effect, resulting in a value for the standard enthalpy of formation of about -61 kJ/mol H_2. A comparative study between Mg/Pd and Mg/M/Pd samples in the low temperature range allows us to deduce the effect of Pd clamping on the thermodynamics and hysteresis behavior of magnesium hydride films. The stress-strain

analysis, developed in chapter 4, proves to be valid also for metal hydrides with a structure transformation as it quantitatively predicts a hysteresis increase in MgH_2 thin films, with respect to the bulk hydride. We find that with a proper temperature correction, the stress-strain theory can be used in a very wide temperature range.

The following chapter is submitted to special issue *"Hydrogen Storage Alloys" of Crystal.*

6.2 Thermodynamic properties, hysteresis behavior and stress-strain analysis of MgH_2 films studied in a wide temperature range

Abstract:

Using a thin film optical approach (Hydrogenography) we investigate the thermodynamic parameters and hysteresis behavior in Mg films in the temperature range from 333K to 553 K.

The enthalpy and entropy of hydride decomposition, ΔH_{des} = -78.3 kJ/molH_2, ΔS_{des} = -136.1 J/ K molH_2, estimated from the Van 't Hoff analysis, are in a good agreement with bulk results, while the absorption thermodynamic properties, ΔH_{abs} = -61.6 kJ/molH_2, ΔS_{abs} = -110.9 J/K molH_2, appear to be substantially affected by the clamping effect. The influence of the substrate is negligible at high temperatures, T>523 K, as the (de-)hydrogenation behavior in Mg/Ta/Pd films is in line with the bulk volumetric measurements. At lower temperature, the clamping effect is considerable, as the hysteresis in Mg/Ta/Pd films at RT increases by a factor of 16 as compared to extrapolated values derived from MgH_2 bulk. The hysteresis increases even further in Mg/Pd films, most likely due to the formation of a Mg-Pd alloy at the Mg/Pd interface. The stress-strain analysis of the Mg/Ta/Pd films at 300-333 K proves that the increase of the hysteresis takes place as a result of a larger elastic and plastic expansion work of the films during loading and unloading hydrogenation cycle. With a proper temperature correction, our stress-strain analysis quantitatively and qualitatively explains the hysteresis behavior in thin films as compared to bulk materials in the whole temperature range.

6.2.1 Introduction

In the search for light-weight hydrogen storage materials, Mg and Mg-based alloys play a prominent role [1-7]. High volumetric (~110 kgH_2/m^3) and gravimetric capacity (of 7.6 wt%) of MgH_2, low price and high abundance make magnesium a promising hydrogen storage material [7]. However, the practical application of magnesium hydride is limited due to its high thermodynamic stability (-74.5 kJ/mol H_2), which requires very high temperatures (approximately 573 K) for hydrogen decomposition to occur around hydrogen pressure of 1 bar. At room temperature (de-)hydrogenation takes place in the millibar range, which is insufficient for operation in conjunction with a PEM fuel cell.

To study the effect of alloying on the enthalpy and entropy of hydride formation of Mg, we use our combinatorial Hydrogenography technique. An optical thin film approach substantially reduces the preparation and measurement time. However, we need to be sure of the general applicability of the thermodynamic parameters obtained. Large mechanical compressive stresses in thin films during (de-)hydrogenation- arising as a results of the rigid substrate- could influence the thermodynamics properties of thin films as compared to bulk materials. This so-called clamping effect could lead to false results and, therefore, need to be analyzed in more detail..

The clamping effect has been thoroughly studied previously in Pd films in Chapters 3 and 4. However, the influence of the substrate on the (de-)hydrogenation properties of Mg films is expected to differ substantially from that of Pd. First of all, Mg possesses a very high volume expansion (about 32%), which will lead to a larger expansion work during the hydrogen (de-)absorption cycle. In addition, due to the metal-to-insulator transition, MgH_2 more stiff (the bulk modulus increases and the compressibility, correspondingly, lowers) with respect to Mg metal. This results in extra compressive stresses acting on the β-hydride upon phase transformation. Last but not least, the hcp-bct structure transformation taking place in magnesium upon hydrogenation could influence the apparent thermodynamic properties of these films.

In this work we investigate the thermodynamic properties and hysteresis behavior of MgH_2 thin films. Using Hydrogenography we investigate (de-)hydrogenation in Mg/Pd and Mg/M/Pd (where M=Ta, Ti, Fe) multilayers to determine the enthalpy and entropy of the hydride formation and decomposition of Mg. We show that desorption thermodynamics of Mg/Ta/Pd films is similar to that of MgH_2 bulk, whereas absorption parameters differ substantially from it. A thorough analysis of the hysteresis behavior reveals that the large difference between hydride formation and decomposition at low temperatures is caused by the clamping effect. By applying a proper temperature correction, the stress-strain model can quantitatively explain the hysteresis behavior in these thin films in a wide temperature

range. A comparison between Mg/Pd and Mg/Ta/Pd films shows a widening of the hysteresis by a factor 15 at 363 K for films which is due to a chemical interaction at the Mg-Pd interface.

6.2.2 Experimental details

Thin Mg films were sputtered in a dc/rf magnetron deposition system (background pressure 10^{-7} Pa, deposition argon pressure 0.3 Pa) on 10×10 mm fused glass substrates. For one set of samples (Fig. 6.1) a layer of Pd was directly deposited on top of Mg to prevent oxidation and to catalyze the hydrogen dissociation. For another set, an intermediate layer M (M = Ta, Ti, Fe) with a thickness of 10 nm was deposited in-between Mg and Pd to prevent inter-alloying between Mg and Pd [9]. Thus, Mg/M/Pd samples were studied in a wide temperature range (333-545 K), whereas Mg/Pd films were measured at temperature below 393 K. According to Krozer and Kasemo [10], Pd-Mg intermixing takes place only above 375 K. It is worth mentioning, however, that a thin (1-3 monolayers) intermixed layer of Mg-Pd could be already formed at 300 K as results of the sputtering or/and hydrogen absorption process [11-13].

After deposition, the metal films were transferred to the hydrogenography setup to study their (de-)hydrogenation properties. A more detailed explanation of the Hydrogenography technique and the experimental procedure can be found elsewhere [14,15].

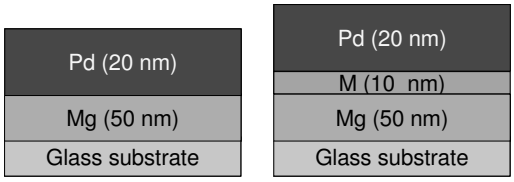

Fig. 6.1. Schematic representation of the deposited Mg films studied in this work.

Hydrogenography experiments were conducted in the temperature range from 333 K till 545 K. For each temperature run we used a fresh film from the same deposition batch to ensure that no sample degradation or alloying could affect the experimental results. At first, Mg films were subjected to a few (3-4) fast loading and unloading cycles at 333 K. The absorption was performed in hydrogen atmosphere within one hour, whereas desorption was carried out in oxygen to speed up desorption kinetics. Afterwards, when the steady-state condition has been reached, the equilibrium Pressure-Transmission-Isotherms

(PTI's) were measured using slow (de-)hydrogenation cycles (from 116 hours at 333 K to 5 hours at 545 K).

The absorption/desorption pressures were determined from the midpoint of the corresponding PTI's. These pressures were plotted in a Van 't Hoff plot, from which the enthalpy and entropy of hydride formation/decomposition were obtained from the slope of the linear fit (ΔH)and from the cross-point of this fit with the y-axis (ΔS), respectively.

6.2.3 Results and discussion

The thermodynamic properties of three different Mg films, namely Mg/Ti/Pd, Mg/Ta/Pd and Mg/Fe/Pd were investigated using Hydrogenography. All of them show qualitatively and quantitatively similar results. Consequently, experimental data for only one set of films, i.e. Mg/Ta/Pd are presented here.

Hydrogenography experiments on Mg/Ta/Pd films

Mg hydride is known for its slow kinetics, especially at low temperatures. To verify the quasi-equilibrium state of the hydrogenation process at these temperatures, loading at 333 K was performed twice with a different measuring time. Based on our previous experience, the time of the first loading was set to 35 hours and during the second one it was increased to 44 hours. Both absorption isotherms show the same (de-)hydrogenation behavior, proving that no kinetic factor is influencing the experimental results. It is worth mentioning that the unloading isotherm was measured for 72 hours.

The pressure-transmission-isotherms of Mg/Ta/Pd thin films for the whole temperature range measured are collected in Fig. 6.2. All isotherms possess very flat plateaus in both absorption and desorption. As a sloping pressure plateau in nano-sized materials is often related to kinetic problems [15, 16], this is an additional proof that we indeed probe the equilibrium properties of the Mg/Ta/Pd films.

It can be seen from Fig. 6.2 that some of the desorption PTI's, namely at 333 K and 363 K show an unusual behavior – an increase of the $\ln T/T_o$ during a decrease of the hydrogen pressure. This effect is connected to the sequence of the hydrogenation of the layers within the stack and does not mean that the hydrogen concentration in the material is increasing. If we compare the enthalpy of hydride formation/decomposition between different layers in Mg/Ta/Pd film, the first layer that should load is MgH_2 (ΔH= -74.5 kJ/molH_2 [17]), the next one is TaH_x (ΔH= -72.4 kJ/molH_2 [18]) and, finally, PdH_x (ΔH= -39 kJ/molH_2 [19]). The unloading procedure proceeds in a reversed order: Pd – Ta – Mg. It is worth mentioning, that Mg and Ta behave oppositely, i.e. Ta darkens during hydrogen

loading and transmits more light during hydrogen unloading. Thus, Mg/Ta/Pd film becomes darker ($\ln T/T_M$ increases) on dehydrogenation due to Ta layer.

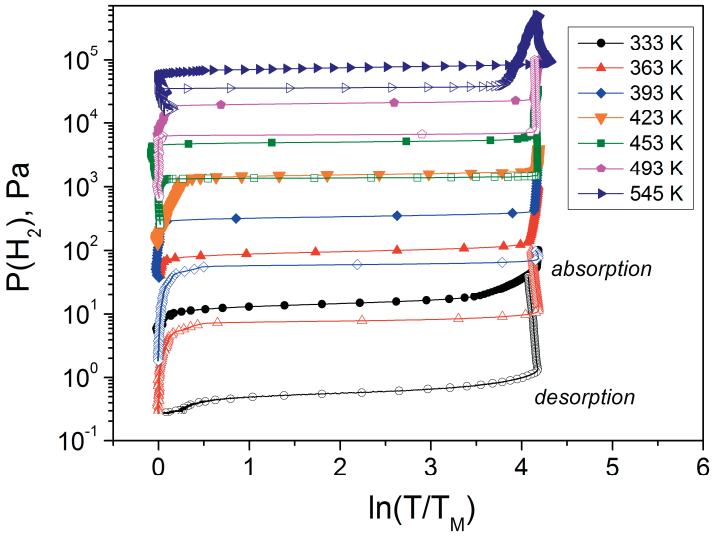

Fig. 6.2. Pressure-transmission-isotherms of the Mg/Ta/Pd thin films during hydrogen absorption (filled symbols) and hydrogen desorption (open symbols) in a wide temperature range.

From the equilibrium plateau pressures of the corresponding PTI's the Van 't Hoff plot was constructed (Fig. 6.3). The calculated enthalpy and entropy of hydride formation and decomposition are: ΔH_{abs} = -61.6 kJ/molH_2, ΔS_{abs} = -110.9 J/K molH_2 and ΔH_{des} = -78.3 kJ/molH_2, ΔS_{des} = -136.1 J/ K molH_2, respectively.

There is a substantial scattering of the reported desorption bulk enthalpies of MgH_2 [17, 21-28], ranging from -67.0 kJ/molH_2 [17] to -81.3 kJ/molH_2 [27, 28]. The thermodynamic properties of our Mg films in desorption are in a very good agreement with few bulk references [22, 23] and, in general, fall within the experimental spread. Among this spread Bohmhammel et al. [21] calculated the mean value, which appears to be close to Stampfer result [17], i.e. -74.5 kJ/molH_2. By taking this average (Stampfer) value as a reference one, the enthalpy of hydride decomposition of the Mg/Ta/Pd films, measured by the Hydrogenography, is then lower by 3.8 kJ/molH_2 as compared to bulk data.

A comparison of hydrogenation thermodynamics of Mg bulk with thin films is much more difficult. Most of the literature values on bulk MgH_2 rely on desorption

experiments, whereas only a few references could be found describing formation enthalpies and entropies of magnesium hydride [29, 30]. The enthalpy and entropy of hydride formation, measured by Vigeholm et al. [29] in the temperature range 533–698 K is -70 kJ/molH_2 and -126 J/K molH_2, respectively, which agree pretty well with theoretical predictions by Selvam et al. [30]. Taking the Vigeholm [29] data as a reference, the hydrogenation enthalpy of Mg/Ta/Pd films deduced from our optical approach is by 8.4 kJ/molH_2 higher as compared to magnesium bulk.

There exist several studies devoted to the thermodynamics of magnesium hydride at low temperatures (T< 393 K) using films. Thus, based on room temperature electrochemical measurements of hydrogen equilibrium pressures, Vermeulen et al. [31] calculated the enthalpy of hydride formation (-72 kJ/molH_2) and decomposition (-74 kJ/molH_2) in 200 nm MgH_2 films, which is found quite similar to bulk values mentioned above. Their estimates, however, are based on one temperature only (298 K) and assume the entropy of hydride formation of -130.8 J/K molH_2 in absorption and desorption. Somewhat contradictive results have been measured on 380 nm Mg films in the temperature range 290-370 K by piezoelectric quartz crystal microbalance (gravimetric method) [10]. The enthalpy of hydride formation derived from the pressure-concentration-isotherms is -60.7±6.3 kJ/molH_2, which is very close to the Hydrogenography results. The enthalpy of hydride decomposition, -71.0±4.2 kJ/molH_2, is relatively close to the electrochemistry data, but in a disagreement with the Hydrogenography.

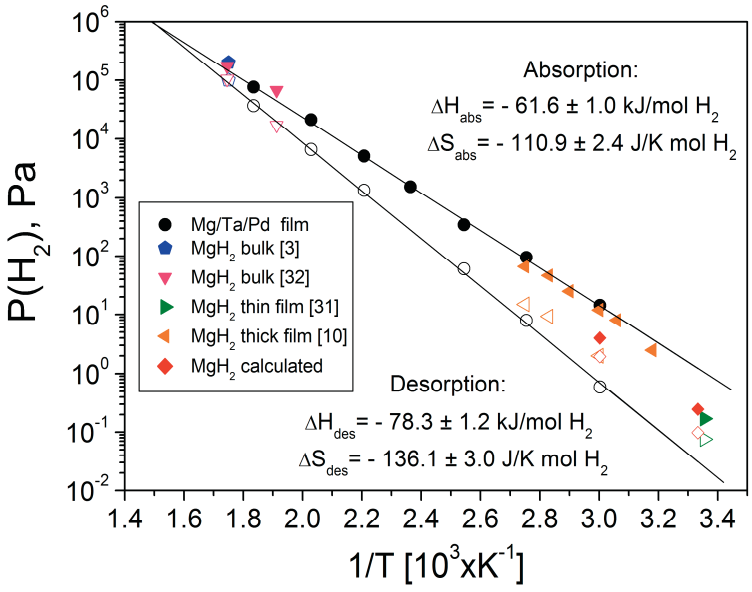

Fig. 6.3. Van 't Hoff plot of the Mg/Ta/Pd films. Filled and open symbols represent absorption and desorption, respectively. Thermodynamic parameters are calculated from the regression analysis. Data for bulk MgH_2 [3] and MgH_2–V 3at.%–Ti 2at.% [32], thin [31] and thick MgH_2 films [10] are shown for comparison. Red diamonds are the calculated absorption and desorption equilibrium pressures from the Van' t Hoff equation using Vigeholm [29] and Stampfer [17] thermodynamic parameters, respectively.

The difference in thermodynamics of Mg films studied by means of Hydrogenography and Electrochemistry/Gravimetry follows from the difference in the (de-)hydrogenation pressures and, accordingly, hysteresis behavior (Fig. 6.3). A possible cause for the discrepancy between various techniques is connected, in our opinion, to the different hydrogen concentration in the films upon hydrogenation. Thus, due to relatively high current densities used in the electrochemical measurements, 300 nm thick Mg films were loaded only up to 1.2 H/M [38]. In order to prevent delamination of the films from the substrate in the gravimetric experiments, thick Mg films (380-800 nm) were allowed to absorb no more than 0.3 H/M [10]. As the hydrogen-induced deformations is directly related to the amount of hydrogen in a sample [39], one can conclude that not fully hydrided thick Mg films, measured by electrochemistry and gravimetry, possess a lower stress state with respect to the fully hydrided one. Lower mechanical stresses along with a smaller volume expansion will inevitably result in a smaller expansion work in thick Mg

films. This, consequently, would lead to a lower substrate influence as compared to thin Mg films, studied by Hydrogenography. Hydrogenography samples to have a full hydrogen capacity because: (i) a larger pressures range and/or a longer measuring time as compared to thicker films and (ii) the fact that the transmission/reflection optical spectra of MgH_2 thin films could be accurately modeled using the bulk MgH_2 dielectric functions.

Hysteresis behavior and the Stress-strain analysis of Mg/Ta/Pd thin films

A comparison between Mg/Ta/Pd films and Mg bulk reveal two distinct characters of the hysteresis behavior, depending on the temperature (Fig. 6.3). At high temperatures, T ≥ 523 K, the ratio between absorption and desorption equilibrium pressures in films becomes essentially the same as in bulk [3, 32], i.e. $P_{abs}/P_{des} \approx 2$, proving that thin film optical results are in line with the bulk volumetric data. At lower temperatures (T < 423 K) the difference in hysteresis between thin films and bulk becomes much more pronounced. The largest deviation is observed at 300 K and 333 K, where the experimentally derived hysteresis is 40.4 at and 20.2, respectively, which is much larger than in magnesium bulk at the same temperatures (Fig. 6.3, red diamonds); since there is no bulk data available at these temperatures, the bulk pressures are extrapolated from the high temperatures using absorption and desorption enthalpies and entropies of Vigeholm [29] and Stampfer [17], respectively.

A larger hysteresis in Mg/Ta/Pd films as compared to bulk Mg at low temperatures is assumed to be caused by the clamping effect. One way to check this is to apply the stress-strain model, similar to one presented in Chapter 4, to Mg/Ta/Pd films.

According to the stress-strain model (Chapter 4), the hysteresis increase in films with respect to bulk takes place as a consequence of the expansion constraints related to the substrate and, consequently, a larger elastic+plastic work upon (de-)hydrogenation:

$$\frac{1}{2}RT\ln\left((P_{abs}/P_{des})_{film}/(P_{abs}/P_{des})_{bulk}\right) = V_M/(c_\beta - c_\alpha)\cdot\int_0^{\varepsilon_{max}}\sigma\, d\varepsilon_V \qquad (6.1)$$

Here R is the gas constant, T is the absolute temperature, V_M is the molar volume of the metal, $c_{\beta,\alpha}$ is the maximum hydrogen concentration in the β and α phase and σ and ε correspond to the stresses and volume strain in the Mg/Ta/Pd thin films, respectively. To prove that our assumption is correct, we need to solve numerically the right part of the Eq. (6.1) and compare it with the experimentally measured hysteresis in thin films and bulk Mg. However, as Mg films are X-Ray amorphous in the hydrogenated state, it is impossible to utilize the same approach as used in Chapter 4 to calculate stresses

and strains upon hydrogen loading and unloading. Thus, in this calculation we rely mostly on literature values of ($c_\beta - c_\alpha$), σ and ε of MgH_2 thin films.

According to the Mg-H phase diagram [20], the solubility of hydrogen at temperatures below 650 K is negligible (3×10^{-6} H/M at 300 K [20]) in the α-phase and close to the theoretical capacity of MgH_2, i.e. 2 H/M, in the β-phase. The width of the plateau, (c_β–c_α) in bulk systems is therefore close to 2. In thin films, due to a larger amount of grain boundaries [16] the α- and the β-phase solubility limits are usually affected by the high defect concentration, changing the actual plateau width. Indeed, recent electrochemical studies observe a substantial - 2 orders of magnitude - increase of the α-phase solubility in Mg films as compared to bulk [38]. The same authors observed a decrease in the β-phase solubility down to 1.8 H/M for 165 nm thick Mg film. As the value of c_α remains very small, 2×10^{-4} H/M at 300 K, the plateau width is basically controlled by the β-phase hydrogen solubility and equals to 1.8. Because of a sufficiently long loading times (24 hours at 333 K) used in the Hydrogenography measurements and a 3 times lower film thickness, we believe that Mg/Ta/Pd films can achieve hydrogen capacities on similar level as 1.8 H/M or even higher. For our calculations, we assume the plateau width in Mg/Ta/Pd films to be 1.8 H/M.

Using curvature bending technique, Ludwig measured mechanical stresses in Pd [40] and Mg_2Ni [41] films during hydrogen loading. In spite of the fact that these materials represent two completely different classes of hydrogen storage materials, namely interstitial and complex hydrides, the experimentally measured in-plane compressive stresses of Pd and Mg_2Ni films are found to be comparable: -1.2 GPa and -1.4 GPa, respectively. Surprisingly, the approximately 3 times larger volume expansion and the presence of a structure transformation in Mg_2Ni upon hydrogenation do not have any substantial influence on the stress build up in these films. Following the same logic, the in-plane mechanical stresses in Mg films should be of the same order of magnitude. Thus, in the calculation the maximum hydrogenation stress in Mg film is taken equal to Mg_2Ni, i.e. -1.4 GPa, since Mg is much more similar to Mg_2Ni in terms of structure transformation and volume expansion than to Pd.

It was observed in Chapter 4, that the expansion of clamped Pd films is very similar to that of Pd bulk. This volume expansion occurs by means of plastic deformations and only in the vertical direction, i.e. by increasing the film thickness. A similar situation is assumed to take place in Mg/Ta/Pd films. Recent experiments on thick Mg films [42] and Mg/Ti multilayers [43] by means of profilometry and X-ray reflectometry, show a thickness increase of about 30%, which is very similar to the expansion in magnesium hydride bulk. Thus, the volume strain in Mg/Ta/Pd films, ε_v, is assumed to resemble Mg bulk upon hydrogen loading as well.

Values for the in-plane compressive stress and the volume expansion were used to construct the stress-strain curve and to calculate the expansion (elastic+plastic) work in Mg/Ta/Pd films during (de-)hydrogenation cycle (Fig. 6.4). Since there is no experimental data on tensile stresses to implement it in the strain-stress analysis, no change of the sign is depicted in the stress-strain curve. Therefore, a simplified picture with only the compressive stresses in Mg films was used in this work.

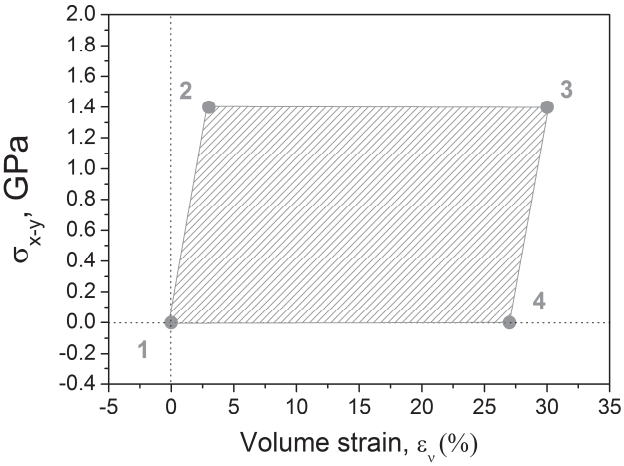

Fig. 6.4. Stress-strain curve of the Mg/Ta/Pd thin films during (de-)hydrogenation; numbers represent different hydrogenation and dehydrogenation steps, namely elastic expansion of the film (1-2), plastic deformations (2-3), elastic recovery (3-4) and plastic deformations (4-1), returning the films to its initial state (1). The positive numbers on the y-axis represent the compressive stress, whereas the negative numbers stand for the tensile stress in Mg/Ta/Pd films.

At point 1, the Mg film is in the metallic state. The initial compressive stress is taken as zero. As was observed in the clamped Pd films (Chapter 4), the mechanical stress changes from tensile to compressive during hydrogen loading and unloading. Analogous behavior is expected to occur in Mg/Ta/Pd films, i.e. non-zero tensile stress in the metallic state. Since the presence of a tensile stress would just shift the whole stress-strain curve downwards while not affecting quantitative conclusions, in this particular case we assumed a zero initial stress.

By absorbing a very small amount of hydrogen the Mg film expands elastically. As it reaches the Yield point, point 2, the nature of the deformation changes from elastic to plastic. The Yield point is taken the same as the maximum stress in Mg/Ta/Pd film,

considering the elasto-plastic behavior of our samples [15]. The elastic volume strain, calculated from the Hooke's law and by taking into account the Young modulus of Mg (45 GPa [44]) is equal to 3.1 %. Following hydrogen absorption results in a substantial volume increase of the Mg film with no variation in the stress state. The film deforms only plastically until it reaches the total volume strain of 30 %, point 3 (Fig. 6.4).

Upon dehydrogenation, first elastic relaxation shrinks the film to point 4. The elastic recovery involves the same amount of stress decrease and the same amount of volume change as during the loading process, namely 3 % (1-2). Then plastic deformations return the film to the initial state, point 1. It is worth mentioning that the dehydrogenation (step 4-1) in Mg films is expected to take place with a change of the stress-state from compressive to tensile, which is the driving force for the unloading reaction [15]. However, for simplicity, we neglect here the negative stresses.

The mechanical work, performed by the Mg film upon (de-)hydrogenation cycle evaluated from the area of the polygon in Fig. 6.4 [45]. A substitution of the estimated mechanical work, $\int_{o}^{\varepsilon_{\max}} \sigma d\varepsilon_V$ =0.378 GJ/m^3, molar volume of Mg, V_M=13.97×10^{-6} m^3/mol and Mg film phase boundaries, (c_β–c_α)=1.8 into the left side of eq. (6.1) yields the Gibbs free energy change, ΔG_{hyst} of 2.93 kJ/(mol H). Substituting the hydrogenography data for the experimentally observed hysteresis (P_{abs} / P_{des}) in Mg film (40.4) and the calculated hysteresis for Mg bulk (2.5) (Fig. 6.3, red diamonds) at 300 K with the gas constant, R=8.314 J/(K·mol) into the right hand side of eq. (6.1) leads to a value of 3.47 kJ/(mol H). The agreement between experimentally measured *hysteresis* in Mg/Ta films and Mg bulk (left side of eq. (6.1)) and the calculated mechanical work (right side of the eq. (6.1)) is remarkable and proves that the hysteresis increase Mg films is related to the substrate clamping and caused by an expansion (mostly plastic) work during (abs-)desorption cycle.

A similar type of calculations has been conducted for Mg/Ta/Pd films at 333 K. The Gibbs free energy change is taken the same, because of a minor influence of the temperature on the stress-strain curve of Mg films at 333 K with respect to 300 K. The measured hysteresis of the Mg/Ta/Pd films, plugged in the right-side of the Eq. (6.1) along with the Mg bulk hysteresis (Fig. 6.3, red diamonds) give the value of 3.18 kJ/(mol H), which again fits very well the calculated Gibbs free energy, ΔG_{hyst} of 2.93 kJ/(mol H).

These examples clearly show a good agreement between the stress-strain theory and experimental results at low temperatures. However, at elevated temperatures the agreement becomes poor. In fig. 6.4 we plot the Hydrogenography measured absorption/desorption pressures ratio (black circles) for Mg/Ta/Pd and a calculated one (red diamonds) using Eq. (6.1) in the whole temperature range. In the estimated pressure ratio we assume no

temperature dependence of the stress-strain model parameters, namely stress, volume strain, molar volume and the plateau width. As it can bee seen, the slope of the lines is not the same and the difference between them is increasing with temperature. Obviously, the stress-strain parameters do require a temperature correction.

A temperature correction of the stress-strain analysis

There are four parameters in the stress-strain model, i.e. $V_M(T)$, $(c_\beta - c_\alpha)(T)$, $\sigma(T)$, $\varepsilon_v(T)$, whose temperature dependence should be considered.

The temperature dependence of the molar volume of metallic Mg can be assessed from the coefficient of thermal expansion (CTE) of a material. Using the linear CTE of Mg, $\alpha = 24.8 \times 10^{-6}\ K^{-1}$ and assuming an isotropic linear expansion, the molar volume change upon temperature increase is estimated from the following equation:

$$V_M(T) = V_M^{RT}(3\alpha\Delta T + 1) \tag{6.2}$$

Here V_M^{RT} and ΔT are the molar volume of metallic Mg at room temperature (RT) and the difference between the operating temperature and RT, respectively. The temperature dependence of the molar volume was used to recalculate the hysteresis in Mg/Ta/Pd films (fig. 6.5, open squares). As expected, the temperature correction of Mg molar volume has a minor effect on the calculated pressures ratio, since the thermal expansion coefficient is of the order of 10^{-6}.

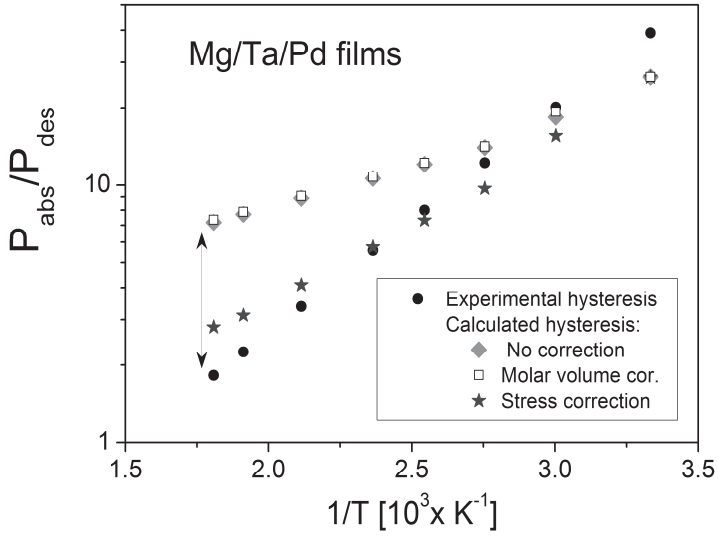

Fig. 6.5. Comparison of the experimentally measured hysteresis (P_{abs}/P_{des}) in Mg/Ta/Pd films (black circles) and the calculated one with no temperature correction (red diamonds), with a molar volume temperature correction (open squares) and with a stress temperature correction (blue stars).

For the same reason, i.e. very small thermal expansion coefficient, the volume strain of Mg films, ε_v, should not strongly depend on the temperature. No substantial temperature variation of the width of the plateau, ($c_\beta - c_\alpha$), is expected either for Mg films below 573 K, taking into account the phase diagram of MgH_2 [20].

Hydrogenation stresses, on the other hand, should dependent strongly on temperature. Hydrogenation stress is composed of an elastic and a plastic parts, changing with temperature. The maximum elastic stress or elastic limit or Yield point (point 2 on the stress-strain curve, Fig. 6.4) depends on the Young modulus of a material and elastic strain, whereas the plastic stress, which defines the maximum mechanical stress (point 3 on the stress-strain curve, Fig. 6.4), depends on the stress relaxation, mainly by means of dislocations movement. In our analysis we consider the elasto-plastic behavior of Mg films, which implies the equality of maximum elastic and plastic stresses. However, there are separate physical phenomena responsible for their temperature dependence.

One of the reasons why the elastic limit is decreasing with temperature is connected to a temperature dependence of Young modulus, E and its influence on the elastic limit. The magnitude of the Young modulus is a measure of the resistance to separation of

adjacent atoms, which, in fact, represents the interatomic bonding force. As the atomic forces are decreasing with temperature (due to an increase of atomic separation distance, r), the Young modulus also diminishes with temperature.

The temperature dependence of the Young modulus for most of materials could be described by the theoretical relationship proposed by Varshni [46]:

$$E = E(0) - s/(\exp(\theta_E / T) - 1) \tag{6.3}$$

where *E(0)* is the Young modulus at zero temperature, θ_E is the Einstein characteristic temperature in the absence of electronic effects and *s* is the high temperature limit of the temperature derivative *dE/dT*. At lower temperatures the *E/T* curve is non-linear, whereas at higher temperatures (T>273 K) the *E* vs. T dependence could be approximated by a linear equation [47]. Based on the parameters proposed by Varshni [46] for Mg, we constructed the dependence of the Young modulus on temperature and calculated the slope of the linear part of the curve, *dE/dT* in the temperature range 300-600 K (inset in Fig. 6.6). The temperature dependence of Mg, *dE/dT*= -18×10^6 Pa/K is found relatively week as compared to other materials, like Aluminum (-46×10^6 Pa/K) and Nickel alloys (-68×10^6 Pa/K) [47]. According to this dependence, the young modulus of Mg of 45 GPa at ambient temperature reduces to 40.8 GPa at 553 K.

An increase in the temperature should also influence the strain ε as the hydrogen solubility depends on T [20]. However, taking into account a minor hydrogen concentration in the α-phase in the temperature range 300-553 K, the elastic strain in Mg considers virtually the same. From the Hooke's equation it follows that a decrease of Young modulus with no change in strain results in a decrease of the Elastic limit. In Fig. 6.6 we plot the Yield point, σ_y in Mg/Ta/Pd films as a function of the Young modulus, estimated at different temperatures; the elastic strain is taken the same as in the stress-strain curve, Fig. 6.4 (point 2). According to our calculations, the elastic limit decreases from 1.4 GPa to 1.26 GPa when the temperature increases from RT to 553 K. The temperature dependence of the Yield stress in the whole temperature range is presented in Fig. 6.7 (B, blue line).

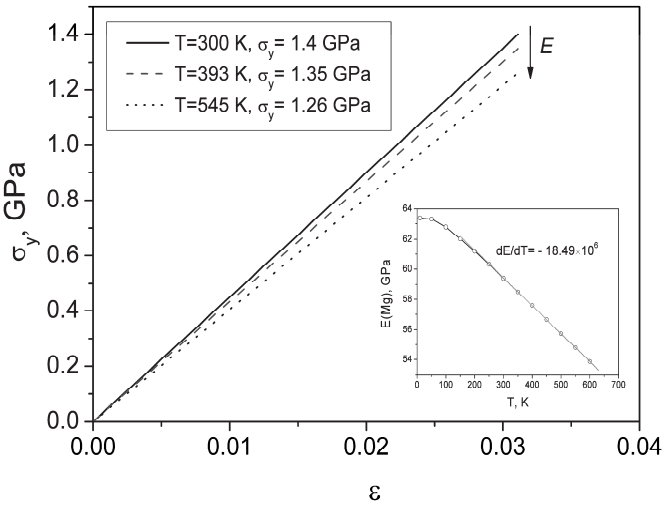

Fig. 6.6. Temperature dependence of the Elastic limit/Yield stress, σ_y in Mg films. The inset shows the temperature dependence of the Young modulus of Mg, reproduced using Eq. (6.3) and the parameters from Varshni [46]; the slope of the linear part of the curve is calculated from the regression analysis.

Besides the Young modulus, the Elastic limit is also influenced by the grain size via the Hall-Petch relationship [48]:

$$\sigma = \sigma_o + k_y (D)^{-\frac{1}{2}} \tag{6.4}$$

where σ_o is a materials constant for the starting stress for dislocation movement, k_y is the strengthening coefficient and D is the average grain diameter. This relation is essentially empirical and was proposed to describe the Yield stress of materials with grain size in the micrometer range. It has been proven recently to be valid also for a nanocrystalline metals with grain size down to 20 nm [49].

The Yield stress dependence on Mg grain size is presented in Fig. 6.7 (A). For the calculation, the literature values of the Hall-Petch slope, $k_y=0.28\times10^6$ Pa×m$^{1/2}$ and $\sigma_o=126$ MPa at room temperature of polycrystalline magnesium with 26-1000 nm grain were used [50, 51]; a temperature dependence of the parameters in Eq. (6.4) has been disregarded. From Fig 6.7 (A) it can be concluded that the initial (at 300 K, before temperature treatment) grain size of Mg/Ta/Pd films is about 40 nm, taking into account that the Yield stress of Mg films is 1.4 GPa at room temperature (Fig. 6.4). A similar grain size was estimated from the room temperature XRD experiments of Mg/Ta/Pd films (Fig. 6.8), where the analysis of

(002) reflection of Mg structure, using the Scherrer formula, gives the average grain size of 20 nm.

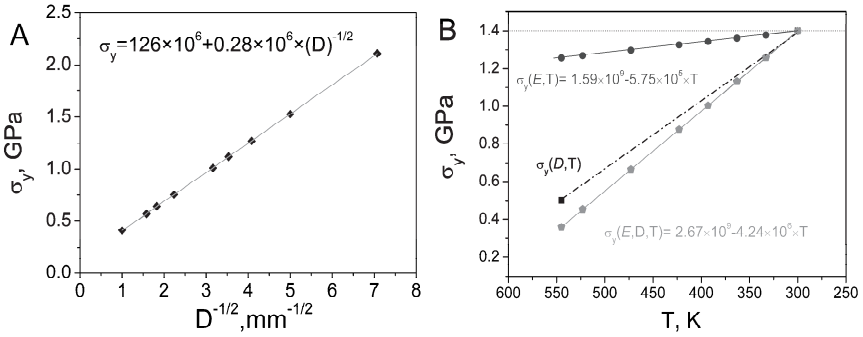

Fig. 6.7. (A) Dependence of the Yield strress on grain size in Mg films. (B) Effect of the Young modulus, $\sigma_y(E,T)$ (blue line), grain size $\sigma_y(D,T)$ (black dotted line) and their combined influence, $\sigma_y(E,D,T)$ (red line) on the Yield stress in Mg films. Solid lines are linear fits with the corresponding temperature dependences and the dotted line is just a guide to the eye. Dashed line at 1.4 GPa represents the Yield stress of Mg film with no temperature correction.

The analysis of the grain growth in Mg films with temperature is somewhat difficult. Grain growth is a temperature-activated and non-linear process [52]. It proceeds more rapidly as temperature increases, which is connected to an enhancement of diffusion rate with rising temperature. In addition to the temperature effect, the grain growth is also facilitated by means of hydrogen-induced Ostwald ripening [53]. An increase of the grain size of about 3 times during hydrogen cycling of Pd films was observed even at room temperature [54]. Because of a scarcity of the experimental data, the mathematical description of the grain size growth with temperature and its influence on the Yield stress has not been conducted. However, in order to have an idea on the order of numbers, an attempt was made to estimate the Yield stress in Mg films at the highest experimental temperature, 545 K.

Our preliminary analysis indicate that hydrogenation cycling at 333 K, followed by an annealing at 545 K for about 1-2 hours should result in a grain growth up to 300-400 nm. The Elastic limit of magnesium film with an average grain size of 350 nm is then reduces to about 0.5 GPa at 553 K, which is noticeably lower as compared to the Elastic limit of Mg film with 40 nm grain size at RT (Fig. 6.7 (A)). By comparing the influence of the Young modulus change, $\sigma_y(E,T)$ and grain growth, $\sigma_y(D,T)$ with temperature on the

Yield stress in Fig. 6.7 (B), we concluded that the latter has a much more pronounced effect.

A combination of $\sigma_y(E,T)$ and $\sigma_y(D,T)$ gives a total reduction of the Yield point. Since there are limited amount of points on the $\sigma_y(D,T)$ dependence, only two temperatures, namely 300 K and 553 K have been considered. Adding up of both contributions resulted in the Elastic limit of 0.37 GPa and 1.4 GPa at 545 K and 300 K, respectively. Assuming that the combined dependence, as well as the $\sigma_y(E,T)$, has a linear character we have made a linear fit through these two points (red line, Fig. 6.7 (B)) and estimated the Yield stress in the whole temperature range. It is worth mentioning that the final Yield stress at 545 K in Mg films, 0.37 GPa is very close to that one of Pd buckled film, 0.4 GPa (Chapter 4). The fact that both, Pd buckled films and Mg/Ta/Pd films at 533 K resembles behavior of the corresponding bulk materials means the same minor influence of the clamping effect, which support our calculations of the Yield point in Mg films.

Apart from the Yield stress change, the temperature increase also reduces the maximum mechanical stress in the plastic regime upon film hydrogenation (point 3, Fig. 6.4). Plastic deformations occur by the glide of dislocations, which require certain activation energy. The energy that has to be provided for dislocation to overcome the barrier during slip determines the dependence of the stress on temperature. When the energy barrier is sufficiently small for thermal energy (~kT) to be significant, thermal vibrations of the crystal atoms may assist the dislocation to move and overcome obstacles, opposing dislocation motion [55]. Therefore, at low temperatures this energy is provided in the form of mechanical work, while with increasing temperature the thermal energy contributes to the total energy and enables partly or fully to overcome the barrier, lowering the mechanical work. Furthermore, a reduction of the mechanical work also takes place at the expanse of a decrease of grain boundaries, which acts as a pinning centre for dislocation slip.

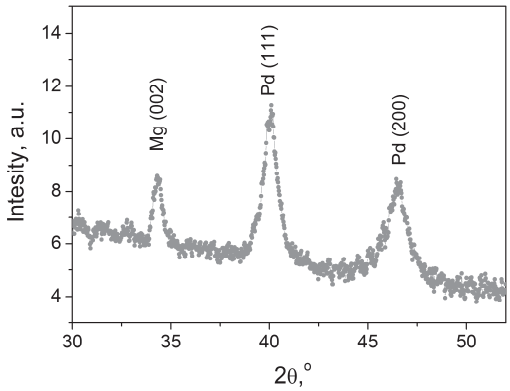

Fig. 6.8. XRD scan of the Mg(50 nm)/Ta(10 nm)/Pd(20 nm) film at room temperature.

A decrease of the Yield stress (point 2) and the maximum stress, point 3 on the stress-strain curve (Fig. 6.4) with temperature leads to a decrease of the total elastic+plastic expansion work in Mg/Ta/Pd films during (de-)hydrogenation cycle. By using the temperature dependence of the Yield stress, σ_y(E,D,T) and taking into account the elasto-plastic behavior of Mg films we then calculate the Gibbs free energy change, ΔG_{hyst} in the whole temperature range. The recalculated pressure ratio with the stress-temperature correction (blue stars, Fig. 6.5) now exhibit a very good agreement with the experimental hysteresis (black circles). This example proves that the stress-strain theory with a proper temperature correction of the involved parameters is able to predict hysteresis behavior in metal hydride thin films in a wide temperature range.

Hydrogenography experiments on Mg/Pd films

Mg films with direct contact with Pd are measured simultaneously with Mg/Ta/Pd films to study the effect of the Pd cap-layer on the thermodynamic properties. Because of an extensive alloying between Mg and Pd [10] on one hand and kinetics issues on the other hand, the temperature range is reduced to 333–393 K, where we measure three PTI's in absorption and only two in desorption (Fig. 6.9).

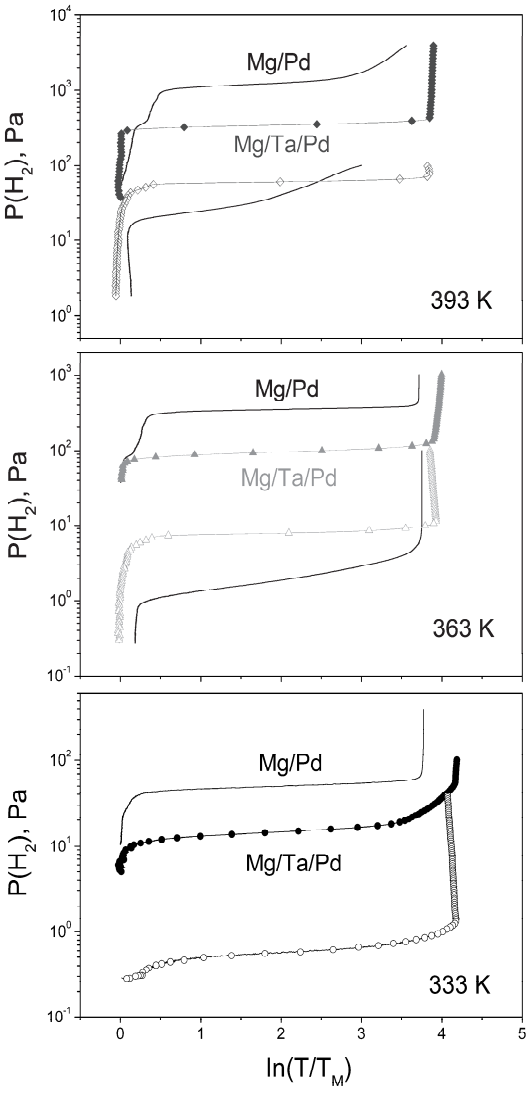

Fig. 6.9. Comparison between PTI's of the Mg/Pd and Mg/Ta/Pd films in the temperature range 333–393 K. Solid and solid+symbol lines represent (de-)hydrogenation behavior of Mg/Pd and Mg/Ta/Pd films, respectively.

Absorption equilibrium pressures in Mg/Pd films increases by 3.6-3.7 times at each temperature in the studied temperature range. Thus, the upwards shift of absorption by means of Pd capping layer is almost parallel with respect to Mg/Ta/Pd films (Fig. 6.10).

It is difficult to draw any solid conclusion form the desorption measurements. First of all, there are only two experimental points, which is not enough to calculate the thermodynamic parameters. Secondly, tilted desorption isotherms point out that the equilibrium conditions have not been established during the experiments due to kinetics and/or alloying reasons and that the pressure estimation error is quite high. Nevertheless, it is clear that the hydrogen unloading in Mg films with a direct contact with Pd capping layer takes place at lower hydrogen pressure (about 2.5-4 times lower) with respect to Mg films without the Mg/Pd interface (Fig. 6.9, Fig. 6.10).

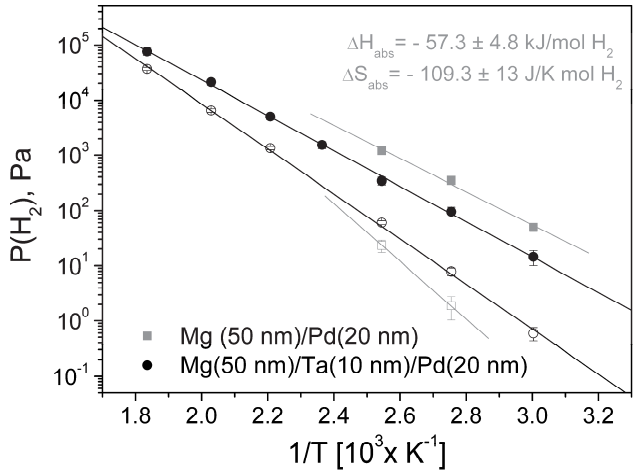

Fig. 6.10. Van 't Hoff plot of Mg films with (red squares) and without (black circles) a direct contact with Pd cap-layer. The error bars of the equilibrium pressure estimation are also presented.

The exact reason why the hysteresis expands when the Mg/Pd interface is present remains unclear. Baldi et al. [8] have proposed an explanation based on the elastic clamping of Mg layer by means of Pd, having affinity to form an alloy with Mg. This model suffers from explaining the complete (de-)hydrogenation behavior of Mg films, still, we think that the formation of Mg-Pd alloy at the interface is the main reason for the destabilization, observed in Pd capped Mg films.

Temperature, hydrogen treatment or even sputtering process can lead to an interdifussion of Mg into Pd layer and vice versa [10], forming a Mg-rich Mg-Pd alloy (Mg_9P_1, Mg_6Pd_1). This interface alloy, apparently, remains coherent with the rest of the film and becomes stiffer as compared to Mg itself. Upon hydrogenation, a larger expansion (elastic and plastic) work is therefore required to expand Mg films with the interface Mg-Pd alloy than without it, shifting absorption plateau to a higher pressures. A similar phenomenon is responsible for a decrease of the equilibrium pressure during desorption, expanding the whole hysteresis. Obviously, there is no difference whether the Mg-Pd alloy is formed at the interface or dispersed throughout whole volume of Mg film, as the (de-)hydrogenation behavior of the Mg/Pd films is in very good agreement with co-sputtered $Mg_{98}Pd_2$ samples [56] (Fig. 6.11)

In conclusion, to measure the intrinsic thermodynamics and hysteresis behavior of a Mg film, it should be decoupled from the Pd capping layer, by, for instance, an additional layer in-between Mg and Pd. This layer should not form any alloy with Mg and, preferably, with Pd and should be penetrable for hydrogen diffusion. These precautions should be taken into account for any metal hydride material under consideration, which forms an alloy with Pd

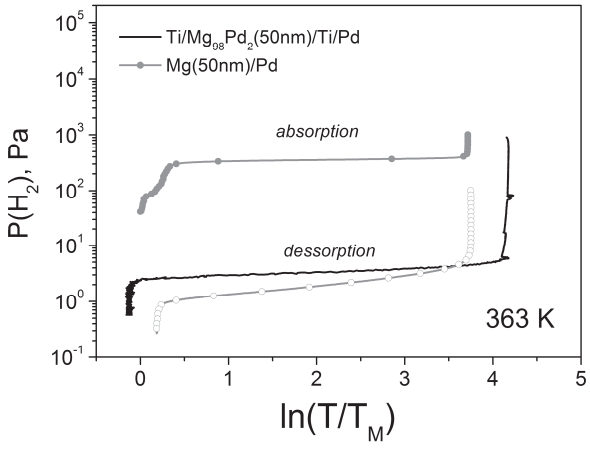

Fig. 6.11. Pressure-transmission-isotherms of the co-sputtered $Mg_{98}Pd_2$ and sandwiched Mg/Pd film at 363 K.

6.2.4 Conclusion

(De-)hydrogenation behavior of Mg/M/Pd (M=Ti, Ta, Fe) films has been studied in a wide temperature range (333–553 K). The enthalpy and entropy of hydride decomposition, estimated from the Van 't Hoff analysis, ΔH_{des} = -78.3 kJ/molH_2 and ΔS_{des} = -136.1 J/ K molH_2, respectively are found in a very good agreement with the bulk volumetric results. Contrary to desorption properties, absorption thermodynamic parameters, ΔH_{abs} = -61.6 kJ/molH_2, ΔS_{abs} = -110.9 J/K molH_2 are found noticeably higher as compared to bulk MgH_2, which is caused by the clamping effect.

The clamping effect is only present at low temperatures. The stress-strain analysis of the Mg/Ta/Pd films at 300–333 K proved that the increase of the hysteresis takes place as a result of a larger elastic+plastic expansion work of the films during loading and unloading hydrogen cycle. At elevated temperature (T>523 K) the ratio between absorption and desorption equilibrium pressures in films is essentially the same as in bulk, meaning a decrease of the expansion mechanical work.

A temperature dependence of the parameters, involved in the stress-strain theory showed that the Yield stress has the biggest influence on the mechanical work. Using a proper temperature correction of this parameter, it is possible to quantitatively and qualitatively explain hysteresis behavior in thin films as compared to bulk in a wide temperature range.

A direct contact between Mg and Pd in Mg/Pd films leads to an enhancment of hysteresis as compared to films without this interface, i.e. Mg/Ta/Pd. Absorption in Mg/Pd samples is increasing by a factor of 3.6-3.7, whereas desorption is decreasing by a factor of 2.5-4 with respect to Mg/Ta/Pd films in the temperature range 333–393 K. An increase of the hysteresis of about 15 times in Mg/Pd films at 363 K is, most likely, caused by formation of a stiffer Mg-Pd alloy at the Mg/Pd interface during deposition process and temperature/hydrogen treatment.

6.2.5 References

[1] D.G. Ivery, R.I. Chittim, K.J Chittim and D.O. Northwood, Metal hydrides for energy storage, J. Materials for energy systems 3(3) (1981) 3.

[2] A. Zaluska, L. Zaluska, J.O. Strom-Olsen, Nanocrystalline magnesium for hydrogen storage, J. Alloys Comp. 288 (1999) 217.

[3] T. Klassen, W. Oelerich, R. Bormann, Nanocrystalline Mg-based hydrides: hydrogen storage for the zero-emission vehicle, Journal of Metastable and Nanocrystalline Mat. 10 (2001), 603.

[4] B. Sakintuna, F. Lamari-Darkrim, M. Hircher, Metal hydrides for solid hydrogen storage: A review, Int. J. Hydrogen energy 32 (2007) 1121.

[5] M. Dornheim, S. Doppiu, G. Barkhordarian, U. Boesenberg, T. Klassen, O. Gutfleisch and R. Bormann, Hydrogen storage in magnesium-based hydrides and hydride composites, Scripta Mater. 56 (2007) 841.

[6] G. Prinsipi, F. Agresti, A. Maddalena, S.Lo Russo, The problem of solid hydrogen storage, Energy 34 (2009) 2087.

[7] I.P. Jain, C. Lal, A. Jain, Hydrogen storage in Mg: a most promising material, Int. J. Hydrogen energy 35 (2010) 5133.

[8] A. Baldi, M. Gonzalez-Silveira, V. Palmisno, B. Dam and R. Griessen, Destabilization of the Mg-H system through elastic constraints, Physical Review Letters 102 (2009) 226102.

[9] X. Tan, C. Harrower, B.S. Amirkhiz, D. Mitlin. Nano-scale bi-layer Pd/Ta, Pd/N and Pd/Fe catalysts for hydrogen sorption in magnesium thin films, Int. J. Hydrogen energy 34 (2009) 7741.

[10] A. Krozer, B. Kasemo, Hydrogen uptake by Pd-coated Mg: absorption-decomposition isotherms and uptake kinetics, J. Less Common Metals 160 (1990) 323.

[11] A. Fischer, A. Krozer and L. Schlapbach, Mg/Pd and Ba/Pd interfaces with without hydrogen, Surface Science 269-270 (1992) 737.

[12] K. Yoshimura, Y. Yamada, M. Okada, Hydrogenation of Pd capped Mg thin films at room temperature, Surface Science 556-568 (2004) 751.

[13] G. Silveiro, V. Bello, G. Mattei, P. Mazzoldi, G. Battaglin, N.Bazzanella, R. Checchetto, A. Moitello, Structural evolution of Pd-capped Mg thin films under H_2 absorption and desorption cycles, Int. J. Hydrogen energy 34 (2009) 4817.

[14] R. Gremaud, C. Broedersz, D. Borsa, A. Borgschulte, P. Mauron, H. Schreuders, B. Dam and R. Griessen, Hydrogenography: An optical combinatorial method to find new light-weight hydrogen-storage materials, Adv. Mater. 19 (2007) 2813.

[15] Y. Pivak, H. Schreuders, M. Slaman, R. Griessen, B. Dam, Thermodynamics, stress release and hysteresis behavior in highly adhesive Pd-H films, Int. J. Hydrogen energy 36(6) (2011) 4056.
[16] A. Pundt, Hydrogen in nano-sized metals, Adv. Eng. Materials 6 (2004) 11.
[17] J.F. Stampfer, C.E. Holley, J.F. Suttle, The magnesium-hydride system, J. American Chemical Society 82 (7) (1960) 3504.
[18] A.Y. Esayed and D.O. Northwood, Metal hydrides: a review of group V transition metals – Niobium, vanadium and tantalum, Int. J. Hydrogen Energy 17(1) (1992) 41.
[19] H. Friske and E. Wicke, Ber. Bunsenges. Phys. Chem. 77 (1972) 48.
[20] F.D. Manchester, Phase diagrams of binary hydrogen alloys, ASM International, Materials Park, 2000.
[21] F.H. Ellinger, C.E. Holley, Jr. , B.B. McInteer, D. Pavone, R.M. Potter, E. Staritsky and W.H. Zachariasen, "The preparation and some properties of magnesium hydride", J. Amer. Chem. Soc. 77 (1955) 2647.
[22] J.J. Reilly, R.H. Wiswall, The Reaction of Hydrogen with Alloys of Magnesium and Nickel and the Formation of Mg_2NiH_4, Inorganic Chemistry 7 (1968) 2254.
[23] E. Akiba, K. Nomura, S. Ono, Y. Minzuno, Journal of the Less Common Metals 83 (2) (1982) L43.
[24] K. Zeng, T. Klassen, W. Oelerich, R. Bormann, Critical assessment and thermodynamic modeling of the Mg-H system, Int. J. Hydrogen Energy 24 (1999) 989.
[25] B. Bogdanovic, K. Bohmhammel, B, Christ, A. Reiser, K. Schlichte, R. Vehlen, U. Wolf, Thermodynamic investigation of the magnesium-hydrogen system, J. Alloys Comp. 282 (1999) 84.
[26] K. Bohmhammel, U. Wolf, G. Wolf, E. Konigsberger, Thermodynamic optimization of the system magnesium-hydride, Thermochimica Acta 337 (1999) 195.
[27] K.J. Gross, P. Spatz, A. Zuttel, L. Schlapbach, J. Alloys Comp. 240 (1996) 206.
[28] W. Klose, V. Stuke, Int. J. Hydrogen energy 20 (1995) 309.
[29] A.S. Pedersen, J. Kjoller, B. Larsen, B. Vigeholm, International Journal of Hydrogen Energy 8(3) (1983) 205.
[30] P. Selvam, B. Viswanathan, C.S. Swamy, V. Srinivasan, Int. J. Hydrogen Energy 13(2) (1988) 87.
[31] P. Vermeulen, A. Ledovskikh, D. Danilov, P.H.L. Notten, Thermodynamics and kinetics of the thin film magnesium-hydrogen system, Acta Materialia 57 (2009) 4967.

[32] Z. Dehouche, H.A. Peretti, S. Hamoudi, Y. Yoo, K. Belkacemi, Effect pf activated alloys on hydrogen discharge kinetics of MgH_2 nanocrystals, Journal of Alloys and Compounds 455 (2008) 432.

[33] S. Wagner, H. Uchida, V. Burlaka, M. Vlach, M. Vlcek, F. Lukac, J. Cizek, C. Baehtz, A. Bell and A. Pundt, Achieving coherent phase transition in palladium-hydrogen thin films, Scripta Materialia 64 (2011) 978.

[34] R. Feenstra, D.G. de Groot, J.H. Rector, E. Salomons and R. Griessen, Gravimetric determination of pressure-compositional-isotherms of thin PdH_c films, J. Phys. F: Met. Phys. 16 (1986) 1953.

[35] M. W. Lee, and R. Glosser, Pressure-Concentration Isotherms of Thin Films of the Palladium-hydrogen System as Modified by Film Thickness, Hydrogen Cycling, and Stress. J. Appl. Phys. 57 (1985) 5326.

[36] E. Lee, J.M. Lee, J.H. Koo, W. Lee, T. Lee, Hysteresis behavior of electrical resistance in Pd thin films during the process of absorption and desorption of hydrogen gas, Int. J. Hydrogen energy 35 (2010) 6984.

[37] P. Vermeulen, A. Ledovskikh, D. Danilov, P.H.L. Notten, The impact of layer thickness on the thermodynamic properties of Pd hydride thin film electrodes, J. Phys. Chem. B 110 (2008) 20350.

[38] H. T. Uchida, R. Kirchheim and A. Pundt, Influence of hydrogen loading conditions on the blocking effect of nanocrystalline Mg films, Scripta Materialia, (2011), doi: 10.1016/j.scriptamat.2011.01.036.

[39] R.B. Schwartz, A.G. Khachaturyan, Thermodynamics of open two-phase systems with coherent interfaces: Application to metal-hydrogen systems, Acta Mater. 54(2006) 313.

[40] A. Ludwig, J. Cao, A. Savan, M. Ehmann, High-throughput characterization of hydrogen storage materials using thin films on micromachined Si substrates, Journal of Alloys and Compounds 446-447 (2007) 516.

[41] A. Ludwig, J. Cao, B. Dam, R. Gremaud, Opto-mechanical characterization of hydrogen storage properties of Mg–Ni thin film composition spreads, Applied Surface Science 254 (2007) 682.

[42] M. Pasturel, M. Slaman, H. Schreuders, J.H. Rector, D.M. Borsa, B. Dam and R. Griessen, Hydrogen absorption kinetics and optical properties of Pd-doped Mg thin films, J. Applied Physics 100 (2006) 023515.

[43] A. Baldi, G. K. Pálsson, M. Gonzalez-Silveira, H. Schreuders, M. Slaman, J. H. Rector, G. Krishnan,B. J. Kooi, G. S. Walker, M. W. Fay, B. Hjörvarsson, R. J. Wijngaarden, B. Dam, and R. Griessen, Mg/Ti multilayers: Structural and hydrogen absorption properties, Phys. Rev. B 81 (2010) 224203.

[44] T.H. Courtney, Mechanical Behavior of Materials, McGraw-Hill, New York, 1990.
[45] G. Simmons, H. Wang, Single Crystal Elastic Constants, 2nd ed., MIT Press, Cambridge, 1971.
[46] Y.P. Varshni, Temperature Dependence of the Elastic Constants, Phys. Rev. B 2 (1970) 3952.
[47] H.M. Ledbetter, Temperature behavior of Young's moduli of forty engineering alloys, Cryogenics, 1982.
[48] W.D. Callister, Fundamentals of Materials Science and Engineering, 2nd ed., Wiley & Sons. pp. 252.
[49] N. Hansen, Hall-Petch relation and boundary strengthening, Scripta Mater. 51 (2004) 801.
[50] F.E. Hauser, P.R. Landon, J.E. Dorn, Fracture of magnesium alloys at low temperatures, Trans AIME 206 (1956) 589.
[51] F. Ebrahimi and H. Li, Grain growth in electrodeposited nanocrystalline fcc Ni-Fe alloys, Scripta Mater. 55 (2006) 263.
[52] M. Di Vece, D. Grandjean, M. J. Van Bael, C. P. Romero, X. Wang, S. Decoster, A. Vantomme and P. Lievens, Hydrogen-Induced Ostwald Ripening at Room Temperature in a Pd Nanocluster Film, Phys. Rev. Lett. 100 (2008) 236105.
[53] R. Gremaud, M. Gonzalez-Silveira, Y. Pivak, S. de Man, M. Slaman, B. Dam and R. Griessen, Hydrogenography of PdH_x thin films: Influence of H-induced stress relaxation processes, Acta Mater. 57(4) (2008) 1209.
[54] D. Hull and D.J. Bacon, Introduction to Dislocations, 4th ed., Elsevier Butterworth-Heinemann, Oxford, 2001.
[55] A. Baldi, Hydrogenography experiments on $Mg_{1-Y}Pd_y$ (y=0.02-0.3) films, private communication.

Chapter 7

Hydrogenography of Mg-based complex hydrides

7.1 Introduction

Complex hydrides, where hydrogen is covalently bonded to central atoms in complex anions, are an important class of hydrogen storage materials. Depending on the central atom in the complex, one distinguishes alanates (AlH_4), amides (NH_2) and borohydrides (BH_4) [1]. These materials promise a gravimetric capacity in the range of 7–18 wt%, which makes them very attractive candidates for hydrogen storage [2]. However, their complicated, sometimes two-stage (de-)hydrogenation reaction usually requires too high temperatures, which limits their practical application. At the moment, a lot of attention is focused on improving the kinetics and thermodynamics of complex hydrides.

In the previous chapters a stress-strain model was developed to quantitatively predict the shift of the equilibrium pressure plateaus in thin films with respect to bulk. According to this model, an increase of the hysteresis takes place as a consequence of the substrate clamping resulting in a larger mechanical work required during the hydrogenation of films. The stress-strain model was successfully probed for interstitial PdH_x, YH_x, and MgH_x thin films. However, the formation of complex hydrides is even more intricate since it involves reactions between various solid phases and transitions to totally different crystal systems. In chapter 7.2 we study (de-)hydrogenation behavior of complex Mg_2NiH_4 hydride thin films using Hydrogenography. The reason why Mg_2NiH_4 is chosen as a model system to investigate the clamping effect in complex hydrides rather than another promising light weight complex hydride such as $NaAlH_4$- prepared recently in thin films [3]- is connected to its reversibility and fast kinetics, while sodium alanate thin films could not yet be made fully reversible. Pressure-transmission-isotherms of Mg_2NiH_4, measured in

a wide temperature range 303–513 K, were used to calculate thermodynamic parameters. We show that the enthalpy and entropy of hydride formation and decomposition are almost symmetrically affected by the clamping effect. The hysteresis in Mg_2NiH_4 spans more than 3 orders of magnitude around room temperatures and is a factor 1000 larger as compared to extrapolated bulk data at the same temperature. The clamping effect does not completely disappear at high temperatures, as the hysteresis in thin films is still larger with respect to bulk by a factor of 23 at 513 K. Our stress-strain analysis, performed to explain the hysteresis increase in Mg_2NiH_4 thin films, suggests a substantial influence of the structure transformation on the equilibrium pressures. Based on the difference between calculated mechanical work performed by the film against the in-plane compressive stresses and the experimental hysteresis, we conclude that the fact that the film transforms between two preferential orientations in structures with different symmetry, adds to the hysteresis. We suggest that the energy involved in this reorientation is related to the hexagonal-to-monoclinic structure transformation.

The following chapter is submitted to *Acta Materialia.*

7.2 Clamping effect in complex hydride Mg_2NiH_4 thin films

Abstract:

The thermodynamic properties and hysteresis behavior in Mg_2NiH_4 thin films were studied using Hydrogenography in the 303–513 K temperature range. For the enthalpy of hydride formation and decomposition, as estimated from a Van 't Hoff analysis, we find ΔH_{abs} = -51.2 kJ/molH_2, and ΔH_{des} = -76.3 kJ/molH_2. These values are affected by the clamping to the substrate. However, the average enthalpy of the (de-)hydrogenation reaction, $\Delta H=(\Delta H_{abs}+\Delta H_{des})/2$= -63.5 kJ/mol$H_2$ is in remarkable agreement with the average bulk data, -64 kJ/molH_2. The hysteresis in pressure in Mg_2NiH_4 thin films is about 1826 at 303 K, which is by a factor of 45 larger as compared to MgH_2 films. This behaviour is believed to originate from the fact that the phase transition in Mg_2NiH_4 films occurs between two preferentially oriented phases. We assume that the energy involved in the necessary re-orientation is related to the monoclinic to hexagonal structure transformation. By adding this term, the stress-strain analysis is able to explain the enormous difference between absorption and desorption equilibrium pressures in Mg_2NiH_4.

7.2.1 Introduction

Mg_2NiH_4 is the most successful example of destabilization of MgH_2 by means of alloying with transition metals [4]. An enthalpy of hydride decomposition of ΔH_{des} = -64.4 kJ/molH_2 and a moderate hydrogen storage capacity of 3.6 wt% makes Mg_2NiH_4 a promising medium for hydrogen storage. Mg_2NiH_4 belongs to a class of hydrogen storage materials, where hydrogen does not reside interstitially or ionically, but forms covalently bonded NiH_4^{4-} units ionically bonded to the Mg^{2+} matrix instead. Because of its robust kinetics, which allows for fast and, more important, reversible (de-)hydrogenation reactions even at room temperatures [5], Mg_2NiH_4 represents a unique candidate to study the influence of a substrate, i.e. clamping effect, on the thermodynamic properties and hysteresis behavior in complex hydride thin films. The knowledge of the substrate effect on the equilibrium properties will help us to validate the use of thin film combinatorial techniques to search for new complex metal hydride storage materials with appropriate thermodynamic properties.

Due to the volume expansion on hydrogenation, which is usually proportional to the hydrogen concentration of a film, in-plane mechanical stresses arise during hydrogen loading and unloading. These stresses are affected by various factors such as mechanical properties, grain size, crystal structure and the nature of the interatomic bonds. Mechanical properties such as the Young and Bulk modulus indicate the ability of a material to be deformed. Grain size variation leads to a change of the yield stress, which defines the onset of plastic deformations [6]. The crystal structure of the metal hydride determines the amount and type of slip systems. Materials having a relatively large number of slip systems (at least 12), such as metals with FCC or BCC crystal structures, are quite ductile because extensive plastic deformation is normally possible along the various directions. Conversely, HCP metals, having few active slip systems, are normally quite brittle [3]. The nature of the interatomic bonds, metallic, covalent or ionic, defines the activation energy for a dislocation to slip or, in other words, represents how readily the plastic deformations and stress relaxation can occur.

In this work we investigate the thermodynamic properties and hysteresis behavior of Mg_2NiH_4 thin films in a wide temperature range (303–513 K). Using Hydrogenography we study the (de-)hydrogenation behavior of Mg_2Ni films and determine the enthalpy and entropy of hydride formation and decomposition. By comparing the results with the existing bulk data we show that both hydrogen absorption and desorption parameters are influenced by the clamping of the film to the substrate. The hysteresis at room temperature is enormous and substantially larger with respect to extrapolated bulk data at the same temperature. The stress-strain analysis, performed to explain the huge difference between

hydrogen formation and decomposition pressures suggests a large effect of the structure transformation on the hysteresis behavior. The fact that the film has to switch between two preferentially oriented crystalline phases of different symmetry, makes the hysteresis behavior in Mg_2NiH_4 very distinguishable from that in magnesium hydride.

7.2.2 Experimental details

Mg_2Ni films were co-sputtered in a multitarget dc/rf magnetron deposition system (background pressure 10^{-7} Pa, deposition argon pressure 0.3 Pa) on 10×10 mm^2 fused glass substrates. Without breaking the vacuum, a layer of Pd was directly deposited on top of Mg_2Ni to prevent oxidation and to catalyze the hydrogen dissociation reaction.

The (de-)hydrogenation properties of the Mg_2Ni films were studied using Hydrogenography [8] in a temperature range from 303 to 513 K. Before an equilibrium measurement, several fast hydrogenation cycles were performed at 333 K. The absorption was performed in a hydrogen atmosphere in about hour, while desorption was carried out in oxygen. After this cycling procedure a steady-state condition was reached and the equilibrium Pressure-Transmission-Isotherms (PTI's) were recorded; typical loading and unloading times are 30 hours and 48 hours at 333 K. PTI's were measured using both, a continuous and a step-scan mode of pressure changing, where the latter is used to check the kinetics of Mg_2Ni films.

The absorption/desorption equilibrium pressures were used to construct the Van 't Hoff plot. The values for the enthalpy and entropy of hydride formation/decomposition were obtained from the slope of the linear fit (ΔH) and from the cross-point of this fit with the y-axis (ΔS), respectively.

The structural characterization was performed in a Bruker D8 Discover X-ray diffractometer (Cu K_α, $\lambda = 1.5418$ Å) mounted in a $\theta/2\theta$ Bragg-Brentano geometry and equipped with Euler goniometer and a 2D HI-STAR detector. XRD scans were taken in the as-deposited and hydrided state in the angle range $23^o<2\theta<57^o$ at room temperature. Metallic (Mg_2Ni) films were measured in air, while *in- situ* hydrogenation x-ray experiments are conducted with a Beryllium dome at a constant hydrogen pressure of 10^5 Pa.

7.2.3 Results and discussion

Thermodynamic properties and hysteresis behavior of Mg_2NiH_4 thin films

The absorption and desorption pressure-transmission-isotherms of a Mg_2NiH_4 film, measured at 333 K in a step-scan mode is presented in Fig. 7.1. In the step-scan mode, which is used to check the kinetic properties of the complex hydride films during (de-)hydrogenation, the system is allowed to relax in each step, which reveals whether the equilibrium between metal phase and hydrogen gas has been reached or not. Well-defined and flat steps in the α-phase, β-phase and, which is more important, in the coexistence region suggest no kinetic limitations in Mg_2NiH_4 films at this temperature. Thus we estimated that a pressure ramp of around 1.69×10^{-5} log(Pa)/sec and 1.46×10^{-5} log(Pa)/sec is needed in order to work at quasi steady state in absorption and desorption, respectively. These conditions were used in subsequent experiments over the whole temperature range. All isotherms, recorded using a continuous mode of pressure ramping, Fig. 7.2, show flat, non-sloping plateaus, similar to those in Fig. 7.1, pointing towards thermodynamically governed equilibrium measurements.

Absorption and desorption equilibrium pressures, estimated form the midpoint of the corresponding PTI plateau, were used to build up the Van 't Hoff plot (Fig. 7.3) from which the thermodynamic parameters of Mg_2NiH_4 thin films were calculated. The enthalpy and entropy of hydride formation and decomposition, found in this way are: ΔH_{abs} = -51.2 kJ/molH_2, ΔS_{abs} = -108.8 J/K molH_2 and ΔH_{des} = -76.3 kJ/molH_2, ΔS_{des} = -129.2 J/ K molH_2, respectively. The absorption results are in a very good agreement with the previous hydrogenography experiments on Mg-Ni gradient films (Fig. 7.3), though those authors used a substantially smaller temperature range, T<363 K [9]. There is no data on the desorption thermodynamics of complex hydride Mg_2NiH_4 films except for free-standing thick (1.6 μm) Mg_2Ni. The desorption pressures of these free-standing Mg-Ni films, determined gravimetrically in the range 453 K- 669 K by Rogers et al. [10], are consistent with bulk data on Mg_2NiH_4, but no thermodynamic parameters were given.

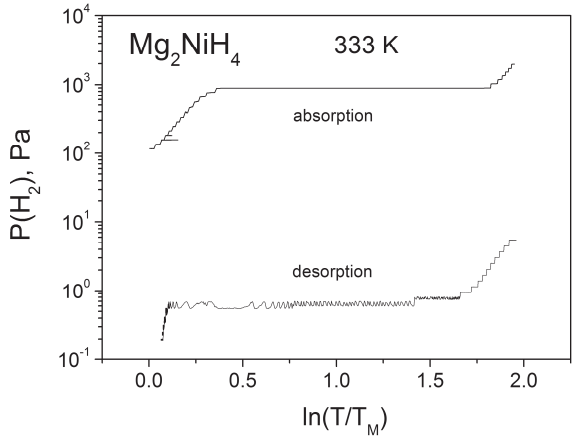

Fig. 7.1. Absorption and desorption pressure-transmission-isotherms of 50 nm Mg_2NiH_4 thin films, taken in a step-scan mode of pressure ramping at 333 K. Note that the hysteresis is not only reflected in a large difference between absorption and desorption equilibrium pressures, but it is also visible from the difference in the boundaries of the two phase region in both branches of the hysteresis.

The thermodynamic parameters of bulk Mg_2NiH_4 have been extensively investigated over the last few decades [3, 11-18]. Most of the experimental results [4, 11-13, 15], measured in the temperature range 493–748 K give the enthalpy of hydride absorption and desorption around -62 kJ/molH_2 and -64 kJ/molH_2, respectively. The only exception is the work of Gross et al. [18], who obtained similar thermodynamic properties to that of Hydrogenography, ΔH_{abs} = -51.2 kJ/molH_2 and ΔH_{des} = -72.9 kJ/molH_2 by studying Mg-based composites, containing Mg, Mg_2Ni and La phases. However, as the thermodynamics of Mg_2NiH_4 was found to depend strongly on the composition, apparently, the nature of the composite material, i.e. the presence of different hydrogen reacting phases affects the hydrogen loading and unloading [18]. A comparison of our thin film results with bulk data clearly shows that both absorption and desorption parameters are substantially influenced by the film-substrate interaction. Thus, the apparent enthalpy of hydride formation and decomposition, determined by means of the optical thin film approach deviates by 10.8 kJ/molH_2 and 12.3 kJ/molH_2, respectively, as compared to bulk Mg_2NiH_4. Still, the average enthalpy, $\Delta H=(\Delta H_{abs}+\Delta H_{des})/2$ remains very similar to that of bulk, i.e. -63.5 kJ/mol H_2, showing that the influence of the substrate on the thermodynamics is quite symmetric. This is in sharp contrast what was observed in MgH_2 films (Chapter 6), where only the absorption was considerably affected by the clamping effect. Furthermore, we find that the

effect on the absorption and desorption enthalpies, $\delta\Delta H=(\Delta H_{abs}-\Delta H_{des})$, is much larger in this complex hydride film as compared to the magnesium hydride film.

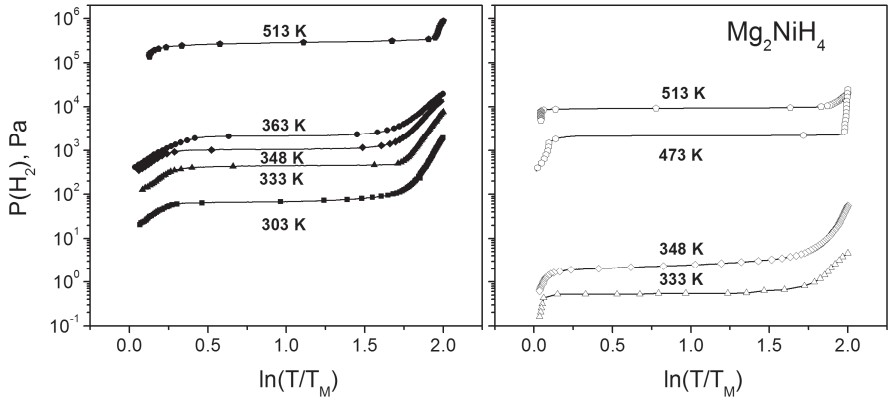

Fig. 7.2. Pressure-transmission isotherms of 50 nm Mg_2NiH_4 films in the temperature range 303–513 K. Hydrogen absorption (left) and desorption (right) are represented by filled and open symbols, respectively.

The large difference in enthalpy on loading and unloading results in a huge hysteresis. The pressure ratio amounts to a factor 1826 at 303 K. It is 45 times larger than in magnesium hydride films and 1014 times larger thah the extrapolated Mg_2NiH_4 bulk data at the same temperature. Since there is no bulk data available at these temperatures, the bulk equilibrium pressures at low temperatures were obtained using an extrapolation from the high temperature results of Song et al. [15] (Fig. 7.3). Note, however, that the accuracy of the bulk pressures estimated in this way are questionable because (i) the (de-)hydrogenation properties of bulk Mg_2NiH_4 have been measured in a small temperature range, 443-501 K, and (ii) therefore need to be extrapolated over a large temperature range, 200 K. Surprisingly, even at elevated temperatures, T > 500 K, the hysteresis in Mg_2NiH_4 films is still much larger (23 times at 513 K) as compared to bulk results, Fig. 7.3. This is opposite to the behaviour of MgH_2 films, where at high temperature (T >500 K) the clamping effect was negligible and the hysteresis was essentially the same as in bulk (Fig. 6.3, chapter 6).

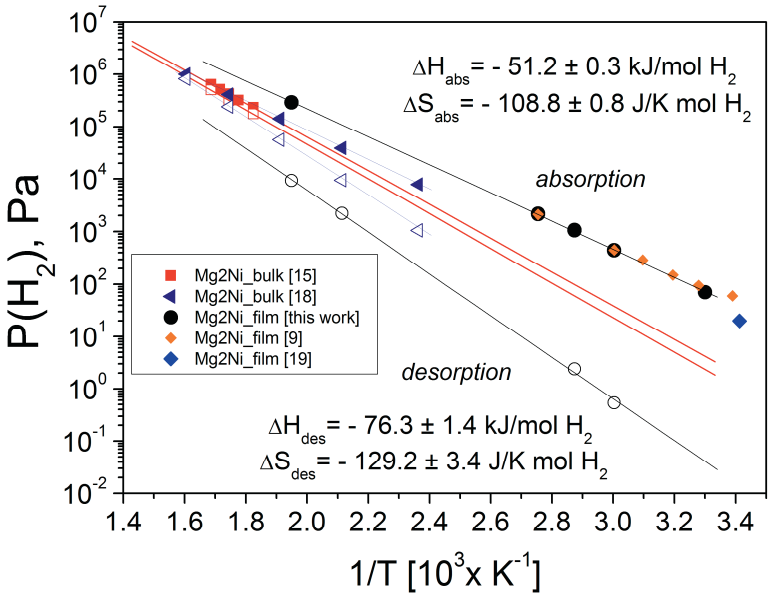

Fig. 7.3. Van 't Hoff plot of the Mg_2NiH_4 films with the calculated enthalpies and entropies of hydride formation and decomposition; thermodynamic parameters are calculated from the linear regression analysis. Additionally, results on Mg_2Ni films, measured by Gremaud et al. [9, 19] using Hydrogenography (orange diamonds) and electrochemistry (blue diamonds) and Mg_2Ni bulk measured by Song et al. [15] (red squares) and Gross et al. [18] (dark blue triangles) are also presented. Solid lines represent fits to thin films and bulk data.

Since there is no protective intermediate layer between Mg_2Ni and Pd, we can not totally exclude interalloying between these layers, which in Mg has a strong influence on the measured equilibrium pressures [20]. However, hydrogenation cycling at 333 reveals a negligible interaction between Mg_2Ni and Pd layer, as the absorption equilibrium pressure only slightly changes between 1st and 4th slow (20 hours) loadings (Fig. 7.4). To reduce and/or prevent possible interalloying at elevated temperature, where diffusion of atoms are known to be higher, every pressure-transmission-isotherm above 333 K was recorded with a new sample from the same sputtering batch.

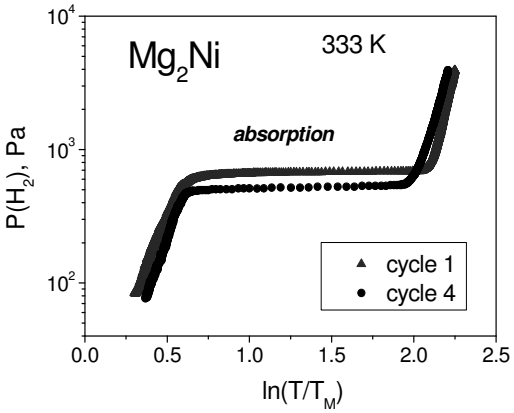

Fig. 7.4. Pressure-transmission isotherms of the Mg_2NiH_4 films during 1st and 4th slow (20 hours) hydrogenation cycles at 333 K [21].

Hence, our Hydrogenography results on Mg_2NiH_4 thin films clearly show an anomalously expanded hysteresis, which is symmetric with respect to the extrapolated bulk values. Thus, we have to answer the question what is the special feature of the clamping of a complex hydride thin film that can explain the increase of the hysteresis by a factor of thousand at near ambient temperatures as compared to bulk.

Stress-strain analysis of complex hydrides

The stress-strain model, developed in Chapter 4, postulates that a widening of the hysteresis in films as compared to bulk occurs due to the expansion constraints imposed by the presence of a rigid substrate which leads to additional expansion work upon (de-)hydrogenation of the films [22]. This work depends on the elastic and plastic deformations, where the plastic contribution is considered to have the larger impact on the hydrogenation pressure. The increase of the hysteresis, which is responsible for changes in thermodynamic parameters of the thin films with respect to bulk, is proportional to the amount of expansion work via the following equation:

$$\frac{1}{2}RT\ln\left((P_{abs}/P_{des})_{film}/(P_{abs}/P_{des})_{bulk}\right)=V_M/(c_\beta-c_\alpha)\cdot\int_o^{\varepsilon_{max}}\sigma\, d\varepsilon_V=\Delta G_{hyst} \quad (7.1)$$

where R is the gas constant, T is the absolute temperature, V_M is the molar volume of the Mg_2Ni metal phase, $c_{\beta,\alpha}$ is the maximum hydrogen concentration in the β and α phase and σ and ε correspond to the stresses and volume strains in Mg_2NiH_4 films, respectively. Note,

that the ΔG_{hyst} is the energy in kJ/mol H, which implies that ($c_\beta - c_\alpha$), corresponding to the width of the equilibrium plateau, is taken as H/formula unit.

Eq. (7.1) was successfully applied to predict an increase of the hysteresis as a result of clamping for Pd (chapter 4) and Mg (chapter 6) hydrides; for Y hydrides the stress-strain model was modified by an additional structural parameter, $\Delta G_{fcc\text{-}hex}$ (chapter 5). It was concluded that this stress-strain model is valid to any interstitial metal hydrides with and without structure transformation. Since Mg_2NiH_4 belongs to the class of complex hydrides, the question arises whether this theory can also be used to explain a widening of the hysteresis in Mg_2NiH_4 thin films.

Similarly to MgH_2, Mg_2NiH_4 exhibits a large volume expansion and a structure transformation during (de-)hydrogenation. However, the formation of hydrogen units in complex hydrides, changing the Mg_2Ni matrix completely and lowering its symmetry to a monoclinic, is what distinguishes Mg_2NiH_4 from MgH_2 (in which the Mg and hydrogen are covalently and ionically bonded). And the interstitial metal hydride such as $PdH_{0.6}$.

To confirm that the stress-strain model is valid for complex hydrides and to check whether the hysteresis in Mg_2NiH_4 films expands in response to additional plastic deformations, we need to numerically solve both parts of eq. (7.1). The right part of the equation contains information on the experimentally measured hysteresis in thin films and bulk Mg_2NiH_4 at a certain temperature, while the left part describes the mechanical work, exerted during the (de-)hydrogenation of the clamped films. The right part of the eq. (7.1) can be calculated from the data shown in the Van 't Hoff plot (Fig. 7.3) in a wide range of temperatures, whereas the mechanical work represents an unknown variable. To compute it, a stress-strain curve, which shows the dependence of the hydrogenation stresses created in a film versus its volume expansion [22], is required.

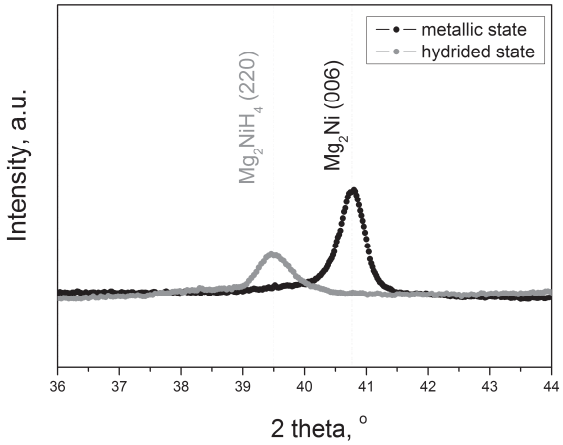

Fig. 7.5. Part of the XRD scans of the 50 nm Mg_2Ni film in the metallic (black line) and hydrided state (red line) at room temperature, showing (006) and (220) peaks of the hexagonal and monoclinic structures, respectively. Hydrogenation has been performed in-situ at a H_2 pressure of 10^5 Pa.

To measure the volume strain we did X-ray diffraction experiments during hydrogenation. Fig. 7.5 shows X-Ray diffraction scans of the as-deposited and hydrogenated Mg_2Ni film at room temperature. The peak at 40.76^o was indexed as the (006) reflection of the hexagonal crystal lattice (Fig. 7.6). From Bragg's law it follows that the *c* lattice parameter equals 13.284 Å, which is in a good agreement with reported literature bulk values of Mg_2Ni [18, 23]. On hydrogenation, the hexagonal structure transforms to a monoclinic phase, which is the low temperature modification of Mg_2NiH_4 (Fig. 7.6). The peak at 39.51^o corresponds to the (220) plane of the monoclinic lattice. The interplanar distance d_{220}=2.281(10) Å, calculated from Bragg's law agrees well with the bulk value in the fully hydrogenated state, i.e. d_{220}=2.2803 Å [24]. Due to the preferential orientation of the crystalline grains in the metallic and hydrogenated state of Mg_2Ni films, only a limited amount of reflections are present in the XRD pattern (Fig. 7.5). It is, therefore, unfeasible to calculate all lattice parameters of the hexagonal and monoclinic structures and, accordingly, the overall volume expansion during the phase transformation in the Mg_2NiH_4 film. However, the agreement between thin film and bulk structural parameters in metallic and hydrided state described above (Fig. 7.5) suggests that the volume expansion in both type samples should be similar as well. The same conclusion was drawn by comparing the volume expansion in Pd/Ti films, studied by XRD, with the volume change in Pd bulk [22].

As a result, we assume that the volume expansion in thin films occurs only in vertical direction and mostly by means of plastic deformations, i.e. material pile-up.

To have an estimate fthe volume expansion in Mg_2NiH_4 films, we took the bulk values in the metallic and hydrided state from Semicic et al. [23] and Noreus et al. [24], which are quite similar. From [23] and [23] it follows that the molar volume of the Mg_2Ni and Mg_2NiH_4 phases are 31.47×10^{-6} m^3/mol and 41.36×10^{-6} m^3/mol. Thus, the volume expansion in Mg_2Ni films during hydrogenation is 31.4 %. It is worth mentioning that a similar volume expansion, e.g. 30% was obtained in thin Mg layers on hydrogen loading of Mg/Ti films by measuring thickness increase using X-ray reflectometry [28].

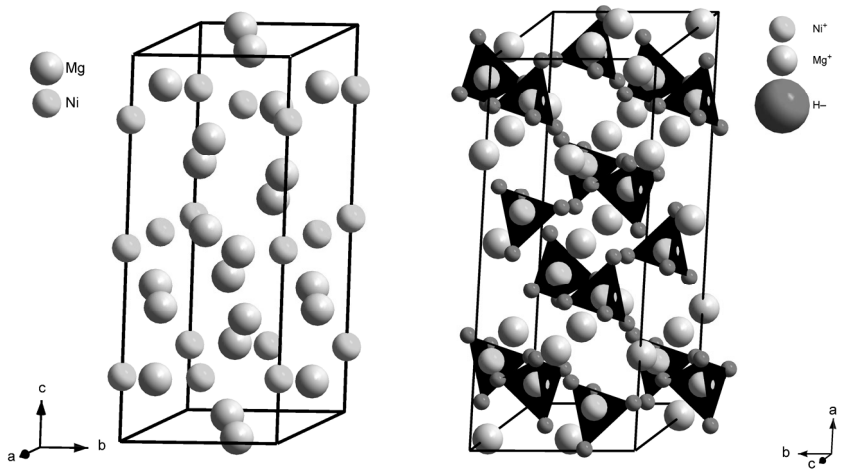

Fig. 7.6. Hexagonal Mg_2Ni (left) and monoclinic Mg_2NiH_4 (right) crystal structures. The size of hydrogen ions in Mg_2NiH_4 structure is reduced to have a better visibility.

The in-plane compressive stresses in Mg_2Ni films during hydrogen loading were measured by Ludwig et al. [29] using the substrate bending technique. The maximum hydrogenation stress in Mg_2Ni reaches about -1.4 GPa, which was assigned as the Yield stress in Mg_2Ni films in the fully hydrogenated state, considering the elasto-plastic behavior of our samples (Chapter 4).

Based on the values of the stresses and volume strains, a simplified stress-strain curve was constructed (Fig. 7.7). As we do not know all the necessary data, this stress-strain curve does not include the change from the compressive to tensile stresses on going from absorption to desorption. It is worth mentioning that the presence of a tensile stress is expected to just shift the whole stress-strain curve downwards, not substantially affecting

the calculations. Therefore, a simplified picture with only the compressive stresses in Mg_2Ni films was used in this work.

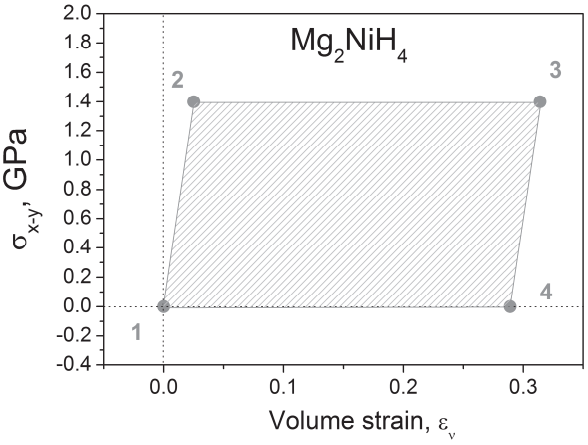

Fig. 7.7. The stress-strain curve of the Mg_2NiH_4 film during (de-)hydrogenation; numbers represent different hydrogenation and dehydrogenation steps, namely elastic expansion of the film (1-2), plastic deformation (2-3), elastic recovery (3-4) and plastic deformations (4-1), returning the films to its initial state (1).

Point 1 on the stress-strain curve corresponds to the metallic state of the Mg_2Ni film. By absorbing a very small amount of hydrogen, the Mg_2Ni film expands elastically. The elastic expansion (1-2) is believed to coincide with the α-phase, or the solid solution of hydrogen in metal after which the nucleation of β-phase starts; this relation between alpha phase and elastic expansion may, however, fail due to clamping. The elastic deformations stop when the in-plane stresses reach the Yield point or Elastic limit, point 2, which represents the beginning of plastic deformations. In the case of Mg_2Ni film, the Yield point is equal to 1.4 GPa.

The elastic expansion can be estimated from the Young modulus and the Yield stress of a material. Unfortunately, there is no data on the Young modulus of Mg_2Ni. Still, it can be estimated from the Bulk modulus, B and Poisson ratio, ν via the following equation: $E = 3B(1-2\nu)$. Taking into account the Bulk modulus of the Mg_2Ni structure, B=60.8 GPa, calculated by Zhang et al. [8] and the Poisson ratio of Mg, ν=0.35 the Young modulus of the alloy equals 54.7 GPa. It is worth mentioning that the Poisson ratio of Mg_2Ni is not expected to differ much from that of Mg because: (i) the Poisson's ratio of Ni is very close to that of Mg, 0.31; (ii) the Poisson ratio for most metals falls between 0.25 to

0.35. The elastic volume strain is then calculated from Hooke's law, taking into account the calculated Young modulus of Mg_2Ni and the Yield stress. The value of 2.6% (Fig. 7.7) agrees reasonably well with the volume expansion of 1.7 % of the $Mg_2NiH_{0.3}$ [24, 26], which is the solid solution phase. During the expansion of 1.7%, which corresponds to the hydrogen concentration of 0.09 H/M, the structure remains hexagonal.

Subsequent hydrogen loading (2-3) occurs at the expense of material rearrangement by means of e.g. dislocation slip. The volume increase associated with the formation of Mg_2NiH_4 is translated into a thickness increase of the Mg_2Ni film with no change in the stress state. It stops when it reaches the total volume strain of 31.4 %, point 3 on the stress-strain curve (Fig. 7.7).

In the absence of experimental data, we assume a similar behavior upon dehydrogenation. First, the film shrinks elastically to point 4. The elastic recovery involves the same amount of stress decrease and the same amount of volume change as during the loading process (1-2), namely 2.6 %. Then, plastic deformations return the film to the initial state, point 1. It is worth mentioning that the dehydrogenation (step 4-1) in Mg_2Ni films is expected to occur similarly to clamped Pd films (Chapter 4) – with a change of the stress-state from compressive to tensile. Tensile stress is very important as it represents the driving force, needed to complete the unloading reaction. In this specific case, in the absence of appropriate data, the presence of the negative stress in the stress-strain curve was neglected (see Chapter 6).

From the area of the polygon in Fig. 7.7 the mechanical work, performed by the Mg_2Ni film upon (de-)hydrogenation cycle was evaluated. A substitution of the estimated mechanical work, $\int_{o}^{\varepsilon_{max}} \sigma d\varepsilon_V$ =0.403 GJ/m^3, molar volume of Mg_2Ni, V_M=31.47×10^{-6} m^3/mol and the width of the plateau of bulk Mg_2Ni, (c_β–c_α)=3.6 H/formula unit into the left side of eq. (7.1) yields the Gibbs free energy change, ΔG_{hyst} of 3.52 kJ/(mol H). The (c_β–c_α) in the films is probably lower than bulk due to a higher amount of grain boundaries in the former samples [30]. However, to have an estimate on ΔG_{hyst} we assumed that the width of the plateau in thin films of complex hydride is similar to that of bulk. Substituting the hydrogenography data for the experimentally observed hysteresis (P_{abs} / P_{des}) in Mg_2Ni film (1826) and an extrapolated hysteresis for Mg_2Ni bulk (1.8) (Fig. 7.3, red line) at 303 K with the gas constant, R=8.314 J/(K·mol) into the left side of eq. (7.1) yields the value of 8.72 kJ/(mol H).

The experimental hysteresis found in Mg_2NiH_4 is much larger than expected from the stress-strain model on the basis of the calculated elastic and plastic work resulting from the volumetric expansion. This finding is rather surprising, as we would expect a similar

hysteresis as in MgH_2 films at low temperatures (303 K). So what is the difference between the two samples?

We propose that this difference originates from the fact that Mg_2NiH_4 switches between two preferentially oriented crystalline states. In contrast the Mg films, certainly after a few cycles, become X-ray amorphous in both the metallic and the hydrogenated state. The preferential orientation of a film usually takes care to have the densest stacking direction normal the surface. Now the details of the structural transition in Mg_2NiH_4 are quite complex. However, when we assume that Mg_2NiH_4 has a pseudo-cubic structure, in any (110) oriented crystallite there are at least 5 other direction which are almost as densely packed. We assume now that all these [110]-directions may transform into an hcp 0001 axis. In that case, in order to preserve the preferential nature of the hcp Mg_2Ni phase, the system has to transform all the misoriented hcp grains and bring them into alignment. Conversely, there is no unique way to transform the hcp Mg_2Ni structure into the hydride. This suggests that, in order to obtain a (110) preferential orientation, again a substantial reorientation is necessary. This rearrangement certainly costs additional energy. Moreover, it explains why this expanded hysteresis is typical for thin films: there is no preferential orientation in bulk. The Mg_2NiH_4 system is however too complex to prove the validity of our model. However, in chapter 5, we saw an example of Y vs La that the phase transformation in relation to a preferential thin film orientation may indeed increase the hysteresis by several orders of magnitude.

In the case of YH_x films we included an additional parameter, $\Delta G_{fcc-hex}$, which represents the energy involved in the fcc-hex structure transformation, in the stress-strain equation (chapter 5). Similarly, we modify eq. (7.1) by the ΔG_{str} parameter, associated with the hcp-monoclinic and monoclinic-hcp structure transformations in Mg_2NiH_4 films during (de-)hydrogenation cycle:

$$\frac{1}{2}RT\ln\left((P_{abs}/P_{des})_{film}/(P_{abs}/P_{des})_{bulk}\right)=V_M/(c_\beta-c_\alpha)\cdot\int_0^{\varepsilon_{max}}\sigma\, d\varepsilon_V+\Delta G_{str} \quad (7.2)$$

By a simple reorganization of eq. (7.2), the energy of the structure transformation in Mg_2NiH_4 can be estimated. A substitution of the experimentally observed hysteresis in Mg_2NiH_4 films (8.72 kJ/mol H) at 303 K along with the calculated mechanical work done by the film upon (de-)hydrogenation cycle (3.52 kJ/mol H) in the right side of the eq. (7.2), yields the value of 5.2 kJ/(mol H) for the ΔG_{str}. The calculated value is very similar to the energy involved in the fcc-hex structure transformation in YH_x films [32]. This finding supports our assumption that the increase of the hysteresis in Mg_2NiH_4 films with respect to MgH_2 takes place due to the preferential orientation in both phases and the structure

transformations needed to maintain this on cycling. It also suggests that the stress-strain model may by able to qualitatively predict the experimental hysteresis in Mg_2NiH_4 films if the energy of the structure transformation can be calculated separately.

The size of the hysteresis is not the only difference between the MgH_2 and Mg_2NiH_4 thin films. In Mg_2NiH_4 films the expansion of the hysteresis is symmetrical with respect to the reference bulk data (Fig. 7.3), contrary to magnesium hydride. The asymmetry in MgH_2 comes from the fact that the elastic contribution to the hysteresis is quite sizeable and enhances the plastic contributions upon hydrogenation but counteracts it during dehydrogenation (chapter 4). In Mg_2NiH_4, the elastic contribution becomes substantially smaller as compared to the overall plastic contribution, since the hysteresis becomes largely affected by the ΔG_{str} . This term, which reflects the energy involved in the grain reorientation upon the structure transformation, enhances the plastic contribution both in, absorption and desorption. As the plastic contribution itself leads to a symmetric expansion of the hysteresis (chapter 4) and the elastic contribution is very small, it implies that the structure transformation should be symmetric as well.

A large difference between thin films and bulk remains in Mg_2NiH_4 films even at elevated temperatures (513 K), while the hysteresis in MgH_2 films was found essentially the same as in bulk at 523 K. By analogy with MgH_2 films (chapter 6), a decrease of the Yield stress (point 2) and the maximum stress, point 3, on the stress-strain curve (Fig. 7.7) with temperature is considered to be the cause of a decrease of the mechanical work in Mg_2NiH_4 films during the (de-)hydrogenation cycle at 513 K. From the experimental results we conclude that the mechanical properties in Mg_2NiH_4 are not as temperature dependent as in MgH_2; similarly, a low temperature dependence is expected for ΔG_{str} , which also affects the hysteresis. A possible origin for this behavior might be connected to about 500 K difference in the melting temperature between Mg_2Ni (1419 K) and Mg (923 K) [16], which has a direct influence on the Young modulus [31]. The magnitude of the Young modulus represents the interatomic bonding force, which decreases with increasing temperature (due to an increase of atomic separation distance). As the melting temperature in Mg_2Ni is larger as compared to Mg, the decline of the Young modulus with temperature is expected to be slower in the former case.

7.2.4 Conclusion

The (de-)hydrogenation behavior of complex Mg_2NiH_4 thin films has been investigated for the first time in absorption and desorption over a wide temperature range 303–513 K using Hydrogenography. The thermodynamic parameters calculated from the

Van 't Hoff plot are substantially influenced by the clamping of the film to the substrate. Optically measured enthalpies of hydride formation and decomposition in Mg_2NiH_4 films were found to deviate by about 10.8 kJ/molH_2 and -12.3 kJ/molH_2, respectively, from bulk Mg_2NiH_4. The widening of the hysteresis is quite symmetric, since the average enthalpy appears to be the same as in bulk, i.e. -63.5 kJ/molH_2. The hysteresis in these complex hydride thin films is more than 3 orders of magnitude at near ambient temperatures. It is larger by a factor of 1000 as compared to bulk Mg_2NiH_4 data, extrapolated from high temperatures and by a factor of 45 larger as compared to magnesium hydride films. The substantially larger influence of the substrate on the hysteresis behavior of Mg_2NiH_4 films as compared to MgH_2 is caused by the transformation between two preferentially oriented crystalline phases of different symmetry in the former case. The stress-strain analysis is able to explain the large hysteresis increase as compared to bulk at 303 K when the energy of the monoclinic-hcp structure transformation is taken into account. This difference between thin films and bulk remains even at the highest experimental temperature, 513 K, where no effect of the substrate was found for MgH_2 films. The difference in temperature dependence is probably due to the difference in melting point, which causes only a slight variation of the elastic parameters in this temperature range.

In any metal hydride films with a structure transformation where metal and hydride phase are structurally related and retain their preferential orientation, a structurally related parameter should be included in the stress-strain equation in order to quantitatively explain the experimental hysteresis in thin films. With the proper ΔG_{str} parameter, the stress-strain model, initially developed to quantitatively describe the difference between the hysteresis behavior in buckled and clamped Pd films, can be also used to predict the clamping effect in complex hydride thin films.

7.2.5 References

[1] B. Sakintuna, F. Lamari-Darkrim, M. Hirscher, Metal hydride materials for solid hydrogen storage: A review, Int. J. Hydrogen energy 32 (2007) 1121.

[2] P. Jena, Materials for hydrogen storage: Past, present, and future. J. Phys. Chem. Lett. 2 (2011) 206.

[3] M. Filippi, J.H. Rector, R. Gremaud, M.J. van Setten and B. Dam, Lightweight sodium alanate thin films grown by reactive sputtering, App. Phys. Let. 95 (2009) 121904.

[4] J.J. Reily and R.H. Wiswall, The Reaction of Hydrogen with Alloys of Magnesium and Nickel and the Formation of Mg_2NiH_4, Inorganic Chemistry 7 (1968) 2254.

[5] T.J. Richardson, J.L. Slack, R.D. Armitage, R. Kostecki, B. Farangis and M.D.Rubin, Switchable mirrors based on nickel-magnesium films, Appl. Phys. Lett. 78 (2001) 3047.

[6] W.D. Callister, Fundamentals of Materials Science and Engineering, 2nd ed., Wiley & Sons. pp. 252.

[7] J. Zhang, D.W. Zhou, L.P. He, P. Peng, J.S. Liu, First-principles investigation of Mg_2Ni phase and high/low temperature Mg_2NiH_4 complex hydrides, J. Phys. Chem. Solids 70 (2009) 32.

[8] R. Gremaud, C. Broedersz, D. Borsa, A. Borgschulte, P. Mauron, H. Schreuders, B. Dam and R. Griessen, Hydrogenography: An optical combinatorial method to find new light-weight hydrogen-storage materials, Adv. Mater. 19 (2007) 2813.

[9] R. Gremaud, C.P. Broedersz, A. Borgschulte, M.J. van Setten, H. Schreuders, M. Slaman, B. Dam, R. Griessen, Hydrogenography of $Mg_yNi_{1-y}H_x$ gradient films: Interplay between the thermodynamics and kinetics of hydrogenation, Acta Materialia 58 (2010) 658.

[10] M. Rogers, S. Barcelo, X. Chen, T.J. Richardson, V. Berube, G. Chen, M.S. Dresselhaus, C.P. Grigoropoulos, S.S. Mao, Hydrogen storage characteristics of nanograined free-standing magnesium-nickel films, Appl. Phys. A 96 (2009) 349.

[11] H.M. Lutz, O.D. Pous, in: Proceeding of the 2nd International Congress on Hydrogen in Metals, 2 (1977) 1F5.

[12] K. Nomura, E. Akiba and S. Ono, Kinetics of the reaction between Mg_2Ni and hydrogen, Int. J. Hydrogen energy 6(3) (1981) 295.

[13] E. Akiba, K. Nomura, S. Ono, Y. Minzuno, Pressure-composition isotherms of Mg-Ni-H_2 alloys, J. Less-Common Metals 83 (1982) L43.

[14] P. Selvam, B. Viswanathan, C.S. Swamy and V. Srinivasan, Magnesium and magnesium alloy hydrides, Int. J. Hydrogen energy 11(3) (1986) 169.

[15] M.Y. Song, H.R. Park, Pressure-composition isotherms in the Mg_2Ni-H_2 system, J. Alloys Comp. 270 (1998) 164.

[16] K. Zeng, T. Klassen, W. Oelerich, R. Bormann, Thermodynamics analysis of the hydriding process of Mg-Ni alloys, J. Alloys Comp. 283 (1999) 213.

[17] D. Sun, H. Enoki, F. Gingl, E. Akiba, New approach of synthesizing Mg-based alloys, J. Alloys Comp. 285 (1999) 279.

[18] K.J. Gross, P. Spatz, A. Zuttel, L. Schlapbach, Mechanically milled Mg composites for hydrogen storage - The transition to a steady state composition, J. Alloys Comp. 240 (1996) 206.

[19] A. Baldi, M. Gonzalez-Silveira, V. Palmisno, B. Dam and R. Griessen, Destabilization of the Mg-H system through elastic constraints, Physical Review Letters 102 (2009) 226102.
[20] V. Palmisano et al., to be published.
[21] R. Gremaud, PhD thesis: Hydrogenography. A thin film optical combinatorial study of hydrogen storage materials, Vrije Universiteit Amsterdam, 2008.
[22] Y. Pivak, H. Schreuders, M. Slaman, R. Griessen, B. Dam, Thermodynamics, stress release and hysteresis behavior in highly adhesive Pd-H films, Int. J. Hydrogen energy 36(6) (2011) 4056.
[23] M.V. Simicic, M. Zdujic, R. Dimitrijevic, L. Nikolic-Bujanovi, N.H. Popovic, Hydrogen absorption and electrochemical properties of Mg_2Ni-type alloys synthesized by mechanical alloying, J. Power Sources 158 (2006) 730.
[24] D. Noreus and P.-E. Werner, The structure of the low temperature phase Mg_2NiH_4 (LT), Mat. Res. Bull. 16 (1981) 199.
[25] S. Ono, Y. Ishido, K. Imanari, T. Tabata, Y.K. Cho, R. Yamamoto and M. Doyama, Phase transformation and thermal expansion of Mg-Ni alloys in a hydrogen atmosphere, J. Less-Common Metals 88 (1982) 57.
[26] B. Darriet, J.L. Soubeyroux, M. Pezat, D. Fruchart, Structural and hydrogen diffusion study in the Mg_2Ni-H_2 system, J. Less-Com. Metals 103 (1984) 153.
[27] H. Hayakawa, Y. Ishido, H Uruno and S. Ono, Phase transformation among three polymorphs of Mg_2NiH_4, J. Less-Common Metals 103 (1984) 277.
[28] A. Baldi, G. K. Pálsson, M. Gonzalez-Silveira, H. Schreuders, M. Slaman, J. H. Rector, G. Krishnan,B. J. Kooi, G. S. Walker, M. W. Fay, B. Hjörvarsson, R. J. Wijngaarden, B. Dam, and R. Griessen, Mg/Ti multilayers: Structural and hydrogen absorption properties, Phys. Rev. B 81 (2010) 224203.
[29] A. Ludwig, J. Cao, B. Dam, R. Gremaud, Opto-mechanical characterization of hydrogen storage properties of Mg–Ni thin film composition spreads, Applied Surface Science 254 (2007) 682.
[30] A. Pundt, Hydrogen in nano-sized metals, Adv. Eng. Materials 6 (2004) 11.
[31] W.D. Callister, Fundamentals of Materials Science and Engineering, 2nd ed., Wiley & Sons. pp. 252.
[32] E. S. Kooij, A. T. M. van Gogh, D. G. Nagengast, N. J. Koeman, and R. Griessen, Hysteresis and the single-phase metal-insulator transition in switchable YH_x films, Phys. Rev. B 62 (2000) 10088.

Chapter 8

Enthalpy-entropy compensation in the quaternary Mg-Ti-Al-H system

8.1 Introduction

The clamping effect, which is caused by the presence of a rigid substrate, affects the thermodynamics and hysteresis behavior of thin films with respect to bulk materials. A thorough study of this effect in various metal hydrides thin films (PdH_x, YH_x. MgH_2, Mg_2NiH_x) led us to the development of a qualitative and quantitative stress-strain model. This model, which postulates that the clamping is proportional to the expansion mechanical work done by films and, in the case of YH_x and Mg_2NiH_x, due to the structure transformation between two preferentially oriented phases, allows for a much deeper understanding of the substrate influence in thin films. However, there is another phenomenon able to affect the thermodynamic properties of metal hydrides.

In the following chapter we investigate an effect of Al additions on the thermodynamic properties of Mg-Ti-H films. By exploring the combinatorial nature of Hydrogenography, we study the hydrogenation behavior of thousands of compositions in the ternary Mg-Ti-Al phase diagram simultaneously. We find, that the enthalpy of hydride formation of $Mg_{0.50}Ti_{0.15}Al_{0.35}H_x$, as calculated from the Van 't Hoff analysis, has increased to -42.4 kJ/mol H_2 compared to MgH_2 (-74.5 kJ/ mol H_2). Even when the clamping effect is taking into account, the resultant enthalpy of $Mg_{0.50}Ti_{0.15}Al_{0.35}H_x$, e. g. -50.8 kJ/mol$H_2$, is remaining substantially higher as compared to bulk magnesium hydride. However, a real destabilization effect (an increase of the equilibrium pressure) is not achieved because of the enthalpy-entropy compensation, increasing the entropy value of this alloy as well.

The following chapter is submitted to *International Journal of Hydrogen Energy*.

8.2 Destabilization effect in $Mg_{1-x-y}Ti_xAl_yH_z$ films as studied by Hydrogenography

Abstract:

Using Hydrogenography, we studied a destabilization effect in Mg-Ti-Al-H thin films. We show that additions of Al to $Mg_{1-x}Ti_x$ increase the enthalpy of formation, in accordance with recent DFT calculations. The composition of $Mg_{0.50}Ti_{0.15}Al_{0.35}H_x$, has a substantially destabilized enthalpy of formation of about -42.4 kJ/mol H_2. However, due to a compensation between the enthalpy and the entropy, the actual equilibrium pressures in this composition range are barely changed with respect to Mg-Ti films.

8.2.1 Introduction

Mg hydride is too stable thermodynamically, meaning that the required equilibrium pressure of 1 bar requires very high temperatures (around 573 K), which is not very practical. One of the ways to solve this problem is to destabilize MgH_2 (increase enthalpy of hydride formation) by means of alloying.

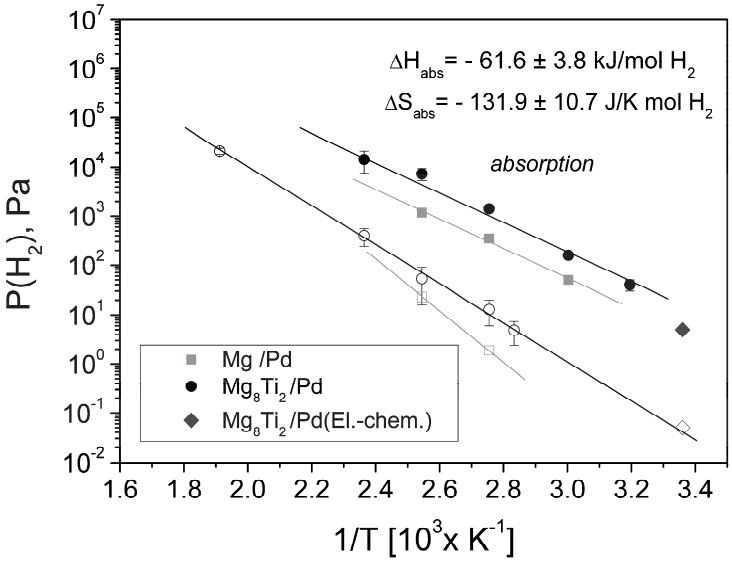

Fig. 8.1. Van 't Hoff plot comparing (de-)hydrogenation pressures of Mg and Mg_8Ti_2 films, measured by means of hydrogenography (black circles and red squares, respectively). Equilibrium pressures of hydride formation and decomposition of Mg_8Ti_2 films, measured using electrochemistry [16] (blue diamonds), is presented for comparison. The enthalpy and entropy of hydride formation of the Mg_8Ti_2 thin film, measured by Hydrogenography, is calculated from the linear fit to the experimental data.

A lot of work has been done to alloy Mg with another element (Ni, Fe, Co, Al, Cu, V, Ti) to increase the equilibrium pressure plateaus [1-11]. One example of a destabilization attempt, namely Mg-Ti, is of particular interest. According to the bulk phase diagram [12], it should not exist, while non-equilibrium preparation methods, like film deposition techniques, succeeded in preparing this metastable alloy [13, 14]. Moreover, it appears to be stable on prolonged hydrogenation [15]. A high gravimetric capacity of $Mg_{1-x}Ti_x$ (x=0.2–0.3) alloys [13, 14, 16] along with an improved loading/unloading kinetics (due

to a formation of an fcc MgH_2-lattice) made this material a very promising candidate for hydrogen storage. However, a more closer examination revealed that this alloying just lead to a small shift to higher equilibrium pressures as compared to pure Mg films [16], as visible from the Van 't Hoff plot (Fig. 8.1), meaning that a further destabilization of Mg-Ti-H is required.

Recently, DFT calculations were applied to probe the thermodynamics of several Mg-Ti-Al compositions. It was found that a substitution of about 13% of Ti with Al in the disordered $Mg_{0.75}Ti_{0.25}$ lattice leads to an increase of the enthalpy of hydride formation to about -48 kJ/mol H_2 [17]. Moreover, electrochemical experiments showed that adding Al to Mg-Ti does not substantially affect the hydrogen storage properties: while doping with up to 15% of Al hydrogen capacity larger than 5 wt% is maintained [18]. This makes Mg-Ti-Al alloys very interesting from a practical point of view.

To confirm the DFT calculations and to explore comprehensively the Mg-Ti-Al-H phase diagram, we investigate the (de-)hydrogenation behaviour in $Mg_{1-y-z}Ti_yAl_zH_x$ ($y \approx 0.05$-0.45; $z \approx 0.05$-0.45) thin films using combinatorial Hydrogenography. The hydrogenation properties of thousands of compositions in the Mg-Ti-Al ternary phase diagram were studied simultaneously in the temperature range 313–383 K. Using the Van 't Hoff analysis, the entropy and enthalpy of hydrogenation in the Mg-Ti-Al-H system have been calculated. Indeed, an increase in enthalpy is observed. It was found that the composition of $Mg_{0.50}Ti_{0.15}Al_{0.35}H_x$ exhibits an enthalpy of formation close to -42.4 kJ/mol H_2. By subtracting the effect of the substrate, i.e. 8.4 kJ/molH_2, from the measured thin film enthalpy, e.g. -42.4 kJ/molH_2, the corresponding bulk enthalpy can be estimated. The resultant value of -50.8 kJ/molH_2 is substantially lower (in absolute value) as compared to bulk MgH_2, confirming the destabilization. However, no pressures destabilization is achieved, as we observe enthalpy-entropy compensation effects for a wide range of Mg-Ti-Al compositions.

8.2.2 Experimental details

Thin $Mg_{1-y-z}Ti_yAl_z$ films are prepared in an AJA 7-gun ultra-high-vacuum dc/rf magnetron sputter deposition system (background pressure 10^{-7} Pa, deposition argon pressure 0.3 Pa). The films are deposited on 7.6 cm diameter circular sapphire substrate at room temperature. By co-sputtering with 3 off-axis targets positioned ever 120^o on a circle, $Mg_{1-y-z}Ti_yAl_z$ films with a compositional gradient (each position on the sample correspond to a different Mg:Ti:Al composition) are obtained. The gradient and the relative amount of each element are controlled by the tilt angle and the power of the targets. These parameters determine the compositional range of the sample. Due to a thickness gradient, which as a

side effect of a compositional gradient, the Mg thickness of the film varies from about 40 nm on the Mg-poor side to about 90 nm on the Mg-rich side. The difference in thickness creates a different in the optical contrast in the PTI's (see Fig. 8.4). The films are covered in-situ with a 20 nm Pd protective layer.

The composition and thickness gradients are determined by Rutherford Backscattering Spectrometry (RBS) using 2 MeV He^+ ions with a 1 mm^2 spot size on films deposited on 13 glassy carbon substrates placed in a triangular radial pattern (yellow dots in Fig. 8.2(a)). This deposition is done under the same sputtering conditions as the Hydrogenography wafers. The carbon substrates do not contribute to the background for energies above approximately 0.5 MeV. The composition of each point on a Hydrogenography wafer is then interpolated from the RBS results. The relative composition accuracy is estimated to be between 2 % and 5 %, the closer to the six axis probed by RBS the better [19].

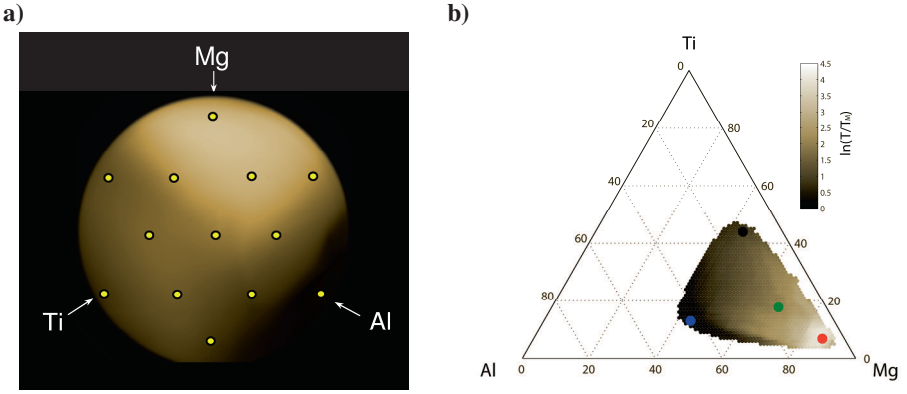

Fig. 8.2. (a) A photograph of the partially loaded ($P(H_2)=1.6\times10^3$ Pa) $Mg_{1-y-z}Ti_yAl_z$ film taken at 313 K during Hydrogenography measurements; to have a more clear difference between various regions in the sample, we used false colors instead of original black-and-white colors. The relative position of the Mg, Ti and Al targets (marked by arrows), along with a position of compositions used for the RBS measurements (yellow dots) are presented. (b) A ternary composition diagram representation of the natural logarithm of the normalized optical transmission ($ln(T/T_M)$) of the $Mg_{1-y-z}Ti_yAl_z$ film shown in (a).

The hydrogenation properties of metallic $Mg_{1-y-z}Ti_yAl_z$ films are studied using Hydrogenography in a combinatorial way [19]. The maximum temperature of the loading experiments is limited to 383 K to prevent/reduce interalloying between Mg and Pd, known to take place at higher temperatures. Prior to equilibrium measurements, films were

subjected to 10 fast (1-2 hours) (de-)hydrogenation cycles, where loading is performed in hydrogen atmosphere (pressure range 12-4×10^3 Pa) and unloading is done in oxygen-argon mixture (Ar-10%O_2). Note, that during absorption equilibrium measurement, the unloading is performed with an oxygen-argon mixture as well.

In order to check the pressure range where the $Mg_{1-y-z}Ti_yAl_z$ film reacts with hydrogen, equilibrium measurement at 313 K were conducted in two steps. First, the films were hydrogenated in a low pressures range, e.g. 1-100 Pa using the 0.1%H_2-Ar mixture and then, using the pure H_2 gas, the film were loaded in a high pressure range, e.g. 1.5×10^3-10^6 Pa; 10^6 Pa is the highest achievable pressure in the Hydrogenography setup. A photograph of the partially loaded ($P(H_2)$=1.6×10^3 Pa) $Mg_{1-y-z}Ti_yAl_z$ film is shown in Fig. 8.2(a). Typical loading times are 35 hours and 40 hours during the low and high pressure experiments, respectively. Equilibrium measurements of $Mg_{1-y-z}Ti_yAl_z$ film at higher temperatures were conducted only within one pressure range.

The equilibrium pressures for all compositions (about 10^4 isotherms) in the sample were determined automatically using a matlab script. First, the number of isotherms was lowered by averaging of the optical transmission during a pressure sweep experiment over 5×5 pixels in order to decrease the noise. Then, a number of numerical operations, including slope determination have been performed for every isotherm. The point with the lowest slope is indicated as the equilibrium pressure (P_{eq}); in case there is more than one plateau, the program is able to resolve and determine P_{eq} for several plateaus. The detailed calculation procedure can be found elsewhere [20].

The enthalpies and entropies of the individual compositions are estimated from the Van 't Hoff plots using the linear regression analysis. Typical errors of estimation of ΔH and ΔS lie within 2 kJ/mol H_2 and 5 J/K molH_2, respectively.

8.2.3 Results and discussion

Hydrogenography measurements of Mg-Ti-Al-H_x thin films

Figure 8.3 shows the hydrogen induced change in optical transmission of a $Mg_{1-y-z}Ti_yAl_z$ gradient sample at several pressures during a hydrogenation experiment at T = 313 K. The change in transmission is dramatic and both the pressure at which this change occurs and the magnitude of the change depend strongly on composition.

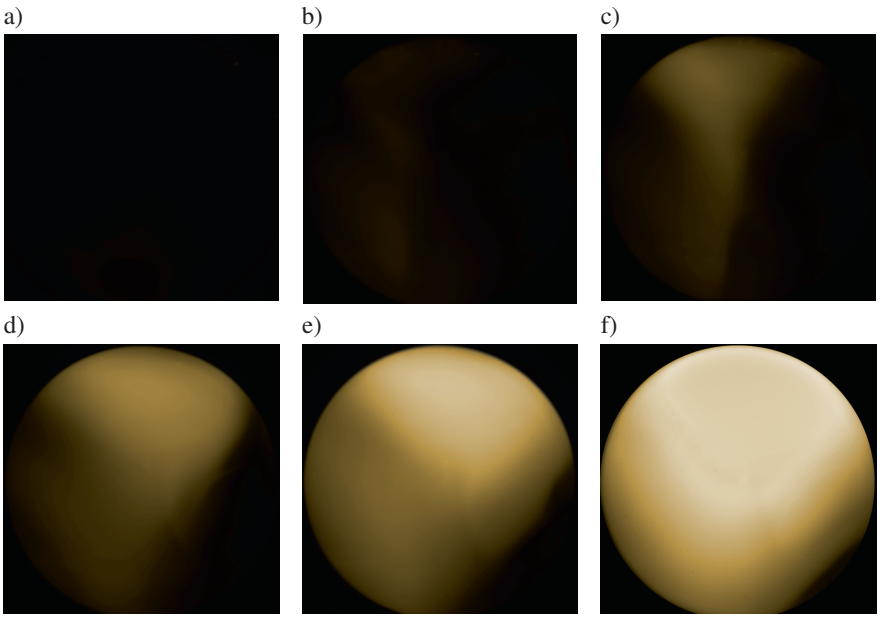

Fig. 8.3. Evolution of the optical transmission of a $Mg_{1-y-z}Ti_yAl_z$ thin film during hydrogen loading at 0.3 Pa (a), 18 Pa (b), 250 Pa (c), 574 Pa (d), 1.6×10^3 Pa (e) and 10^6 Pa at 313 K. Instead of black and white representation, false colors are used. Positions of the Mg, Ti and Al targets are the same as shown in Fig. 8.2(a).

At low hydrogen pressures (Fig. 8.3(b)), the Ti-rich part of the sample becomes slightly transparent, which we attribute to the formation of the highly stable TiH_2 (ΔH_{bulk}= -130 kJ/mol H_2). As the pressure increases (Fig. 8.2 (c, d)), the Mg-rich side of the $Mg_{1-y-z}Ti_yAl_z$ film reacts with hydrogen and this changes its optical appearance. At this stage the formation of MgH_2 with an enthalpy of formation of -74.5 kJ/mol H_2 (bulk value) is taking place. Apart from a small region in the Al-rich side, remaining black, essentially the whole wafer is loaded at 1.6×10^3 Pa (Fig. 8.3 (e)). At 10^6 Pa the black region almost disappears, suggesting a complete hydrogenation. Note that the very bright, not colored, region is due to a very large optical change, taking place in the Mg-rich side of the sample. In this part the optical transmission is quite close to the saturation limit.

To demonstrate the variation of the shape of the isotherms depending on the composition, several PTI's of the $Mg_{1-y-z}Ti_yAl_z$ loaded at 313 K are presented in Fig. 8.4. Positions, from which the various pressure-transmission-isotherms are taken, are shown in Fig. 8.2 (b) by color dots; the same color scheme is used in Fig. 8.4.

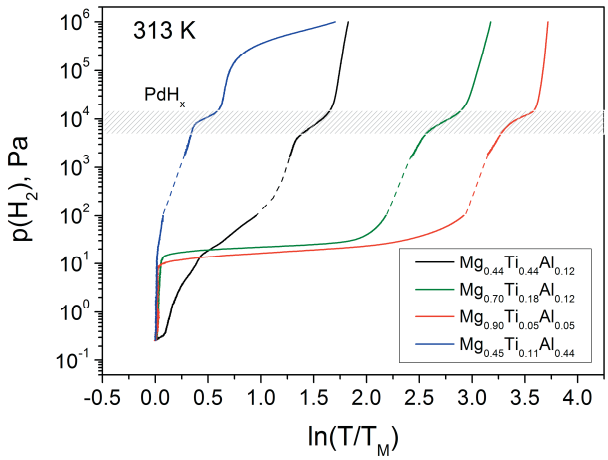

Fig. 8.4. Pressure-transmission-isotherms of certain alloys in the Mg-Ti-Al-H system. The second plateau corresponds to hydrogenation of the Pd cap-layer. Dotted lines correspond to the part of the isotherms, where experimental data is not available.

The black curve, which represents the Ti-rich part of the sample, has a strongly sloping plateau. Experiments at higher temperatures revealed that Ti-rich compositions are not stable as there is more than one plateau present in the isotherms. Red and green curves, which correspond to the Mg-rich part and the center composition, respectively, represent the majority of the isotherms measures at 313 K. They possess well-defined and flat plateaus.

A very peculiar case is the blue curve, measured in the Al-rich part. In the pressure range 1-100 Pa, where most of compositions with a high Mg content are loading, the blue curve does not exhibit any plateau. Further increase in hydrogen pressure just results in a small change of the optical transmission, followed by a plateau at around 10^4 Pa corresponding to the formation of PdH_x. Surprisingly, the beginning of an additional plateau becomes visible at substantially larger pressures – around 10^6 Pa, which is too high to be related to formation of MgH_2-based materials. Although the Mg:Al ratio is only 1:1, the fact that the plateau of $Mg_{0.45}Ti_{0.11}Al_{0.44}$ phase is not reversible on subsequent hydrogenation and appears at very high pressures might suggest a local formation of the magnesium alanate. Formation of the $Mg(AlH_4)_2$ complex hydride in Mg-Al thin films was previously reported by Gremaud et al. [21]. However, due to the non-crystalline nature of the forming phase(s) in $Mg_{0.45}Ti_{0.11}Al_{0.44}$, no reflections can be observed in XRD pattern,

from which we can not disregard or confirm our assumption. Therefore, a more elaborate (EXAFS) study is required to confirm formation of $Mg(AlH_4)_2$ in $Mg_{1-y-z}Ti_yAl_z$ films.

By numerical analysis of all the isotherms, the pressure map of $Mg_{1-y-z}Ti_yAl_z$ film at 313 K was constructed (Fig. 8.5). Black regions on this map relate to compositions having no, or more than one plateau. It can be seen that the pressure difference between various compositions is quite small. The majority of the equilibrium pressures fall within the range 10 - 40 Pa with a small region in the Al rich part of the sample, having absorption pressures in the range 60 - 80 Pa. It is worth to mention that the equilibrium pressures of $Mg_{1-y-z}Ti_yAl_z$ are at similar level as those observed for Mg and $Mg_{0.8}Ti_{0.2}$ films (Fig. 8.1)

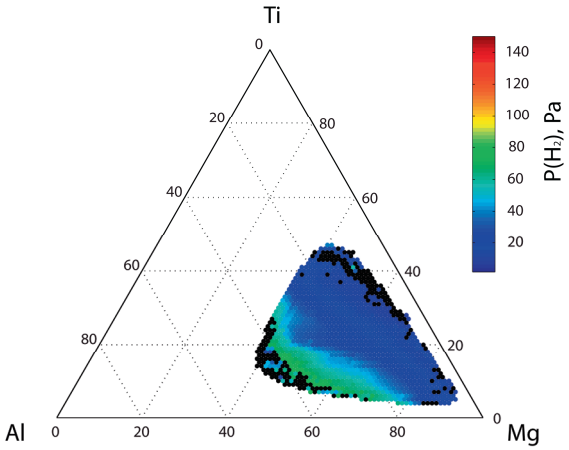

Fig. 8.5 Absorption equilibrium pressure map for $Mg_{1-y-z}Ti_yAl_z$ at 313 K. Black regions represent compositions with no or more than two plateaus.

Following the same numerical procedure, pressures maps at 333 K, 363 K and 383 K similar to the one at 313 K were constructed. From these pressure maps, the Van 't Hoff plots were plotted for each composition. From this the enthalpy and entropy maps were estimated (Fig. 8.6). Similarly to pressure maps, black parts correspond to compositions having no or more than one plateau, suggesting their limited stability.

From the enthalpy map it follows that an addition of Al to Mg-Ti structure results in a gradual increase of the enthalpy of hydrogenation. The largest enthalpy range, i.e. from -70 to -60 kJ/molH_2, is observed for compositions with of 5–20 wt% of Al (red and yellow region). The entropy of hydrogen formation is found to be in the range from -140 to-120 J/K molH_2. Further increase in Al concentration to 30 wt% and 35 wt% rises the enthalpy

and entropy values to about -55 kJ/molH_2 and -110 J/K molH_2 (green region) and -50 kJ/molH_2 and -100 J/K molH_2 (cyan/light blue region), respectively. Note that the concentration value given for every region is the average value since the boundaries between different color regions is not exactly parallel to the Al equi-concentrational lines (diagonal dotted lines in Fig. 8.6 representing equal Al concentrations) and, therefore, varies depending on Mg and Ti concentrations.

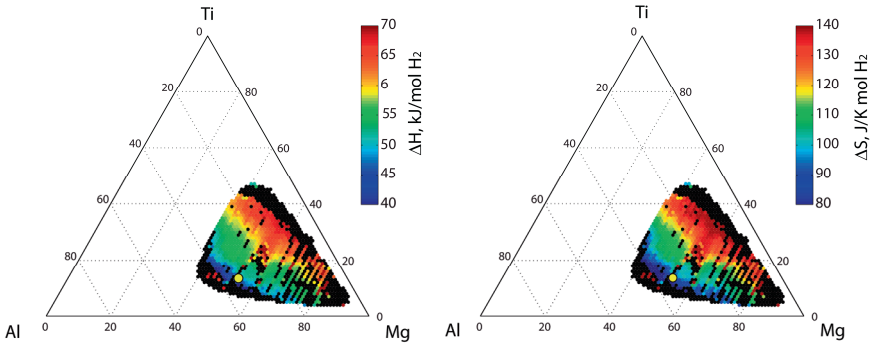

Fig. 8.6. Maps of hydrogenation enthalpies and entropies, calculated from the pressure maps, at different temperatures. The presented thermodynamics parameters (ΔH, ΔS) possess a negative sign. The yellow dot in the dark blue region represents the $Mg_{0.50}Ti_{0.15}Al_{0.35}$ phase.

The largest destabilization effect is observed in the (dark) blue region, with enthalpy values ranging from-45 to -40 kJ/molH_2. The composition of $Mg_{0.50}Ti_{0.15}Al_{0.35}$, shown by a yellow dot in Fig. 8.6, has the enthalpy of hydride formation of -42.4 kJ/molH_2, which is very attractive from the practical point of view. However, the entropy of formation we derive for this alloy is about -76 J/K molH_2, which is substantially higher with respect to the ideal value of the entropy, i.e. -130 J/K molH_2. As a result, the absorption pressure (e.g. 70 Pa at 313 K) is only slightly higher as compared to Mg or Mg_8Ti_2 films at the same temperature (Fig. 8.1, Fig. 8.5)

It is important to mention that, because of the presence of the substrate, the thermodynamic parameters we derive for the $Mg_{0.50}Ti_{0.15}Al_{0.3}$ thin films are expected to deviate from the corresponding bulk sample. To get the bulk values from the Hydrogenography measurements, the experimental results should be corrected for the clamping effect.

The way to account for the clamping effect is to perform the stress-strain analysis, explained in detail in the previous chapters, and recalculate the bulk pressures from the

equilibrium pressures measured by the Hydrogenography. From these pressures the correct (unaffected by the substrate) thermodynamic properties, e.g. enthalpy and entropy, can be evaluated. However, in this case desorption is difficult to measure. Hence, instead we use the stress-strain correction term previously derived for $Mg_{0.8}Ti_{0.2}$ films (Fig. 8.1), which we assume to be very similar to that of $Mg_{1-y-z}Ti_yAl_z$.

According to the experimental results, the enthalpy of hydride formation of $Mg_{0.8}Ti_{0.2}H_x$ film is -61.6 kJ/molH_2 (Fig. 8.1). As there is no bulk result for Mg-Ti alloy, MgH_2 bulk data is taken as a reference for the calculations. Similarly to chapter 6, we used the enthalpy of hydrogenation of -70 kJ/molH_2, which was measured by Vigeholm et al. [22]. By taking the difference between $\Delta H_{film}(Mg_{0.8}Ti_{0.2}H_x)$ of the clamped films and $\Delta H_{bulk}(MgH_2)$ of the "free" material we get 8.4 kJ/molH_2, which represents the energetic value of the clamping effect in $Mg_{0.8}Ti_{0.2}H_x$ films as well as in $Mg_{1-y-z}Ti_yAl_zH_x$ films, assuming that the substrate influence of these metal hydride systems is similar. The 'corrected' enthalpy of the $Mg_{0.48}Ti_{0.15}Al_{0.38}$ then can be estimated by subtracting the clamping effect. i.e. 8.4 kJ/molH_2, from the measured thin film enthalpy, e.g. -42.4 kJ/molH_2. The resultant value of -50.8 kJ/molH_2 corresponds to the bulk enthalpy of hydride formation of $Mg_{0.50}Ti_{0.15}Al_{0.35}$ film, if there would be no substrate. This value confirms the trend of the previously quoted DFT calculations [17]. Addition of Al to the structure of Mg-Ti leads to a destabilization effect as compared to magnesium hydride.

Enthalpy-entropy compensation

Despite the higher enthalpy of hydride formation measured in some Mg-Ti-Al alloys, no considerable pressure change is taking place as observed from Fig. 8.1 and Fig. 8.5. The reason becomes obvious considering the resemblance between the enthalpy and entropy maps (Fig. 8.6), where an increase in the enthalpy is accompanied by an increase in the entropy.

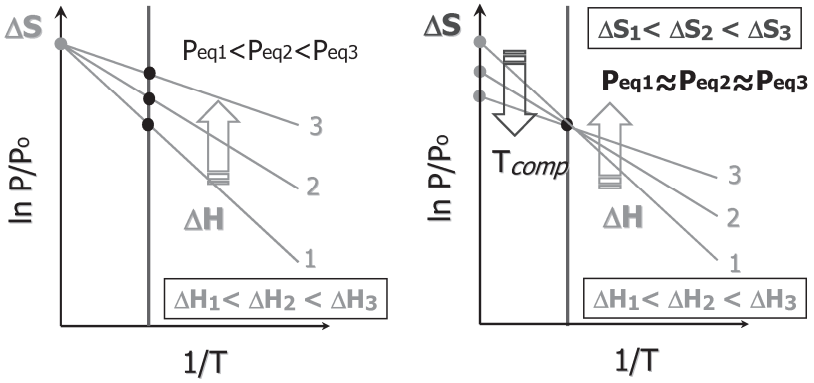

Fig. 8.7. Schematic representation of the destabilization effect in a material with (right) and without (left) enthalpy-entropy compensation; the enthalpies and entropies are taken as absolute values. T_{comp} is the compensation temperature, which is defined as the point where equilibrium pressures are equal for lines with different enthalpies, e.g. 1, 2, 3.

In the ideal situation in which the entropy stays fixed, an increase of the enthalpy results always in a change in pressure (Fig. 8.7, left). In the case of enthalpy-entropy compensation, i.e. when a change in ΔH is accompanied by a simultaneous change in ΔS, having the opposite sign (Fig. 8.7, right), a linear relation between the logarithm of the equilibrium pressure and enthalpy does not hold anymore. In this case there exists one pressure/temperature, which is identical for all compositions considered.

To check whether such a point exists for Mg-Ti-Al alloys a linear fit to the experimentally measured equilibrium pressures of various compositions in the measured ternary phase diagram is plotted against the inverse temperature (Fig. 8.8). The experimental temperature range, which is limited to 383 K for Hydrogenography, is extended in the fitting procedure to the 500 K. It can easily be seen that all lines are crossing at a temperature around 379 K, at which the equilibrium pressures are approximately equal for all compositions in the Mg-Ti-Al-H system (Fig. 8.8). The fact that the compensation temperature exists suggest that indeed, we have enthalpy-entropy compensation in $Mg_{1-y-z}Ti_yAl_zH_x$ films.

The nature of the enthalpy-entropy compensation effect, which was also observed previously in metal-hydride systems [19, 26], is still a subject of debate. A lot of work has been done to answer the question whether it is an artifact or a real physical phenomenon. Thus, by analyzing the compensation effect in two metal hydride systems (Mg and $LaNi_5$), Andreasen et al. [24] concluded that the effect originates from the method of data analysis.

Since the compensation temperature was found very close to the mean experimental temperature, he claimed that whenever the simultaneous determination of the apparent pre-factor and the activation energy using the Arrhenius analysis is taking place, there will be a compensation between these two thermodynamic variables. This, however, does not imply that all compensation observed in metal hydrides are necessarily related to a statistical error. It just means that if the compensation temperature is close to the mean temperature of the experiment, it is very difficult to resolve between the statistical error and a physical compensation. The fact that it falls just on the edge of the experimentally temperature range (it is not the mean experimental temperature) suggest that the compensation effect found in $Mg_{1-y-z}Ti_yAl_zH_x$ films is genuine. Additionally, the temperature and the pressure window, where the T_{comp} is observed are very small, pointing towards a small calculation (statistical) errors.

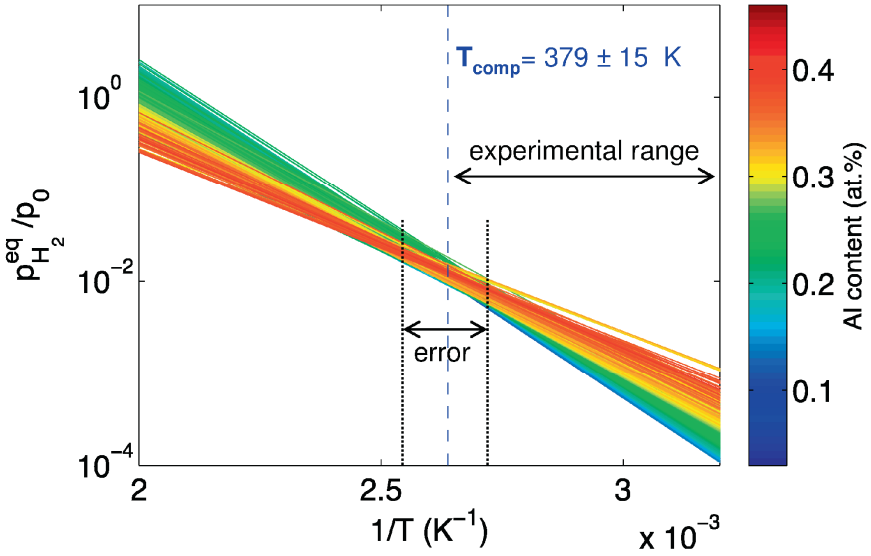

Fig. 8.8. Temperature dependence of the equilibrium pressures in $Mg_{1-y-z}Ti_yAl_zH_x$ films; different colors show different Al concentrations. The blue dashed line indicates the compensation temperature, where all the lines are crossing and all isotherms have approximately the same equilibrium pressures; vertical dotted lines indicate the error range of estimation of the compensation temperature. p_o is the atmospheric pressure, 1.013×10^5 Pa.

It is difficult to identify which physical phenomenon is the cause of the compensation effect in Mg-Ti-Al films. It might be simply connected to a gradual decrease of the hydrogen concentration with Al additions, or by a lattice contraction/expansion depending on Al doping or by different stress gradients. To answer the question a more thorough investigation, involving the calorimetry as a separate way to measure the thermodynamic properties of the sample independently, is prerequisite.

Note, that the derived entropy value may be affected by the clamping effect too. Given the fact that elastic contribution disappears at critical temperature (T_c), below T_c the change in ΔH due to the elastic contribution is necessarily coupled to ΔS, with the T_c as temperature. As the T_c for Mg-based compounds is well over 500 K (chapter 6), we do not think that clamping is the main cause for the compensation we observe in this case.

8.2.4 Conclusion

The hydrogenation behavior of quaternary Mg-Ti-Al-H system has been investigated for the first time using Hydrogenography, a combinatorial thin film optical technique. Thousands of compositions in the Mg-Ti-Al phase diagram were studied simultaneously in the temperature and pressure range 313–383 K and $0.1\text{-}10^6$ Pa, respectively. Using a numerical procedure, the absorption pressures for every composition at every temperature were estimated and the enthalpy/entropy maps were constructed. We found, that the enthalpy of hydride formation of $Mg_{0.50}Ti_{0.15}Al_{0.35}H_x$ alloy, as calculated from the Van 't Hoff analysis, has increased to -42.4 kJ/mol H_2, which is very attractive from the practical point of view. Considering the influence of the substrate on the thermodynamic properties, about the bulk value is estimated to be about -50.8 kJ/molH_2. This is still substantially higher as compared to bulk magnesium hydride, confirming the destabilization effect. The equilibrium pressure, however, is barely changed due to the enthalpy-entropy compensation effect increasing the entropy value of this alloy as well.

The compensation temperature is found around 380 K, which is close to the highest experimental temperature used in the Hydrogenography measurements. As all the isotherms cross each other in a small region of the p-T diagram the compensation temperature, T_{comp} is rather well determined, i.e. 380 K ± 15 K. suggesting small statistical errors, presented in the calculations. Therefore, the enthalpy-entropy compensation in $Mg_{1-y-z}Ti_yAl_zH_x$ films is considered to be a genuine effect and not due to artifacts of the data analysis.

8.2.5 References

[1] J.J. Reily and R.H. Wiswall, The Reaction of Hydrogen with Alloys of Magnesium and Nickel and the Formation of Mg_2NiH_4, Inorganic Chemistry 7 (1968) 2254.

[2] J. J. Didisheim, P. Zolliker, K. Yvon, P. Fischer, J. Schefer, M. Gubelmann, A. F. Williams, Dimagnesium iron(II) hydride, Mg_2FeH_6, containing octahedral FeH_{64}-anions, Inorg. Chem., 23 (1984) 1953.

[3] P. Zolliker, K. Yvon, P. Fischer, J. Schefer, Dimagnesium cobalt(I) pentahydride, Mg_2CoH_5, containing square-pyramidal pentahydrocobaltate(4-)(CoH54-) anions, Inorg. Chem. 24 (1985) 4177.

[4] G. Liang, J. Huot, S. Boily, A. Van Neste, R. Schulz, Catalytic effect of transition metals on hydrogen sorption in nanocrystalline ball milled MgH_2-Tm (Tm=Ti, V, Mn, Fe and Ni) systems, J. Alloys Comp. 292 (1999) 247.

[5] Huaiyu Shao, Yuntao Wang, Hairuo Xu, Xingguo Li, Preparation and hydrogen storage properties of nanostructured Mg_2Cu alloy, J. Solid State Chem. 178 (2005) 2211.

[6] A. Andreasen, Hydrogenation properties of Mg-Al alloys, Int. J. Hydrogen energy 33 (2008) 7489.

[7] D. Kyoi, T. Sato, E. Rönnebro, N. Kitamura, A. Uedac, M. Ito, S. Katsuyama, S. Hara, D. Noréus, T. Sakai, A new ternary magnesium–titanium hydride Mg_7TiH_x with hydrogen desorption properties better than both binary magnesium and titanium hydrides, J. Alloys Comp. 372 (2004) 213.

[8] K. Asano, E. Akiba, Direct synthesis of Mg–Ti–H FCC hydrides from MgH_2 and Ti by means of ball milling, J. Alloys Comp. 481 (2009) L8.

[9] W.P. Kalisvaart, H.J. Wondergem and F. Bakker, and P.H.L. Notten, Mg–Ti based materials for electrochemical hydrogen storage, J. Mater. Res. 22 (2007) 1640.

[10] P. Selvam, B. Viswanathan, C. S. Swamy and V. Srinivasan, Magnesium and Magnesium Alloys Hydrides, Int. J. Hydrogen energy 11 (1986) 169.

[11] I.P. Jain, C. Lal, A. Jain, Hydrogen storage in Mg: a most promising material, Int. J. Hydrogen energy 35 (2010) 5133.

[12] T. Massalskim P.S.H. Okamoto, and L. Kasprzak, Binary Alloy Phase Diagrams, American Society for Metals, Metals Park Oh, 1990.

[13] D. M. Borsa, R. Gremaud, A. Baldi, H. Schreuders, J.H. Rector, B. Kooi, P. Vermeulen, P.H.L. Notten, B. Dam and R. Griessen, Structural, optical and electrical properties of $Mg_yTi_{1-y}H_x$ thin films, Phys. Rev. B 75 (2007) 205408.

[14] P. Vermeulen, R.A.H. Niessen, P.H.L. Notten, Hydrogen storage in metastable $Mg_yTi_{(1-y)}$ thin films, Electrochemistry Comm. 8 (2006) 27.

[15] M. Slaman, B. Dam, M. Pasturel, D. M. Borsa, H. Schreuders, J. H.Rector, R. Griessen, Sensor Actuat. B-Chem 123 (2006) 538.

[16] P. Vermeulen, H.J. Wondergem, P.C.J. Graat, D. M. Borsa, H. Schreuders, B. Dam. R. Griessen and P.H.L. Notten, In situ electrochemical XRD study of (de)hydrogenation of Mg_yTi_{100-y} thin films, J. Mater. Chem. 18 (2008) 3680.

[17] S. Er, G. A. de Wijs, and G. Brocks, Tuning the Hydrogen Storage in Magnesium Alloys, J. Phys. Chem. Lett. 1 (2010) 1982.

[18] P. Vermeulen, E. F. M. J. van Thiel, and P. H. L. Notten, Ternary MgTiX-alloys: A promising route towards low temperature, high capacity, hydrogen storage materials, Chem. Eur. J. 33 (2007) 9892.

[19] R. Gremaud, C. Broedersz, D. Brosa, A. Borgschulte, P. Mauron, H. Schreuders, B. Dam and R. Griessen, Hydrogenography: an optical combinatorial method to find new light-weight hydrogen storage materials, Adv. Mater. 19 (2007) 2813.

[20] C. Boelsma, Enthalpy-entropy correlation in metal-hydrides studied for to magnesium-based systems, MSc thesis, VU University, Amsterdam, 2011.

[21] R. Gremaud, A. Borgschulte, W. Lohstroh, H. Schreuders, A. Züttel, B. Dam, R. Griessen, Ti-catalyzed $Mg(AlH_4)_2$: A reversible hydrogen storage material, J. Alloys Comp. 404-405 (2005) 775.

[22] A.S. Pedersen, J. Kjoller, B. Larsen, B. Vigeholm, International Journal of Hydrogen Energy 8(3) (1983) 205

[23] J. Lu, Y. J. Choi, Z. Z. Fang, H. Y. Sohn and E. Rönnebro, Hydrogen storage properties of nanosized MgH_2-0.1TiH_2 prepared by ultrahigh-energy–high-pressure milling, J. Am. Chem. Soc. 131 (2009) 15843.

[24] A. Andreasen, T. Vegge, and A. Pedersen, Compensation effect in the hydrogenation/dehydrogenation kinetics of metal hydrides, J. Phys. Chem. B 109 (2005) 3340.

[25] A. Cornish-Bowden. Enthalpy-entropy compensation: a phantom phenomenon. J. Biosci, 27 (2002) 121.

[26] Q. Zheng, Y. Pivak, L.P.A. Mooij, A. M. J. van der Eerden, H. Schreuders, P. E. de Jongh, J. H. Bitte, B. Dam, EXAFS investigation of the destabilization of the Mg-Ni-Ti (H) system, submitted to Int. J. Hydrogen Energy.

Summary

Hydrogenography is a combinatorial optical thin film technique to study the thermodynamic properties of metal hydride storage materials. It allows to study thousands of compositions simultaneously with exactly the same experimental conditions. Hydrogenography can pin point the most interesting regions/compositions in binary, ternary, quaternary etc. M-H phase diagrams. This valuable information can then be used in bulk experiments to measure other parameters such as the hydrogen volumetric density.

The main advantage of Hydrogenography comes from the possibility to create thin film compositional gradients, allowing for fast and efficient screening. The main drawback of this approach is the presence of the rigid substrate, used to support the metal thin films. During (de-)hydrogenation reaction the substrate exerts a force, due to the clamping, leading to a modification of the thermodynamics properties as measured by Hydrogenography. Therefore, before drawing conclusions on the corresponding bulk materials, the Hydrogenography experiment should be properly analyzed.

First, it is important to verify whether the film remains clamped to the substrate or has a tendency to delaminate. Delaminated or buckled films, as in the case of Pd, exhibit thermodynamic properties similar to bulk materials; in this case no correction to the enthalpies or entropies should be applied, i.e. $\Delta H_{film} \approx \Delta H_{bulk}$, $\Delta S_{film} \approx \Delta S_{bulk}$. Similar conclusion holds for other metal hydride systems, if the film under investigation is protected from the interaction (alloying) with the capping layer (Pd, Ni) by means of a buffer layer. Otherwise, a larger influence of the substrate on the thermodynamics is expected.

Second, one needs to be aware of an expanded hysteresis and, consequently, affected thermodynamic parameters when the film remains in full contact with the substrate. The enthalpy of formation- which is always modified by a bulk hysteresis term- obtains an additional component due to the clamping by the substrate ($\Delta H_{film} \approx \Delta H_{bulk} + \Delta H_{clamping}$). The proper way to estimate the thermodynamics of the bulk from the thermodynamics of the clamped film, is then to perform a stress-strain analysis at several temperatures. The stress-strain model, developed in this thesis, is able to quantitatively predict the clamping effect. It postulates that the increase of the hysteresis in thin films is taking place due to severe 'reversible' plastic deformations. Bulk metal hydrides disproportionate into small grains, when the hydrogenation stresses become higher than the Yield stress, thus releasing most of the stresses. This behavior is not possible in films due to presence of the substrate.

The outcome of the stress-strain analysis is ΔG_{hyst} parameter, which represents an additional mechanical work, performed by the film during the (de-)hydrogenation cycle due to the expansion constraints. This mechanical work increases when increasing the

'complexity' of the hydrogen storage system. For the metal hydrides studied in this thesis it ranges from 1.69 kJ/mol H for $PdH_{0.6}$, 2.93 kJ/mol H for MgH_2, 3.52 kJ/mol H for Mg_2NiH_4 to 4.25 kJ/mol H for YH_3. ΔG_{hyst} can be used to recalculate back the equilibrium pressures of the free-standing film (film without a substrate). From the linear fit to the new pressure values the enthalpy and entropy of the corresponding bulk materials can be evaluated.

This approach, however, is only valid for metal hydrides with no structure transformation (Pd case) or for metal hydrides which become amorphous on subsequent (de-)hydrogenation, such as MgH_2. When the material cycles between preferentially oriented crystalline metal and metal hydride states, as in the case of YH_3 and Mg_2NiH_4, the equilibrium pressures become affected by an additional parameter, ΔG_{str}. It represents the energy involved in the structure transformation and should be added to ΔG_{hyst} in order to fully describe the hysteresis behavior in these films. The ΔG_{str} equals to 5.2 kJ/(mol H) and 4.5 kJ/(mol H) for YH_3 and Mg_2NiH_4, respectively, which is a quite substantial amount of energy which cannot be disregarded. Thus, any other metal hydride system, possessing a structure transformation and remaining crystalline on cycling, will require this parameter, which can be measured via calorimetry or calculated via first principles methods.

An alternative approach to correct for the clamping effect is to subtract the energetic value of the clamping effect, $\Delta H_{clamping}$ (the change in enthalpy due to clamping in kJ/mol H), from the measured thin film enthalpy: $\Delta H_{bulk} \approx \Delta H_{film} - \Delta H_{clamping}$. This, however, requires knowledge of the $\Delta H_{clamping}$ in advance, which, again, can be estimated from the stress-strain analysis. The problem with this approach is that the entropy cannot be recalculated in this way.

Hydrogenography allows for comparison of thousands of compositions under exactly the same conditions. As a result, by measuring the Mg-Ti-Al-H system we identified an enthalpy-entropy compensation effect. Whenever we saw an increase of the enthalpy, simultaneously the entropy values were increasing (both in absolute sense). As a result, the equilibrium pressures remain almost the same. We can exclude trivial reasons related to the conditions of measurement, presence of the substrate etc. The origin of this effect remains unclear and requires further study. It shows, however, that the analysis of absorption/desorption equilibrium pressure at the relevant temperature is required in addition to the estimated thermodynamic parameters in order to evaluate different metal hydrides as hydrogen storage systems.

Samenvatting

Hydrogenografie is een combinatorische, optische, dunne film techniek om de thermodynamische eigenschappen van metaalhydriden (M-H) te bestuderen. Deze techniek maakt het mogelijk om duizenden chemische composities van deze waterstof opslagmaterialen simultaan bij exact dezelfde experimentele condities te analyseren. Hierdoor kunnen de meest interessante composities in binaire, ternaire, quaternaire, en verdere M-H fase diagrammen gevonden worden. Deze waardevolle informatie kan daarna toegepast worden in bulk experimenten om andere parameters, zoals de volumetrische dichtheid van waterstof, te vinden.

De hierboven genoemde mogelijkheid om vele verschillende materiaal composities te 'screenen' is meteen het grote voordeel van Hydrogenografie. De prijs die hiervoor betaald moet worden is de aanwezigheid van het rigide substraat, dat gebruikt wordt om de dunne metaal lagen op te deponeren. Tijdens de (de-)hydrogenatie reactie oefent het substraat, als gevolg van de adhesie, een kracht uit op de film, wat leidt tot een verandering van de door Hydrogenografie gemeten thermodynamische eigenschappen. Mede hierdoor dient elk Hydrogenografie experiment nauwkeurig te worden geanalyseerd voordat er conclusies uit kunnen worden getrokken ten aanzien van de eigenschappen van de corresponderende bulk materialen.

Ten eerste is het belangrijk te verifiëren of de dunne laag wel of niet vastgeklemd blijft op de substraat. Gedelamineerde, ofwel 'buckled'/ geknikte dunne lagen zoals Pd, vertonen thermodynamische eigenschappen vergelijkbaar met bulk materialen; in dit geval is er geen correctie nodig ten aanzien van de gevonden enthalpie en entropie, dat wil zeggen: $\Delta H_{film} \approx \Delta H_{bulk}$,.$\Delta S_{film} \approx \Delta S_{bulk}$. Een soortgelijke conclusie kan getrokken worden wanneer de onderzochte film wordt beschermd tegen de interactie, zoals het vormen van legeringen, van de katalytische toplaag (Pd of Ni) met behulp van een bufferlaag.

Ten tweede moet men zich bewust zijn van een grotere hysterese en dus veranderde thermodynamische parameters wanneer de film in de vastgeklemde toestand met de substraat blijft. De vormingsenthalpie bestaat nu uit een bulk term en een additionele term door de vastklemming aan het substraat ($\Delta H_{film} \approx \Delta H_{bulk} + \Delta H_{vastklemming}$). De juiste manier om de thermodynamische bulk termen te schatten is een spanning-rek analyse bij meerdere temperaturen. Het spanning-rek model, ontwikkeld in dit proefschrift, kan kwantitatief het effect van vastklemmen voorspellen. Het stelt dat de vergroting van de hysterese in dunne films het gevolg is van 'reversibele' plastische deformaties. Bulk metaalhydriden breken tijdens hydrogenatie op tot kleine korrels wanneer de spanningen groter worden dan de vloeigrens, waarbij de meeste opgebouwde spanning verdwijnt. Dit mechanisme is niet mogelijk in dunne films door de adhesie van de film aan het substraat.

De uitkomst van de spanning-rek analyse is de ΔG_{hyst} parameter. Deze representeert de additionele mechanische arbeid die moet worden verricht door de film tijdens de hydrogenatie cyclus om de beperkingen ten aanzien van de expansie te overbruggen. Deze mechanische arbeid wordt groter wanneer de complexiteit van het waterstof opslagsysteem (de metaalhydride) groter wordt. De in dit proefschrift bestudeerde metaalhydrides vertonen een ΔG_{hyst} van 1.69 kJ/molH voor $PdH_{0.6}$, 2.93 kJ/molH voor MgH_2, 3.52 kJ/molH voor Mg_2NiH_4 tot 4.25 kJ/molH voor YH_3. Met behulp van ΔG_{hyst} is het mogelijk om de evenwichtsdrukken van vrijstaande films (films zonder substraat) te berekenen. Met behulp van de Van 't Hoff vergelijking kunnen hierna de enthalpie en entropie van het corresponderende bulk materiaal berekend worden.

Deze methode geldt echter alleen voor metaalhydriden waarbij zich geen fase transformatie naar een andere structuur voordoet (bijvoorbeeld Pd) en voor metaalhydriden die amorf worden bij (de-)hydrogenatie, zoals MgH_2. Wanneer het materiaal schakelt tussen twee verschillende preferent georienteerde kristalstructuren, zoals het geval is voor YH_3 en Mg_2NiH_4, worden de evenwichtsdrukken beïnvloed door een additionele parameter, ΔG_{str}. Deze parameter staat voor de energie die nodig is voor de fase transitie, en moet bij ΔG_{hyst} opgeteld worden om zodoende de hysterese in deze films volledig te beschrijven. ΔG_{str} is gelijk aan 5.2 kJ/(mol H) en 4.5 kJ/(mol H) voor respectievelijk YH_3 en Mg_2NiH_4, voor beide materialen een substantiële waarde die niet genegeerd mag worden. Voor elk ander metaalhydride systeem waarbij er een fasetransitie tussen twee kristallijne fasen voorkomt zal ΔG_{str} niet te verwaarlozen zijn. ΔG_{str} kan gemeten worden met behulp van calorimetrie of berekend worden met behulp van *ab initio* berekeningen.

Een alternatieve benadering om te corrigeren voor het effect van vastklemmen is door de bijbehorende enthalpie, $\Delta H_{vastklemming}$, van de gemeten enthalpie van hydrogenatie af te trekken: $\Delta H_{bulk} \approx \Delta H_{film} - \Delta H_{vastklemming}$. Dit benodigt echter de *a priori* kennis van de waarde van $\Delta H_{vastklemming}$, welke uit een spanning-rek analyse geëxtraheerd kan worden. Het nadeel hiervan is dat slechts de enthalpie van het bulk materiaal berekent kan worden en niet de entropie.

Als laatste hebben we een fenomeen onderzocht dat gebruikt maakt van het feit dat Hydrogenografie de vergelijking van duizenden samples met verschillende samenstelling mogelijk maakt. Door metingen aan het Mg-Ti-Al-H system konden we een enthalpie-entropie compensatie effect vaststellen. Elke toename in de enthalpie bleek gepaard te gaan met een toename in de entropie (beide in absolute zin). Als gevolg hiervan blijft de evenwichtsdruk vrijwel constant voor een grote groep composities. Door onze methodiek kunnen we uitsluiten dat hieraan triviale oorzaken ten grondslag liggen zoals de aanwezigheid van het substraat of the precieze meetcondities. De oorzaak van dit effect vraagt daarom nadere studie. Het laat echter zien dat het noodzakelijk is de evenwichtsdruk

van de hydrogenatie te meten bij de gewenste temperatuur om de geschiktheid van een metaalhydride als waterstofopslag materiaal vast te stellen.

List of Publications

1. **Y. Pivak**, H. Schreuders, B. Dam, *Clamping effect in Mg_2NiH_4 thin films*, submitted to Acta Materialia.
2. **Y. Pivak**, H. Schreuders, B. Dam, *Thermodynamic properties, hysteresis behavior and stress-strain analysis of MgH_2 films studied in a wide temperature range*, submitted to special issue "Hydrogen Storage Alloys" of Crystal.
3. **Y. Pivak,** L.P.A. Mooij, H. Schreuders, B. Dam, *Destabilization effect in $Mg_{1-x-y}Ti_xAl_yH_z$ films studied by means of Hydrogenography*, submitted to Int. J. Hydrogen Energy.
4. **Y. Pivak,** B. Dam*, Thermodynamic Measurements Using Hydrogenography.* In: K. Gross (Ed.), *Recommended Best Practices for the Characterization of Storage Properties of Hydrogen Storage Materials,* 2012, in preparation.
5. Q. Zheng, **Y. Pivak**, L. P. A. Mooij, A.M.J. van der Eerden, H. Schreuders, P.E. de Joung, J.H. Bitte, B. Dam, *EXAFS investigation of the destabilization of the Mg-Ni-Ti(H) system*, submitted to Int. J. Hydrogen Energy.
6. T. Mongstad , C. Platzer-Björkman, J.P. Maehlen, L.P.A. Mooij, **Y. Pivak**, B.Dam, E. S. Marstein, B. C. Hauback and S.Karazhanov, *A new thin films photochromic material – oxygen-containig yttrium hydride*, Solar Energy Materials and Solar Cells, Volume 95 (2011) 3596.
7. L.P.A. Mooji, A. Baldi, C. Boelsma, K. Shen, M. Wagemaker, **Y. Pivak**, H, Schreuders, R. Griessen and Bernard Dam, *Interface energy controlled thermodynamics of nanoscale metal hydridesI*, Adv. Energy Mater., doi:10.1002/aenm.201100316.
8. **Y. Pivak** , H. Schreuders , M. Slaman, R.Griessen and B. Dam, *Thermodynamics, stress 9release and hysteresis behavior in highly adhesive Pd films,* International journal of hydrogen energy, 2011, Int. J. Hydrogen Energy, 36 (2011) 4056.
9. G. Krishnan, B.J. Kooi, G. Palasantzas, **Y. Pivak**, B. Dam, *Thermal stability of gas phase magnesium nanoparticles,* Journal of Applied physics 107 (2010) 053504.
10. A. Baldi, V. Palmisano, M. Govsalez-Silveira, **Y. Pivak**, M. Slaman, , H. Schreuders, B. Dam, and R.Griessen*, Quasi-free Mg-H thin films,* Applied Physics Letters 95 (2009) 071903.
11. **Y. Pivak**, R. Gremaud, K. Gross, M. Govsalez-Silveira, A. Walton, H. Schreuders, B. Dam, and R.Griessen*, Effect of the film substrate on the thermodynamics properties of the PdH_x studied by hydrogenography,* Scripta Materialia 60 (2009) 348.
12. R. Gremaud, M. Govsalez-Silveira, **Y. Pivak**, S. de Man, M. Slaman, H. Schreuders, B. Dam, and R.Griessen, *Hydrogenography of PdH_x thin films: influence of the H-induced stress relaxation processes,* Acta Materialia 57 (2009) 1209.

Acknowledgements

A large amount of people helped me scientifically, technically, physically and emotionally during my 4 years of PhD in Amsterdam and Delft and prior to that period. Since I'm limited in space, I simply cannot mention everybody here (*otherwise I need to add another chapter to this Thesis*). Nevertheless, you are all in my long lasting memory. In case it will fail, there will be always *Facebook*.

My biggest appreciation belongs to my family and to my daughter, Diana - I couldn't succeed without your love, support and care.

I'm very grateful to my supervisors, Bernard and Ronald for giving me the opportunity to do a PhD in Amsterdam and, later on, in Delft. A proposition for the PhD project in hydrogen storage came partly as a surprise long 4.5 years ago. The decision to move from sunny Portugal to rainy Holland wasn't too hard and I never regretted it. Hopefully, Ronald and Bernard fill the same way.

I must admit, guiding me through the PhD wasn't an easy task, though Bernard and Ronald did it very well. Unavoidable russian accent, gambling with the articles, discussion apathy, presentation marathons, strong non-working attitude advertized by various T-shirts with very peculiar statements like "*Sex Makes You Happy*", "*One Sick Bastard*" or "*Global warming is not cool*" etc. were the obstacles on the way to better me. However, *Their* patients and dedication, huge knowledge, wisdom and experience led to an enormous improvement on my side and made me the scientist I am now – stubborn, critical and asking too many questions. The phrase "I have two questions and a comment" became a habit during the group meetings in TU Delft. Due to the gained qualities also the writing part took a bit longer than expected – due to often, fruitful but sometimes difficult discussions with Bernard during the last year are the main reason for this. On the other hand it helped improved the thesis substantially, resulting in a very nice and well-written document, which even I enjoy to read.

One of the many important things, which came for understanding during PhD, is that the *good research can not be done just in the scientifically strong group*. *Another key ingredient in this equation is the working environment.* Again, I was very lucky here to become a part of a very friendly and a very social group of physicists in VU (expect for Andrea). Thanks to Robin (*father of Hydrogenography*), Erdni, Lennard (*baby face*), Martin, Andrea (*the blondest italian*), Sven, Marta, Valerio (*the Beast*) Davide, Matteo (*Bastardo* and *queen of M.*), Herman, Diana, Jan and, Keer and many more my work in Amsterdam was very joyful and fun. In this atmosphere even the meaning of the word 'work' has changed and with an extensive help of technical masterminds like Martin,

Herman, Jan and Keer my responsibilities basically narrowed to pushing buttons in the Hydrogenography setup and to various discussions during coffee breaks.

Good habits and great working atmosphere of VU followed the group to Delft. Here, however, around new colleges Joost, Wim (*big 'green' man*), Hans, Roel, Yen, Qing-Ping, Arjen, Maria, Fatwa, Qiang, Ali and Cedric the 'hard work' was taken to the next level. It was extended by the extensive ping-pong trainings and even competitions during lunch time, power golf during *ChemE* Open days, group dinners, every week *Borels* etc. The last one, taking place on Wednesdays after the group meetings, where Wim were asking too many questions too, was decreasing the amount of working hours even further, leaving less time for research but bringing a lot of fun.

Of course, great time I had during my PhD could not be possible without many-many new friends I met in the Netherlands. It's all started during the jazz festival in Delft, where I met a group under the code-name 'Ура, товарищи'. After that, I had an opportunity to enjoy the company of Vadim-ka and Oksana, Slava (a.k.a *Milovanovich*), Anton (*Doctor G.*), Sasha and Lina, Vlada, Sigizmund, Lena and Denis, Masha, Dima, Tali, Oleg, Daniela, Stas, Max, Luba, Petya (*Piton*), Olesya, Milan, Katya and many more quite often. There were plenty of birthday parties, relocations, barbeques on Delftse Hout, Halloweens in Zusterlaan, poker nights, weekend *kebabs*, paintball, nights out in Delft in various bars (*Belvedere*, *Kobus Kuch*, *Het Proeflocal*) and even going out in Rotterdam with the gorgeous girl Marla…Slava still can not get her of his mind, as we all. Playing pool while enjoying 'Войско Сербско', drinking *karnemelk* in front of the Church early o sunday morning, swimming in the middle of the night in the sea and in the lake (hopefully not I the canal in front of my house, as it was too contaminated), singing "Хочу Перемен" and "Вырубите на …", going crazy with "Мама, Анархия" and performing *horse fights* during parties at Vlada's place. Thanks to Stas I know all the funny stories about *порутчика Ржевского* and *боцмана*, якорь ему в почку ;-). Genial ideas and propositions of *Doctor G.,* generated "под шафе" always make us laugh. His last speech "Доктора ничего не сломает…" during his defense should be written in stone and putted I front of the Aula. Defense parties of Vlada ad Vadim-ka re-opened physical abilities of my body – amount of sleep were out numbered as compared to party hours and amount of alcohol.

Last but not least, I would like to mention my friends from Portugal. Thanks to them, I gained a lot of experience and knowledge, which was very helpful during the PhD. Thanks to Leha, the bone-crasher Kav, Sash, Serega, Katya and Serega, Dasha the time spent in Portugal was very enjoyable and unforgettable.

Curriculum Vitae

Yevheniy Pivak was born on September 7th 1981 in Lviv, Ukraine. From 1998 to 2003 he studied in Lviv Polytechnical National University at the faculty of semiconductor microelectronis. The master thesis entitled "Crystal structure, thermal expansion and phase transition in $La_{0.92}Sr_{0.08}Ga_{0.92}Ti_{0.08}O_3$ single crystal" was done under the supervision of Dr. L. Vasylechko in the group of Prof. A. Matkovskii. During this graduation project he received a DAAD scholarship in collaboration with Darmstadt Technical University, Germany. From 2003 to 2004 he worked as an engineer in the same group, investigating crystal structures and phase transitions of the RE (rare-earth) complex oxides with perovskite-like structure. In the period from 2005 to 2007 he did a postgraduate research work in the Department of Ceramics and Glass Engineering, University of Aveiro, Portugal in the group of Dr. V. Kharton, where he was involved in the development of the oxygen-ion conducting electrolytes for Solid Oxide Fuel Cells. In 2007 he moved to Amsterdam, The Netherlands, where he started his PhD in the condensed matter physics group at the Vrije Universiteit Amsterdam under the supervision of Prof. Ronald Griessen and Dr. Bernard Dam. After two years, his PhD project was continued in the MECS (Materials for Energy Conversion and Storage) group under the supervision of Prof. Bernard Dam. Research work involved validation of the optical thin film technique called Hydrogenography and the influence of the substrate on the thermodynamic properties and hysteresis behavior of metal hydride films. Since September 2011, he works as a design engineer in the D&E Source and Dose Control department of ASML, a manufacture of the most advanced litho tools.